

BAW-10164-A
Topical Report
Revision 4
November 2002

- RELAP5/MOD2-B&W -

An Advanced Computer Program for
Light Water Reactor LOCA and Non-LOCA
Transient Analysis

Framatome ANP Inc. (Formerly Framatome Technologies Inc.)
P. O. Box 10935
Lynchburg, Virginia 24506

Framatome ANP Inc.
Lynchburg, Virginia

Topical Report BAW-10164-A
Revision 4
November 2002

RELAP5/MOD2-B&W

An Advanced Computer Program for
Light Water Reactor LOCA and Non-LOCA
Transient Analysis

Key Words: RELAP5/MOD2, LOCA, Transient, Water Reactors

Abstract

This document describes the physical solution technique used by the RELAP5/MOD2-B&W computer code. RELAP5/MOD2-B&W is a Framatome Technologies Incorporated (previously known as and referred to in the text as B&W or B&W Nuclear Technologies) adaption of the Idaho National Engineering Laboratory RELAP5/MOD2. The code developed for best estimate transient simulation of pressurized water reactors has been modified to include models required for licensing analysis of zircaloy or zirconium-based alloy fuel assemblies. Modeling capabilities are simulation of large and small break loss-of-coolant accidents, as well as operational transients such as anticipated transient without SCRAM, loss-of-offsite power, loss of feedwater, and loss of flow. The solution technique contains two energy equations, a two-step numerics option, a gap conductance model, constitutive models, and component and control system models. Control system and secondary system components have been added to permit modeling of plant controls, turbines, condensers, and secondary feedwater conditioning systems. Some discussion of the numerical techniques is presented. Benchmark comparison of code

Rev. 4
9/99

predictions to integral system test results are presented in an appendix.

Rev. 4
9/99

ACKNOWLEDGMENT

RELAP5/MOD2-B&W is a modified version of the RELAP5/MOD2 advanced system code developed by the Idaho National Engineering Laboratory. A majority of the RELAP5/MOD2-B&W coding and the descriptive text of this document originates from the INEL personnel connected with the RELAP5 project and acknowledgment is given to their efforts.

B&W Nuclear Technologies (BWNT) also acknowledges the contribution of Nuclear Fuel Industries of Japan for the programming and documentation of the B&W modifications developed under a joint program.

The primary contributors at BWNT to this effort are: J. R. Biller, B. M. Dunn, J. A. Klingenfus, M. E. Mays, C. K. Nithianandan, K. C. Shieh, C. A. Schamp, N. H. Shah, W. T. Sneed, C. R. Williamson, and G. J. Wissinger. Their efforts are acknowledged in creating the modifications necessary to produce RELAP5/MOD2-B&W.

This page is intentionally left blank.

Topical Revision Record

Documentation <u>Revision</u>	<u>Description</u>	Program <u>Change?</u>	Program <u>Version</u>
0	Original issue	—	8.0
1	Typographical corrections	yes	10.0
2	Replace CSO correlation with Condie-Bengston IV. SBLOCA modifications Miscellaneous corrections	yes	18.0
3	EM Pin Enhancements Filtered Flows for Hot Channel Heat Transfer Rupture Area Enhancement for Surface Heat Transfer OTSG Improvements and Benchmarks using the Becker CHF, Slug Drag, and Chen Void Ramp	yes	19.0
4	Zirconium-based alloy pin model changes Option for multiple pin channels in a single core fluid channel Void-dependent core cross flow option Zirconium-based alloy rupture temperature	yes	24.0

Rev. 4
9/99

This page is intentionally left blank.

TABLE OF CONTENTS

	Page
1. INTRODUCTION	1-1
2. METHOD OF SOLUTION	2.1-1
2.1. Hydrodynamics	2.1-1
2.1.1. Field Equations	2.1-3
2.1.2. State Relationships	2.1-28
2.1.3. Constitutive Models	2.1-41
2.1.4. Special Process Models	2.1-88
2.1.5. Special Component Models	2.1-134
2.2. Heat Structure Models	2.2-1
2.2.1. Heat Conduction Model	2.2-1
2.2.2. Heat Structure Convective Boundary Conditions and Heat Transfer Models.	2.2-17
2.3. Reactor Core	2.3-1
2.3.1. Reactor Kinetics	2.3-1
2.3.2. Core Heat Structure Model	2.3-25
2.3.3. Core Heat Transfer Models	2.3-58.11}
2.4. Initial Conditions, Boundary Conditions, and Steady-State Calculations	2.4-1
2.4.1. Initial Conditions	2.4-2
2.4.2. Steady-State Initialization	2.4-3
2.4.3. Boundary Conditions	2.4-21
2.5. Control System	2.5-1
2.5.1. Control Variable Components	2.5-1
2.5.2. Trip System	2.5-13
3. PROGRAMMING METHODS	3.1-1
3.1. Top Level Organization	3.1-1
3.2. Transient and Steady-State Overview	3.2-1
3.3. Solution Accuracy	3.3-1
3.3.1. Time Step Control	3.3-1
3.3.2. Mass/Energy Mitigation	3.3-3
3.3.3. Velocity Flip-Flop	3.3-4

TABLE OF CONTENTS (Cont'd)

	Page
4. REFERENCES	4-1
5. LICENSING DOCUMENTS	5-1
5.1 Responses to Revision 1 Questions: Round 1	5-3
5.2 Responses to Revision 1 Questions: Round 2	5-101
5.3 Revision 1 Safety Evaluation Report (SER)	5-191
5.4 Responses to Revision 2 Questions	5-254
5.5 Responses to Revision 3 Questions	5-268
5.6 Supplemental Information to Revisions 2 and 3	5-300
5.7 Revisions 2 and 3 SER	5-325
5.8 Responses to Revision 4 Questions.	5-403
5.9 Revision 4 SER	5-533
5.10 Pages replaced from Revision 3	5-543
5.11 SER Directed Changes and Typographical Corrections.	5-570

This page is intentionally left blank.

Rev. 3
7/96

TABLE OF CONTENTS (cont'd)

Appendices

A.	RELAP5/MOD2 Models Not Employed in Evaluations	A-1
B.	List of Symbols	B-1
C.	EM Critical Flow Tables	C-1
D.	Thermodynamic Properties	D-1
E.	RELAP5/MOD2 Internally Stored Material Default Properties	E-1
F.	Heat Transfer Regimes and Correlations Identification	F-1
G.	Benchmarks	G-1
	G.1. LBLOCA Benchmark of Semiscale MOD1 Experiment S-04-6	G-2
	G.2. SBLOCA Benchmark of LOFT Experiment L3-5	G-32
	G.3. Conclusion - Large and Small LOCA Benchmark	G-48
H.	Wilson Drag Model Benchmarks	H-1
I.	BWUMV Critical Heat Flux Correlation	I-1
J.	SBLOCA EM Benchmark	J-1
K.	19-Tube OTSG Benchmarks	K-1
L.	MIST Benchmark	L-1

LIST OF TABLES

Table		Page
2.1.3-1.	RELAP5/MOD2 Interfacial Mass Transfer in Bulk Fluid	2.1-76
2.1.4-1.	Critical Flow Logic	2.1-111
2.1.5-1.	Semiscale Dimensionless Head Ratio Difference Data	2.1-149
2.1.5-2.	Head Multiplier and Void Fraction Data	2.1-150
2.3.2-1.	Constants Used in Gas Thermal Conductivity Correlation	2.3-31
2.3.2-2.	Radial Thermal Strain of Zircaloy for 1073 K < T < 1273 K	2.3-37
2.3.2-3.	NUREG-0630 Slow-Ramp Correlations for Burst Strain and Flow Blockage	2.3-42
2.3.2-4.	NUREG-0630 Fast-Ramp Correlations for Burst Strain and Flow Blockage	2.3-43
2.3.3-1.	English-SI Conversion Factors	2.3-78
C.1.	Moody Critical Flow Table	C-3
C.2.	Henry Model Critical Flow Tables	C-6
C.3.	Homogeneous Equilibrium Model Critical Flow Tables	C-8
C.4.	Murdock-Bauman Critical Flow Table for Superheated Vapor	C-13
G.1-1.	Sequence of Events During Test S-04-6	G-13
G.1-2.	Conditions at Blowdown Initiation	G-13
G.2-1.	Initial Conditions for LOFT L3-5	G-39
G.2-2.	Sequence of Events for LOFT L3-5	G-40
H.1.	FOAM2 Comparison Benchmark Cases	H-5
H.2.	ORNL Thermohydraulics Test Facility (THTF) Benchmark Cases	H-6
I.1.	Geometry of Westinghouse Bundles 121, 160, and 164	I-9

LIST OF TABLES (Cont'd)

Table	Page
I.2. Local Condition Analysis: Subchannel Parameters	I-10
I.3. Calculated Local Condition Values	I-11
J.1. Major Design Parameters of LSTF and PWR	J-14
J.2. Initial Test Conditions	J-15
J.3. Sequence of Events	J-16
K.1. Model 19-Tube OTSG Conditions for Steady-State Boiling Length Tests	K-8
K.2. Comparison of Predicted and Measured Boiling Lengths for a 19-Tube Model OTSG	K-8
K.3. Initial Conditions for 19-Tube Model OTSG LOFW Test	K-9
L.1. Comparison of MIST Initial Conditions to RELAP5/MOD2-B&W Values	L-13
L.2. Sequence of Events	L-13

LIST OF FIGURES

Figure	Page
2.1.1-1. Relation of Central Angle θ to Void Fraction α_g	2.1-22
2.1.1-2. Difference Equation Nodalization Schematic	2.1-24
2.1.3-1. Sketch of Vertical Flow Regime Map	2.1-42
2.1.3-2. Vertical Flow Regime Map Including the Vertically Stratified Regime	2.1-43
2.1.3-3. Slug-Flow Pattern	2.1-51
2.1.3-3.1 Typical RELAP5 Void Profile: Smoothed and Unsmoothed Curves	2.1-52.4
2.1.3-4. Comparison of Friction Factors for the Colebrook and Improved RELAP5 Friction Factor Models	2.1-73

LIST OF FIGURES (Cont'd)

Figure	Page
2.1.3-5. Two Vertical Vapor/Liquid Volumes	2.1-87
2.1.4-1. Equilibrium Speed of Sound as a Function of Void Fraction and Virtual Mass Coefficient	2.1-95
2.1.4-2. Coefficient of Relative Mach Number for Thermal Equilibrium Flow as a Function of Void Fraction and Virtual Mass Coefficient	2.1-96
2.1.4-3. Subcooled Choking Process	2.1-98
2.1.4-4. Orifice at Abrupt Area Change	2.1-114
2.1.4-5. Schematic Flow of Two-Phase Mixture at Abrupt Area Change	2.1-117
2.1.4-6. Simplified Tee Crossflow	2.1-124
2.1.4-7. Modeling of Crossflows or Leak	2.1-125
2.1.4-8. Leak Flow Modeling	2.1-127
2.1.4-9. One-dimensional Branch	2.1-130
2.1.4-10. Gravity Effects on a Tee	2.1-132
2.1.4-11. Volumes and Junction Configurations Available for CCFL Model	2.1-133.1
2.1.5-1. Typical Separator Volume and Junctions	2.1-135
2.1.5-2. Vapor Outflow Void Donoring	2.1-136
2.1.5-3. Liquid Fallback Void Donoring	2.1-136
2.1.5-4. Typical Pump Characteristic Four- Quadrant Curves	2.1-141
2.1.5-5. Typical Pump Homologous Head Curves	2.1-142
2.1.5-6. Typical Pump Homologous Torque Curves	2.1-143
2.1.5-7. Single-Phase Homologous Head Curves for 1-1/2 Loop MOD1 Semiscale Pumps	2.1-145
2.1.5-8. Fully Degraded Two-Phase Homologous Head Curves for 1-1/2 Loop MOD1 Semiscale Pumps	2.1-146
2.1.5-9. Torque Versus Speed, Type 93A Pump Motor	2.1-152

LIST OF FIGURES (Cont'd)

Figure	Page
2.1.5-10. Schematic of a Typical Relief Valve in the Closed Position	2.1-162
2.1.5-11. Schematic of a Typical Relief Valve in the Partially Open Position	2.1-163
2.1.5-12. Schematic of a Typical Relief Valve in the Fully Open Position	2.1-163
2.1.5-13. Typical Accumulator	2.1-170
2.2.1-1. Mesh Point Layout	2.2-3
2.2.1-2. Typical Mesh Points	2.2-4
2.2.1-3. Boundary Mesh Points	2.2-5
2.2.2-1. Logic Chart for System Wall Heat Transfer Regime Selection	2.2-34
2.3.2-1. Gap Conductance Options	2.3-27.1
2.3.2-2. Fuel Pin Representation	2.3-34
2.3.2-3. Fuel Pin Swell and Rupture Logic and Calculation Diagram	2.3-48
2.3.3-1. Core Model Heat Transfer Selection Logic	
a) Main Driver for EM Heat Transfer	2.3-62
b) Driver Routine for Pre-CHF and CHF Correlations	2.3-63
c) Driver Routine for CHF Correlations	2.3-64
d) Driver Routine for Post-CHF Correlations	2.3-65
3.1-1. RELAPS Top Level Structure	3.1-1
3.2-1. Transient (Steady-State) Structure	3.2-1
G.1-1. Semiscale MOD1 Test Facility - Cold Leg Break Configuration	G-14
G.1-2. Semiscale MOD1 Rod Locations for Test S-04-6	G-15

LIST OF FIGURES (Cont'd)

Figure		Page
G.1-3.	Semiscale MOD1 Test S-04-6; Pressure Near the Vessel Side Break	G-16
G.1-4.	Semiscale MOD1 Test S-04-6; Pressure Near the Pump Side Break	G-16
G.1-5.	Semiscale MOD1 Test S-04-6; Pressure Near the Intact Loop Pump Exit	G-17
G.1-6.	Semiscale MOD1 Test S-04-6; Pressure in the Broken Loop Near the Pump Simulator Inlet . . .	G-17
G.1-7.	Semiscale MOD1 Test S-04-6; Pressure in the Lower Plenum	G-18
G.1-8.	Semiscale MOD1 Test S-04-6; Pressure in the Upper Plenum	G-18
G.1-9.	Semiscale MOD1 Test S-04-6; Pressure Near the Top of the Pressurizer	G-19
G.1-10.	Semiscale MOD1 Test S-04-6; Pressure in the Intact Loop Accumulator	G-19
G.1-11.	Semiscale MOD1 Test S-04-6; Pressure in the Broken Loop Accumulator	G-20
G.1-12.	Semiscale MOD1 Test S-04-6; Mass Flow Rate Near the Vessel Side Break	G-20
G.1-13.	Semiscale MOD1 Test S-04-6; Mass Flow Rate Near Pump Side Break (Before ECC Injection Point)	G-21
G.1-14.	Semiscale MOD1 Test S-04-6; Mass Flow Rate in the Intact Loop Hot Leg	G-21
G.1-15.	Semiscale MOD1 Test S-04-6; Mass Flow Rate Near the Pump Simulator Inlet	G-22
G.1-16.	Semiscale MOD1 Test S-04-6; Mass Flow Rate in Intact Loop Cold Leg (Before Accumulator Injection Point)	G-22

LIST OF FIGURES (Cont'd)

Figure		Page
G.1-17.	Semiscale MOD1 Test S-04-6; Downcomer Inlet Flow Rate from the Intact Loop	G-23
G.1-18.	Semiscale MOD1 Test S-04-6; Mass Flow Rate at the Core Inlet	G-23
G.1-19.	Semiscale MOD1 Test S-04-6; Mass Flow Rate from the Intact Loop Accumulator	G-24
G.1-20.	Semiscale MOD1 Test S-04-6; Mass Flow Rate from the Broken Loop Accumulator	G-24
G.1-21.	Semiscale MOD1 Test S-04-6; Density Near the Vessel Side Break	G-25
G.1-22.	Semiscale MOD1 Test S-04-6; Density Near the Pump Side Break (Before the ECC Injection Location)	G-25
G.1-23.	Semiscale MOD1 Test S-04-6; Density Near the Core Inlet	G-26
G.1-24.	Semiscale MOD1 Test S-04-6; Fluid Temperature Near the Vessel Side Break	G-26
G.1-25.	Semiscale MOD1 Test S-04-6; Fluid Temperature Near Pump Side Break (Before ECC Injection Location)	G-27
G.1-26.	Semiscale MOD1 Test S-04-6; Fluid Temperature in the Intact Loop Hot Leg	G-27
G.1-27.	Semiscale MOD1 Test S-04-6; Fluid Temperature in Intact Loop Cold Leg (Near ECC Injection Point)	G-28
G.1-28.	Semiscale MOD1 Test S-04-6; Fluid Temperature Near the Core Inlet	G-28
G.1-29.	Semiscale MOD1 Test S-04-6; Fluid Temperature in Upper Plenum	G-29
G.1-30.	Semiscale MOD1 Test S-04-6; Average Power Rod Cladding Temperature at Peak Power Location . .	G-29

LIST OF FIGURES (Cont'd)

Figure		Page
G.1-31.	Semiscale MOD1 Test S-04-6; High Power Rod Cladding Temperature Near Peak Power Location	G-30
G.1-32.	RELAP5 Node and Junction Diagram	G-31
G.2-1.	LOFT System Configuration	G-41
G.2-2.	RELAP5 LOFT Nodalization for Test L-3-5	G-42
G.2-3.	RELAP5 Nodalization for LOFT Test L-3-5 Benchmark Analysis	G-43
G.2-4.	LOFT Test L-3-5; Core Pressure	G-44
G.2-5.	LOFT Test L-3-5; Steam Generator Pressure	G-44
G.2-6.	LOFT Test L-3-5; Pressurizer Water Level	G-45
G.2-7.	LOFT Test L-3-5; Pump Velocity	G-45
G.2-8.	LOFT Test L-3-5; Hot Leg Mass Flow Rate	G-46
G.2-9.	LOFT Test L-3-5; HPIS Mass Flow Rate	G-46
G.2-10.	LOFT Test L-3-5; Leak Node Pressure	G-47
G.2-11.	LOFT Test L-3-5; Steam Generator Pressure	G-47
H.1.	RELAP5 Model of Hypothetical Reactor Core	H-7
H.2.	Comparison of RELAP5 and FOAM2 Predictions: 5% Decay Power, 100 Psia	H-8
H.3.	Comparison of RELAP5 and FOAM2 Predictions: 5% Decay Power, 200 Psia	H-8
H.4.	Comparison of RELAP5 and FOAM2 Predictions: 5% Decay Power, 400 Psia	H-9
H.5.	Comparison of RELAP5 and FOAM2 Predictions: 5% Decay Power, 600 Psia	H-9
H.6.	Comparison of RELAP5 and FOAM2 Predictions: 5% Decay Power, 800 Psia	H-10

LIST OF FIGURES (Cont'd)

Figure		Page
H.7.	Comparison of RELAP5 and FOAM2 Predictions: 5% Decay Power, 1200 Psia	H-10
H.8.	Comparison of RELAP5 and FOAM2 Predictions: 2.5% Decay Power, 100 Psia	H-11
H.9.	Comparison of RELAP5 and FOAM2 Predictions: 2.5% Decay Power, 400 Psia	H-11
H.10.	Comparison of RELAP5 and FOAM2 Predictions: 2.5% Decay Power, 800 Psia	H-12
H.11.	Comparison of RELAP5 and FOAM2 Predictions: 2.5% Decay Power, 1200 Psia	H-12
H.12.	Comparison of RELAP5 and FOAM2 Predictions: 1.5% Decay Power, 1200 Psia	H-13
H.13.	Comparison of RELAP5 and FOAM2 Predictions: 1.5% Decay Power, 1600 Psia	H-13
H.14.	THTF in Small Break Test Configuration	H-14
H.15.	RELAP Model of ORNL Thermal-Hydraulic Test Facility (THTF)	H-15
H.16.	Comparison Between RELAP5 Prediction and ORNL Test Data: Experiment 3.09.10i, 0.68 Kw/ft, 650 Psia	H-16
H.17.	Comparison Between RELAP5 Prediction and ORNL Test Data: Experiment 3.09.10j, 0.33 Kw/ft, 610 Psia	H-16
H.18.	Comparison Between RELAP5 Prediction and ORNL Test Data: Experiment 3.09.10k, 0.10 Kw/ft, 580 Psia	H-17
H.19.	Comparison Between RELAP5 Prediction and ORNL Test Data: Experiment 3.09.10l, 0.66 Kw/ft, 1090 Psia	H-17
H.20.	Comparison Between RELAP5 Prediction and ORNL Test Data: Experiment 3.09.10m, 0.31 Kw/ft, 1010 Psia	H-18

LIST OF FIGURES (Cont'd)

Figure		Page
H.21.	Comparison Between RELAP5 Prediction and ORNL Test Data: Experiment 3.09.10n, 0.14 Kw/ft, 1030 Psia	H-18
H.22.	Comparison Between RELAP5 Prediction and ORNL Test Data: Experiment 3.09.10aa, 0.39 Kw/ft, 590 Psia	H-19
H.23.	Comparison Between RELAP5 Prediction and ORNL Test Data: Experiment 3.09.10bb, 0.20 Kw/ft, 560 Psia	H-19
H.24.	Comparison Between RELAP5 Prediction and ORNL Test Data: Experiment 3.09.10cc, 0.10 Kw/ft, 520 Psia	H-20
H.25.	Comparison Between RELAP5 Prediction and ORNL Test Data: Experiment 3.09.10dd, 0.39 Kw/ft, 1170 Psia	H-20
H.26.	Comparison Between RELAP5 Prediction and ORNL Test Data: Experiment 3.09.10ee, 0.19 Kw/ft, 1120 Psia	H-21
H.27.	Comparison Between RELAP5 Prediction and ORNL Test Data: Experiment 3.09.10ff, 0.08 Kw/ft, 1090 Psia	H-21
H.28.	Comparison Between RELAP5 Prediction and ORNL Test Data: Experiment 3.09.10i, 0.68 Kw/ft, 650 Psia	H-22
H.29.	Comparison Between RELAP5 Prediction and ORNL Test Data: Experiment 3.09.10j, 0.33 Kw/ft, 610 Psia	H-22
H.30.	Comparison Between RELAP5 Prediction and ORNL Test Data: Experiment 3.09.10k, 0.10 Kw/ft, 580 Psia	H-23
H.31.	Comparison Between RELAP5 Prediction and ORNL Test Data: Experiment 3.09.10l, 0.66 Kw/ft, 1090 Psia	H-23

LIST OF FIGURES (Cont'd)

Figure		Page
H.32.	Comparison Between RELAP5 Prediction and ORNL Test Data: Experiment 3.09.10m, 0.31 Kw/ft, 1010 Psia	H-24
H.33.	Comparison Between RELAP5 Prediction and ORNL Test Data: Experiment 3.09.10n, 0.14 Kw/ft, 1030 Psia	H-24
I.1.	Subchannel Model for Westinghouse Test 121 . . .	I-13
I.2.	Subchannel Model for Westinghouse Tests 160 and 164	I-13
I.3.	Frequency Distribution of Mixing Vane CHF Data	I-14
I.4.	Measured-to-Predicted Ratios of BWUMV Data: Quality	I-14
I.5.	Measured-to-Predicted Ratios of BWUMV Data: Pressure	I-15
I.6.	Measured-to-Predicted Ratios of BWUMV Data: Mass Flux	I-15
J.1.	ROSA Large Scale Test Facility Configuration	J-17
J.2.	ROSA Noding Diagram Pressure Vessel	J-18
J.3.	ROSA Noding Diagram for Primary Loops	J-19
J.4.	ROSA SBLOCA EM Noding Diagram for Pressure Vessel	J-20
J.5.	ROSA SBLOCA EM Noding Diagram for Primary Loops	J-21
J.6.	Leak Flow Rate	J-22
J.7.	Primary System Pressure	J-22
J.8.	Core Differential Pressure	J-23
J.9.	Intact Loop Pump Suction Seal Downflow Differential Pressure	J-23

LIST OF FIGURES (Cont'd)

Figure		Page
J.10.	Broken Loop Pump Suction Seal Downflow Differential Pressure	J-24
J.11.	Leak Flow Rate	J-24
J.12.	Primary System Pressure	J-25
J.13.	Pressurizer Level	J-25
J.14.	Intact Loop Steam Generator Pressure	J-26
J.15.	Broken Loop Steam Generator Pressure	J-26
J.16.	Intact Loop Pump Suction Seal Downflow Differential Pressure	J-27
J.17.	Intact Loop Pump Suction Seal Upflow Differential Pressure	J-27
J.18.	Broken Loop Pump Suction Seal Downflow Differential Pressure	J-28
J.19.	Broken Loop Pump Suction Seal Upflow Differential Pressure	J-28
J.20.	Core Differential Pressure	J-29
J.21.	Downcomer Differential Pressure	J-29
J.22.	Intact Loop Steam Generator Inlet Plenum Differential Pressure	J-30
J.23.	Broken Loop Steam Generator Inlet Plenum Differential Pressure	J-30
J.24.	Inlet Loop Steam Generator Tube Upflow Differential Pressure	J-31
J.25.	Broken Loop Steam Generator Tube Upflow Differential Pressure	J-31
J.26.	Upper Plenum Differential Pressure	J-32
J.27.	Inlet Loop Steam Generator Tube Downflow Differential Pressure	J-32

LIST OF FIGURES (Cont'd)

Figure		Page
J.28.	Broken Loop Steam Generator Tube Downflow Differential Pressure	J-33
J.29.	Intact Loop Accumulator Flow Rate	J-33
J.30.	Broken Loop Accumulator Flow Rate	J-34
J.31.	Hot Rod Surface Temperature - Elevation 0.05 Meters	J-34
J.32.	Hot Rod Surface Temperature - Elevation 1.018 Meters	J-35
J.33.	Hot Rod Surface Temperature - Elevation 1.83 Meters	J-35
J.34.	Hot Rod Surface Temperature - Elevation 2.236 Meters	J-36
J.35.	Hot Rod Surface Temperature - Elevation 3.048 Meters	J-36
J.36.	Hot Rod Surface Temperature - Elevation 3.61 Meters	J-37
J.37.	Dimensionless Liquid Velocity at Steam Generator Tube Inlet	J-37
J.38.	Dimensionless Vapor Velocity at Steam Generator Tube Inlet	J-38
J.39.	Wallis Constant at Steam Generator Tube Inlet	J-38
J.40.	Dimensionless Liquid Velocity at Steam Generator Plenum Inlet	J-39
J.41.	Dimensionless Vapor Velocity at Steam Generator Plenum Inlet	J-39
J.42.	Wallis Constant at Steam Generator Plenum Inlet	J-40

LIST OF FIGURES (Cont'd)

Figure		Page
K-1.	Schematic Diagram of the Nuclear Steam Generator Test Facility	K-10
K-2.	19-Tube Once-Through Steam Generator and Downcomer	K-11
K-3.	RELAP5/MOD2-B&W Model of 19-Tube OTSG	K-12
K-4.	Comparison of Measured and Predicted Boiling Lengths in a Model 19-Tube OTSG	K-13
K-5.	Comparison of Measured and Predicted Initial Primary System Fluid Temperatures for 19-Tube OTSG LOFW Test	K-13
K-6.	Comparison of Measured and Predicted Initial Secondary System Fluid Temperatures for 19-Tube OTSG LOFW Test	K-14
K-7.	Comparison of Measured and Predicted Steam Flow During 19-Tube OTSG LOFW Test	K-14
K-8.	Comparison of Measured and Predicted Primary Outlet Temperatures During 19-Tube OTSG LOFW Test	K-15
L-1.	MIST Facility	L-14
L-2.	RELAP5/MOD2-B&W Model of The MIST Facility	L-15
L-3.	Comparison of Predicted and Observed Primary System Pressures for MIST Test 320201	L-16
L-4.	Comparison of Predicted and Observed Secondary System Pressures for MIST Test 320201	L-16
L-5.	Comparison of Predicted and Observed Reactor Vessel Liquid Levels for MIST Test 320201	L-17
L-6.	Comparison of Predicted and Observed SG Secondary Liquid Levels for MIST Test 320201	L-17

1. INTRODUCTION

RELAP5/MOD2 is an advanced system analysis computer code designed to analyze a variety of thermal-hydraulic transients in light water reactor systems. It is the latest of the RELAP series of codes, developed by the Idaho National Engineering Laboratory (INEL) under the NRC Advanced Code Program. RELAP5/MOD2 is advanced over its predecessors by its six-equation, full nonequilibrium two-fluid model for the vapor-liquid flow field and partially implicit numerical integration scheme for more rapid execution. As a system code, it provides simulation capabilities for the reactor primary coolant system, secondary system, feedwater trains, control systems, and core neutronics. Special component models include pumps, valves, heat structures, electric heaters, turbines, separators, and accumulators. Code applications include the full range of safety evaluation transients, loss-of-coolant accidents (LOCAs), and operating events.

RELAP5/MOD2 has been adopted and modified by B&W for licensing and best estimate analyses of PWR transients in both the LOCA and non-LOCA categories. RELAP5/MOD2-B&W retains virtually all of the features of the original RELAP5/MOD2. Certain modifications have been made either to add to the predictive capabilities of the constitutive models or to improve code execution. More significant, however, are the B&W additions to RELAP5/MOD2 of models and features to meet the 10CFR50 Appendix K requirements for ECCS evaluation models. The Appendix K modifications are concentrated in the following areas: (1) critical flow and break discharge, (2) fuel pin heat transfer correlations and switching, and (3) fuel clad swelling and rupture for both zircaloy and zirconium-based alloy cladding types.

This report describes the physical models, formulation, and structure of the B&W version of RELAP5/MOD2 as it will be applied to ECCS and system safety analyses. It has been prepared as a stand-alone document; therefore substantial portions of the text that describe the formulation and numerics have been taken directly from original public domain reports, particularly NUREG/CR-4312¹. Chapter 2 presents the method of solution in a series of subsections, beginning with the basic hydrodynamic solution including the field equations, state equations, and constitutive models in section 2.1. Certain special process models, which require some modification of the basic hydrodynamic approach, and component models are also described. The general solution for heat structures is discussed in section 2.2. Because of the importance of the reactor core and the thermal and hydraulic interaction between the core region and the rest of the system, a separate section is dedicated to core modeling. Contained in section 2.3 are the reactor kinetics solution, the core heat structure model, and the modeling for fuel rod rupture and its consequences. Auxiliary equipment and other boundary conditions are discussed in section 2.4 and reactor control and trip function techniques in section 2.5. Chapter 3 provides an overview of the code structure, numerical solution technique, method and order of advancement, and initialization. Time step limitation and error control are presented in section 3.3.

The INEL versions of RELAP5/MOD2 contain certain solution techniques, correlations, and physical models that have not been selected for use by B&W. These options have been left intact in the coding of the B&W version, but descriptions have not been included in the main body of this report. Appendix A contains a list of those options that remain in the RELAP5/MOD2 programming but are not used by B&W and not submitted for review. A brief description of each along with a reference to an appropriate full discussion is provided in the appendix. Appendix B defines the nomenclature used throughout this report. Appendix G documents

the benchmark calculations performed by BWNT to support the application of RELAP5/MOD2 to safety and ECCS evaluations. Appendix H provides comparisons between Wilson drag benchmarks and the NRC-approved core water level swell code, FOAM2, and between Wilson and ORNL Thermal-Hydraulic Test Facility (THTF) small break LOCA test data. Appendix I provides the derivation of the BWUMV critical heat flux (CHF) correlation. Appendix J presents the small break LOCA evaluation model benchmark. Appendix K presents the once-through steam generator (OTSG) steady-state and loss-of-feedwater with feedwater reactivation benchmarks to validate the OTSG model improvements. Appendix L contains Multi-Loop Integral System Test (MIST) facility benchmarks to demonstrate the integral system performance of RELAP5/MOD2-B&W and further validate the OTSG and drag model improvements.

2. METHOD OF SOLUTION

The general formulation and structure of RELAP5/MOD2 allow the user to define a nodal finite difference model for system transient predictions. Coupling of the major system models (hydrodynamics, heat structures, reactor core, and control system) provides the capability to simulate a range of transients from LBLOCA to operational upsets. In RELAP5/MOD2, the transients are calculated by advancing the one-dimensional differential equations representing a two-fluid, nonhomogeneous, nonequilibrium, two-phase system. Six flow field equations are coupled with the state- and flow regime-dependent constitutive relations in a partially-implicit numerical solution. The control system, heat structures, and reactor core models employ explicitly formulated terms that interface with the solution techniques. Also, special models are included for some system components such as pumps, separators, valves, and accumulators. A description of the formulation and solution method is contained in this section of the report.

2.1. Hydrodynamics

The RELAP5/MOD2-B&W hydrodynamic model is a one-dimensional, transient, two-fluid model for flow of a two-phase steam-water mixture that can contain a noncondensable component in the steam phase and/or a nonvolatile component in the liquid phase. The hydrodynamic model contains several options for invoking simpler hydrodynamic models. These include homogeneous flow, thermal equilibrium, and frictionless flow models, which can be used independently or in combination.

The two-fluid equations of motion that are used as the basis for the RELAP5/MOD2-B&W hydrodynamic model are formulated in terms of area and time average parameters of the flow. Phenomena that depend upon transverse gradients such as friction and heat transfer are formulated in terms of the bulk potentials using empirical transfer coefficient formulations. The system model is solved numerically using a semi-implicit finite difference technique. The user can select an option for solving the system model using a nearly-implicit finite difference technique, which allows violation of the material Courant limit. This option is suitable for steady state calculations and for slowly-varying, quasi-steady transient calculations.

The basic two-fluid differential equations possess complex characteristic roots that give the system a partially elliptic character and thus constitute an ill-posed initial boundary value problem. In RELAP5 the numerical problem is rendered well posed by the introduction of artificial viscosity terms in the difference equation formulation that damp the high frequency spatial components of the solution.

The semi-implicit numerical solution scheme uses a direct sparse matrix solution technique for time step advancement. It is an efficient scheme and results in an overall grind time on the CDC Cyber-176 of approximately 0.0015 seconds. The method has a material Courant time step stability limit. However, this limit is implemented in such a way that single node Courant violations are permitted without adverse stability effects. Thus, single small nodes embedded in a series of larger nodes will not adversely affect the time step and computing cost. The nearly-implicit numerical solution scheme also uses a direct sparse matrix solution technique for time step advancement. This scheme has a grind time that is 25 to 60 percent greater than the semi-implicit scheme but allows violation of the material Courant limit for all nodes.

2.1.1. Field Equations

RELAP5/MOD2-B&W has six dependent variables (seven if a noncondensable component is present), P (pressure), U_g and U_f (gas and fluid internal energies), α_g (void fraction), v_g and v_f (phasic velocities), and X_n (noncondensable mass fraction). The noncondensable quality is defined as the ratio of the noncondensable gas mass to the total gaseous phase mass (i.e., $X_n = M_n / (M_n + M_s)$, where M_n = mass of noncondensable in the gaseous phase and M_s = mass of steam in the gaseous phase). The eight secondary dependent variables used in the equations are phasic densities (ρ_g, ρ_f), vapor generation rate per unit volume (Γ_g), phasic interphase heat transfer rates per unit volume (Q_{ig}, Q_{if}), phasic temperatures (T_g, T_f), and saturation temperature (T^s).

In the following sections, the basic two-fluid differential equations that form the basis for the hydrodynamic model are presented. The discussion is followed by the development of a convenient form of the differential equations used as the basis for the numerical solution scheme. The modifications necessary to model horizontal stratified flow are also discussed. Subsequently, the semi-implicit scheme difference equations, the volume-averaged velocity formulations, and the time advancement scheme are discussed. Finally, the nearly-implicit scheme difference equations are presented.

2.1.1.1. Basic Differential Equations

The differential form of the one-dimensional transient field equations is first presented for a one-component system. The modifications necessary to consider noncondensibles as a component of the gaseous phase and boron as a nonvolatile solute component of the liquid phase are discussed separately.

Vapor/Liquid System

The basic field equations for the two-fluid nonequilibrium model consist of two phasic continuity equations, two phasic momentum equations, and two phasic energy equations. The equations are recorded in differential streamtube form with time and one space dimension as independent variables and in terms of time and volume-average dependent variables.^a The development of such equations for the two-phase process has been recorded in several references^{11,12} and is not repeated here. The equations are cast in the basic form with discussion of those terms that may differ from other developments. Manipulations required to obtain the form of the equations from which the numerical scheme was developed are described in section 2.1.1.2.

The phasic continuity equations are

$$\frac{\partial}{\partial t} (\alpha_g \rho_g) + \frac{1}{A} \frac{\partial}{\partial x} (\alpha_g \rho_g v_g A) = \Gamma_g \quad 2.1.1-1$$

and

$$\frac{\partial}{\partial t} (\alpha_f \rho_f) + \frac{1}{A} \frac{\partial}{\partial x} (\alpha_f \rho_f v_f A) = -\Gamma_g \quad 2.1.1-2$$

Generally, the flow does not include mass sources or sinks and overall continuity consideration yields the requirement that the liquid generation term be the negative of the vapor generation; that is,

$$\Gamma_f = -\Gamma_g \quad 2.1.1-3$$

^aIn all the field equations shown herein, the correlation coefficients are assumed unity so the average of a product of variables is equal to the product of the averaged variables.

The interfacial mass transfer model assumes that total mass transfer consists of mass transfer in the bulk fluid (Γ_{ig}) and mass transfer at the wall (Γ_w); that is,

$$\Gamma_g = \Gamma_{ig} + \Gamma_w . \quad 2.1.1-4$$

The phasic conservation of momentum equations are used, and recorded here, in the so-called nonconservative form. For the vapor phase it is

$$\begin{aligned} \alpha_g \rho_g A \frac{\partial v_g}{\partial t} + \frac{1}{2} \alpha_g \rho_g A \frac{\partial v_g^2}{\partial x} &= - \alpha_g A \frac{\partial P}{\partial x} + \alpha_g \rho_g B_x A \\ - (\alpha_g \rho_g A) FWG(v_g) + \Gamma_g A (v_{gI} - v_g) - (\alpha_g \rho_g A) FIG(v_g - v_f) \\ - C \alpha_g \alpha_f \rho A \frac{\partial (v_g - v_f)}{\partial t} \end{aligned} \quad 2.1.1-5$$

and for the liquid phase it is,

$$\begin{aligned} \alpha_f \rho_f A \frac{\partial v_f}{\partial t} + \frac{1}{2} \alpha_f \rho_f A \frac{\partial v_f^2}{\partial x} &= - \alpha_f A \frac{\partial P}{\partial x} + \alpha_f \rho_f B_x A \\ - (\alpha_f \rho_f A) FWF(v_f) - \Gamma_g A (v_{fI} - v_f) - (\alpha_f \rho_f A) FIF(v_f - v_g) \\ - C \alpha_f \alpha_g \rho A \frac{\partial (v_f - v_g)}{\partial t} . \end{aligned} \quad 2.1.1-6$$

The force terms on the right sides of Equations 2.1.1-5 and 2.1.1-6 are, respectively: the pressure gradient, the body force, wall friction, momenta due to interphase mass transfer, interphase frictional drag, and force due to virtual mass. The terms FWG and FWF are part of the wall frictional drag, which is linear in velocity and are products of the friction coefficient, the frictional reference area per unit volume, and the magnitude of the fluid bulk velocity. The interfacial velocity in the

interphase momentum transfer term is the unit momentum with which phase appearance or disappearance occurs. The coefficients FIG and FIF are parts of the interphase frictional drag, which is linear in relative velocity, and are products of the interphase friction coefficients, the frictional reference area per unit volume, and the magnitude of interphase relative velocity.

The coefficient of virtual mass is the same as that used by Anderson¹³ in the RISQUE code, where the value for C depends on the flow regime. A value of C > 1/2 has been shown to be appropriate for bubbly or dispersed flows,^{14,15} while C = 0 may be appropriate for a separated or stratified flow.

The virtual mass term in Equations 2.1.1-5 and 2.1.1-6 is a simplification of the objective formulation^{16,17} used in RELAP5/MOD1. In particular, the spatial derivative portion of the term is deleted. The reason for this change is that inaccuracies in approximating spatial derivatives for the relatively coarse nodalizations used in system representations can lead to nonphysical characteristics in the numerical solution. The primary effect of the virtual mass terms is on the mixture sound speed, thus, the simplified form is adequate since critical flows are calculated in RELAP5 using an integral model¹⁸ in which the sound speed is based on an objective formulation for the added mass terms.

Conservation of interphase momentum requires that the force terms associated with interphase mass and momentum exchange sum to zero, and is shown as

$$\begin{aligned} \Gamma_g v_{gI} - (\alpha_g \rho_g) FIG(v_g - v_f) - C\alpha_g \alpha_f \rho [\partial(v_f - v_g)/\partial t] \\ + \Gamma_f v_{fI} - (\alpha_f \rho_f) FIF(v_f - v_g) - C\alpha_f \alpha_g \rho [\partial(v_f - v_g)/\partial t] = 0. \end{aligned}$$

2.1.1-7

This particular form for interphase momentum balance results from consideration of the momentum equations in conservative form. The force terms associated with virtual mass acceleration in Equation 2.1.1-7 sum to zero identically as a result of the particular form chosen. In addition, it is usually assumed (although not required by any basic conservation principle) that the interphase momentum transfer due to friction and due to mass transfer independently sum to zero, that is,

$$v_{gI} = v_{fI} = v_I \quad 2.1.1-8$$

and

$$\alpha_g \rho_g F_{IG} = \alpha_f \rho_f F_{IF} = \alpha_g \alpha_f \rho_g \rho_f F_{I}. \quad 2.1.1-9$$

These conditions are sufficient to ensure that Equation 2.1.1-7 is satisfied.

The phasic energy equations are

$$\begin{aligned} \frac{\partial}{\partial t}(\alpha_g \rho_g U_g) + \frac{1}{A} \frac{\partial}{\partial x} (\alpha_g \rho_g U_g v_g A) &= -P \frac{\partial \alpha_g}{\partial t} - \frac{P}{A} \frac{\partial}{\partial x} (\alpha_g v_g A) \\ + Q_{wg} + Q_{ig} + \Gamma_{ig} h_g^* + \Gamma_w h_g^S + DISS_g & \quad 2.1.1-10 \end{aligned}$$

and

$$\begin{aligned} \frac{\partial}{\partial t}(\alpha_f \rho_f U_f) + \frac{1}{A} \frac{\partial}{\partial x} (\alpha_f \rho_f U_f v_f A) &= -P \frac{\partial \alpha_f}{\partial t} - \frac{P}{A} \frac{\partial}{\partial x} (\alpha_f v_f A) \\ + Q_{wf} + Q_{if} - \Gamma_{ig} h_f^* - \Gamma_w h_f^S + DISS_f & \quad 2.1.1-11 \end{aligned}$$

In the phasic energy equations, Q_{wg} and Q_{wf} are the phasic wall heat transfer rates per unit volume. These phasic wall heat transfer rates satisfy the equation

$$Q = Q_{wg} + Q_{wf}, \quad 2.1.1-12$$

where Q is the total wall heat transfer rate to the fluid per unit volume.

The phasic enthalpies (h_g^* , h_f^*) associated with interphase mass transfer in Equations 2.1.1-10 and 2.1.1-11 are defined in such a way that the interface energy jump conditions at the liquid vapor are satisfied. In particular, the h_g^* and vapor interface h_f^s are chosen to be h_g and h_f , respectively for the case of vaporization and h_g and h_f^s , respectively for the case of condensation. The logic for this choice will be further explained in the development of the mass transfer model.

The phasic energy dissipation terms, $DISS_g$ and $DISS_f$, are the sums of wall friction and pump effects. The wall friction dissipations are defined as

$$DISS_g = \alpha_g \rho_g F_{WG} v_g^2 \quad 2.1.1-13$$

and

$$DISS_f = \alpha_f \rho_f F_{WF} v_f^2 \quad 2.1.1-14$$

The phasic energy dissipation terms satisfy the relation

$$\text{DISS} = \text{DISS}_g + \text{DISS}_f, \quad 2.1.1-15$$

where DISS is the energy dissipation. When a pump component is present the associated energy dissipation is also included in the dissipation terms (see section 2.1.5.2).

The vapor generation (or condensation) consists of two parts, that which results from bulk energy exchange (Γ_{ig}) and that due to wall heat transfer effects (Γ_w). Each of the vapor generation (or condensation) processes involves interface heat transfer effects. The interface heat transfer terms appearing in Equations 2.1.1-10 and 2.1.1-11 include heat transfer from the bulk states to the interface due to both interface energy exchange and wall heat transfer effects. The vapor generation (or condensation) rates are established from energy balance considerations at the interface.

The summation of Equations 2.1.1-10 and 2.1.1-11 produces the mixture energy equation, from which it is required that the interface transfer terms vanish, that is,

$$Q_{ig} + Q_{if} + \Gamma_{ig}(h_g^* - h_f^*) + \Gamma_w(h_g^s - h_f^s) = 0 \quad 2.1.1-16$$

The interphase heat transfer terms consist of two parts, that is,

$$Q_{ig} = H_{ig}(T^s - T_g) + Q_{ig}^w \quad 2.1.1-17$$

and

$$Q_{if} = H_{if}(T^s - T_f) + Q_{if}^w \quad 2.1.1-18$$

H_{ig} and H_{if} are the interphase heat transfer coefficients per unit volume and Q_{ig}^W and Q_{if}^W are the wall heat transfer terms. The first term on the right side of Equations 2.1.1-17 and 2.1.1-18 is the thermal energy exchange between the fluid bulk states and the fluid interface, while the second term is that due to wall heat transfer effects and will be defined in terms of the wall vapor generation (or condensation) process.

Although it is not a fundamental requirement, it is assumed that Equation 2.1.1-16 will be satisfied by requiring that the wall heat transfer terms and the bulk exchange terms each sum to zero independently. Thus,

$$H_{ig}(T^S - T_g) + H_{if}(T^S - T_f) + r_{ig}(h_g^* - h_f^*) = 0 \quad 2.1.1-19$$

and

$$Q_{ig}^W + Q_{if}^W + r_w(h_g^S - h_f^S) = 0 \quad 2.1.1-20$$

In addition, it is assumed that $Q_{ig}^W = 0$ for boiling processes where $r_w > 0$. Equation 2.1.1-20 can then be solved for the wall vaporization rate to give

$$r_w = \frac{-Q_{if}^W}{h_g^S - h_f^S}, \quad r_w > 0 \quad 2.1.1-21$$

Similarly, it is assumed that $Q_{if}^W = 0$ for condensation processes in which $\Gamma_w < 0$. Equation 2.1.1-20 can then be solved for the wall condensation rate to give

$$\Gamma_w = \frac{-Q_{ig}^W}{h_g^S - h_f^S}, \Gamma_w < 0 \quad 2.1.1-22$$

The interphase energy transfer terms Q_{ig} and Q_{if} can thus be expressed in a general way as

$$Q_{ig} = H_{ig}(T^S - T_g) - \left(\frac{1-\epsilon}{2}\right) \Gamma_w (h_g^S - h_f^S) \quad 2.1.1-23$$

and

$$Q_{if} = H_{if}(T^S - T_f) - \left(\frac{1+\epsilon}{2}\right) \Gamma_w (h_g^S - h_f^S), \quad 2.1.1-24$$

where $\epsilon = 1$ for $\Gamma_w > 0$ and $\epsilon = -1$ for $\Gamma_w < 0$. Finally, Equation 2.1.1-16 can be used to define the interphase vaporization (or condensation) rate

$$\Gamma_{ig} = - \frac{Q_{ig} + Q_{if}}{h_g^* - h_f^*} - \Gamma_w \frac{(h_g^S - h_f^S)}{h_g^* - h_f^*}, \quad 2.1.1-25$$

which, upon substitution of Equations 2.1.1-23 and 2.1.1-24, becomes

$$\Gamma_{ig} = - \frac{H_{ig}(T^S - T_g) + H_{if}(T^S - T_f)}{h_g^* - h_f^*} \quad 2.1.1-26$$

The phase change process that occurs at the interface is envisioned as a process in which bulk fluid is heated or cooled to the saturation temperature and phase change occurs at the saturation state. The interphase energy exchange process from each phase must be such that at least the sensible energy change to reach the saturation state occurs. Otherwise, it can be shown that the phase change process implies energy transfer from a lower temperature to a higher temperature. Such conditions can be avoided by the proper choice of the variables h_g^* and h_f^* . In particular, it can be shown that they should be

$$h_g^* = \frac{1}{2}[(h_g^s + h_g) + \eta(h_g^s - h_g)] \quad 2.1.1-27$$

and

$$h_f^* = \frac{1}{2}[(h_f^s + h_f) - \eta(h_f^s - h_f)] , \quad 2.1.1-28$$

where

$$\eta = \begin{cases} 1 & \text{for } \Gamma_{ig} \geq 0 \\ -1 & \text{for } \Gamma_{ig} < 0 \end{cases} \quad 2.1.1-29$$

$$2.1.1-30$$

Substituting Equation 2.1.1-26 into Equation 2.1.1-4 gives the final expression for the total interphase mass transfer as

$$\Gamma_g = - \frac{H_{ig}(T^s - T_g) + H_{if}(T^s - T_f)}{h_g^* - h_f^*} + \Gamma_w \quad 2.1.1-31$$

Noncondensibles in the Gas Phase

The basic, two-phase, single-component model just discussed can be extended to include a noncondensable component in the gas phase. The noncondensable component is assumed to be in mechanical and thermal equilibrium with the vapor phase, so that

$$v_n = v_g \quad 2.1.1-32$$

and

$$T_n = T_g, \quad 2.1.1-33$$

where the subscript, n , is used to designate the noncondensable component.

The general approach for inclusion of the noncondensable component consists of assuming that all properties of the gas phase (subscript g) are mixture properties of the steam/noncondensable mixture. The quality, X , is likewise defined as the mass fraction of the entire gas phase. Thus, the two basic continuity equations (Equations 2.1.1-1 and 2.1.1-2) are unchanged. However, it is necessary to add an additional mass conservation equation for the noncondensable component

$$\frac{\partial}{\partial t}(\alpha_g \rho_g X_n) + \frac{1}{A} \frac{\partial}{\partial x}(\alpha_g \rho_g X_n v_g A) = 0, \quad 2.1.1-34$$

where X_n is the mass fraction of the noncondensable component based on the gaseous phase mass.

The remaining field equations for energy and phasic momentum are unchanged, but the vapor field properties are now evaluated for the steam/noncondensable mixture. The modifications appropriate to the state relationships are described in section 2.1.2.

Boron Concentration in the Liquid Field

An Eulerian boron tracking model is used in RELAP5 which simulates the transport of a dissolved component in the liquid phase. The solution is assumed to be sufficiently dilute that the following assumptions are valid:

1. Liquid properties are not altered by the presence of the solute.
2. Solute is transported only in the liquid phase and at the velocity of the liquid phase.
3. Energy transported by the solute is negligible.
4. Inertia of the solute is negligible.
5. Solute is transported at the velocity of the vapor phase if no liquid is present.

Under these assumptions, only an additional field equation for the conservation of the solute is required. In differential form, the added equation is

$$\frac{\partial \rho_B}{\partial t} + \frac{1}{A} \frac{\partial (C_B \alpha_f \rho_f v_f A)}{\partial x} = 0, \quad 2.1.1-35$$

where the concentration parameter, C_B , is defined as

$$C_B = \frac{\rho_B}{\rho(1 - X)} \quad 2.1.1-36$$

C_B is the concentration of dissolved solid in mass units per mass unit of liquid phase.

2.1.1.2. Numerically Convenient Set of Differential Equations

A more convenient set of differential equations upon which to base the numerical scheme is obtained from the basic density and energy differential equations by expanding the time derivative in each equation using the product rule. When the product rule is used to evaluate the time derivative, we will refer to this form as the expanded form.

A sum density equation is obtained by expanding the time derivative in the phasic density equations, Equations 2.1.1-1 and 2.1.1-2, adding these two new equations, and using the relation

$$\frac{\partial \alpha_f}{\partial t} = - \frac{\partial \alpha_g}{\partial t} \quad 2.1.1-37$$

This gives

$$\alpha_g \frac{\partial \rho_g}{\partial t} + \alpha_f \frac{\partial \rho_f}{\partial t} + (\rho_g - \rho_f) \frac{\partial \alpha_g}{\partial t} + \frac{1}{A} \frac{\partial}{\partial x} (\alpha_g \rho_g v_g A + \alpha_f \rho_f v_f A) = 0 \quad 2.1.1-38$$

A difference density equation is obtained by expanding the time derivative in the phasic density equations, Equations 2.1.1-1 and 2.1.1-2, subtracting these two new equations, again using the relation

$$\frac{\partial \alpha_f}{\partial t} = - \frac{\partial \alpha_g}{\partial t} \quad 2.1.1-39$$

and substituting Equation 2.1.1-31 for Γ_g . This gives

$$\begin{aligned} & \alpha_g \frac{\partial \rho_g}{\partial t} - \alpha_f \frac{\partial \rho_f}{\partial t} + (\rho_g + \rho_f) \frac{\partial \alpha_g}{\partial t} + \frac{1}{A} \frac{\partial}{\partial x} (\alpha_g \rho_g v_g A - \alpha_f \rho_f v_f A) \\ & = - \frac{2[H_{ig}(T^S - T_g) + H_{if}(T^S - T_f)]}{h_g^* - h_f^*} + 2\Gamma_w \end{aligned} \quad 2.1.1-40$$

The time derivative of the noncondensable density equation, Equation 2.1.1-34, is expanded to give

$$\rho_g X_n \frac{\partial \alpha_g}{\partial t} + \alpha_g X_n \frac{\partial \rho_g}{\partial t} + \alpha_g \rho_g \frac{\partial X_n}{\partial t} + \frac{1}{A} \frac{\partial}{\partial x} (\alpha_g \rho_g X_n v_g A) = 0 \quad 2.1.1-41$$

The momentum equations are also rearranged into a sum and difference form. The sum momentum equation is obtained by direct summation of Equations 2.1.1-5 and 2.1.1-6 with the interface conditions (Equations 2.1.1-7, 2.1.1-8, and 2.1.1-9) substituted where appropriate, and the cross-sectional area canceled throughout. The resulting sum equation is

$$\begin{aligned} & \alpha_g \rho_g \frac{\partial v_g}{\partial t} + \alpha_f \rho_f \frac{\partial v_f}{\partial t} + \frac{1}{2} \alpha_g \rho_g + \frac{\partial v_g^2}{\partial x} + \frac{1}{2} \alpha_f \rho_f \frac{\partial v_f^2}{\partial x} \\ & = - \frac{\partial P}{\partial x} + \rho B_x - \alpha_g \rho_g v_g^{FWG} - \alpha_f \rho_f v_f^{FWF} - \Gamma_g (v_g - v_f) \end{aligned} \quad 2.1.1-42$$

The difference of the phasic momentum equations is obtained by first dividing the vapor and liquid phasic momentum equations by $\alpha_g \rho_g$ and $\alpha_f \rho_f$, respectively, and subsequently subtracting. Here

again, the interface conditions are used and the common area is divided out. The resulting equation is

$$\begin{aligned} \frac{\partial v_g}{\partial t} - \frac{\partial v_f}{\partial t} + \frac{1}{2} \frac{\partial v_g^2}{\partial x} - \frac{1}{2} \frac{\partial v_f^2}{\partial x} = - \left(\frac{1}{\rho_g} - \frac{1}{\rho_f} \right) \frac{\partial P}{\partial x} \\ - v_g^{FWG} + v_f^{FWF} + \Gamma_g [\rho v_I - (\alpha_f \rho_f v_g + \alpha_g \rho_g v_f)] / \\ (\alpha_g \rho_g \alpha_f \rho_f) - \rho F I (v_g - v_f) - C [\rho^2 / (\rho_g \rho_f)] \\ \cdot \frac{\partial (v_g - v_f)}{\partial t} , \end{aligned} \quad 2.1.1-43$$

where the interfacial velocity, v_I , is defined as

$$v_I = \lambda v_g + (1 - \lambda) v_f . \quad 2.1.1-44$$

This definition for v_I has the property that if $\lambda = 1/2$, the interphase momentum transfer process associated with mass transfer is reversible. This value leads to either an entropy sink or source, depending on the sign of Γ_g . However if λ is chosen to be 0 for positive values of Γ_g and +1 for negative values of Γ_g (that is, a donor formulation), the mass exchange process is always dissipative. The latter model for v_I is the most realistic for the momentum exchange process and is used for the numerical scheme development.

To develop an expanded form of the vapor energy Equation 2.1.1-10 the time derivative of the vapor energy equation, Equation 2.1.1-10, is expanded, the Q_{ig} Equation 2.1.1-23 and the Γ_{ig} Equation 2.1.1-26 are substituted, and the H_{ig} , H_{if} , $\delta \alpha_g / \delta t$,

and convective terms are collected. This gives the desired form for the vapor energy equation

$$\begin{aligned}
 & (\rho_g U_g + P) \frac{\partial \alpha_g}{\partial t} + \alpha_g U_g \frac{\partial \rho_g}{\partial t} + \alpha_g \rho_g \frac{\partial U_g}{\partial t} + \frac{1}{A} \left[\frac{\partial}{\partial x} (\alpha_g \rho_g U_g v_g A) \right. \\
 & \left. + P \frac{\partial}{\partial x} (\alpha_g v_g A) \right] = - \left[\frac{h_f^*}{h_g^* - h_f^*} \right] H_{ig} (T^S - T_g) \\
 & - \left[\frac{h_g^*}{h_g^* - h_f^*} \right] H_{if} (T^S - T_f) + \left[\left(\frac{1+\epsilon}{2} \right) h_g^S \right. \\
 & \left. + \left(\frac{1-\epsilon}{2} \right) h_f^S \right] \Gamma_w + Q_{wg} + DISS_g .
 \end{aligned} \tag{2.1.1-45}$$

To develop an expanded form of the liquid energy Equation 2.1.1-11 the time derivative is expanded, the Q_{if} Equation 2.1.1-24 and the Γ_{ig} Equation 2.1.1-26 are substituted, and

$$\frac{\partial \alpha_f}{\partial t} = - \frac{\partial \alpha_g}{\partial t} \tag{2.1.1-46}$$

is used, then the H_{ig} , H_{if} , $\delta \alpha_g / \delta t$, and convective terms are collected. This gives the desired form for the liquid energy equation

$$\begin{aligned}
 & - (\rho_f U_f + P) \frac{\partial \alpha_g}{\partial t} + \alpha_f U_f \frac{\partial \rho_f}{\partial t} + \alpha_f \rho_f \frac{\partial U_f}{\partial t} \\
 & + \frac{1}{A} \left[\frac{\partial}{\partial x} (\alpha_f \rho_f U_f v_f A) + P \frac{\partial}{\partial x} (\alpha_f v_f A) \right] \\
 & = \left[\frac{h_f^*}{h_g^* - h_f^*} \right] H_{ig} (T^S - T_g) + \left[\frac{h_g^*}{h_g^* - h_f^*} \right] H_{if} (T^S - T_f) \\
 & - \left[\left(\frac{1+\epsilon}{2} \right) h_g^S + \left(\frac{1-\epsilon}{2} \right) h_f^S \right] \Gamma_w + Q_{wf} + DISS_f .
 \end{aligned} \tag{2.1.1-47}$$

The basic density and energy differential equations are used in nonexpanded form in the back substitution part of the numerical scheme. When the product rule is not used to evaluate the time derivative, we will refer to this form as the nonexpanded form.

The vapor, liquid, and noncondensable density equations, Equations 2.1.1-1, 2.1.1-2, and 2.1.1-34, are in nonexpanded form. The Γ_g , from Equation 2.1.1-31, is not substituted into the vapor and liquid density equations (the reason is apparent in the Time Step Solution Scheme, see section 3.1.1.6 of NUREG/CR-4312¹). The vapor energy equation, Equation 2.1.1-10, is altered by substituting Equation 2.1.1-23 for Q_{ig} , substituting Equation 2.1.1-26 for Γ_{ig} and collecting the H_{ig} , H_{if} , and convective terms. This gives

$$\begin{aligned} & \frac{\partial}{\partial t}(\alpha_g \rho_g U_g) + \frac{1}{A} \left[\frac{\partial}{\partial x}(\alpha_g \rho_g U_g v_g A) + P \frac{\partial}{\partial x}(\alpha_g v_g A) \right] \\ & = -P \frac{\partial \alpha_g}{\partial t} - \left[\frac{h_f^*}{h_g^* - h_f^*} \right] H_{ig} (T^S - T_g) - \left[\frac{h_g^*}{h_g^* - h_f^*} \right] H_{if} (T^S - T_f) \\ & + \left[\left(\frac{1+\epsilon}{2} \right) h_g^S + \left(\frac{1-\epsilon}{2} \right) h_f^S \right] \Gamma_w + Q_{wg} + DISS_g . \end{aligned} \quad 2.1.1-48$$

The liquid energy equation, Equation 2.1.1-11, is also altered by substituting Equation 2.1.1-24 for Q_{if} , substituting Equation 2.1.1-26 for Γ_{ig} , using

$$\frac{\partial \alpha_f}{\partial t} = - \frac{\partial \alpha_g}{\partial t} , \quad 2.1.1-49$$

and collecting the H_{ig} , H_{if} , and convective terms. This gives

$$\begin{aligned} & \frac{\partial}{\partial t}(\alpha_f \rho_f U_f) + \frac{1}{A} \left[\frac{\partial}{\partial x}(\alpha_f \rho_f U_f v_f A) + P \frac{\partial}{\partial x}(\alpha_f v_f A) \right] \\ &= P \frac{\partial \alpha_g}{\partial t} + \left[\frac{h_f^*}{h_g^* - h_f^*} \right] H_{ig}(T^S - T_g) + \left[\frac{h_g^*}{h_g^* - h_f^*} \right] H_{if}(T^S - T_f) \\ &- \left[\left(\frac{1+\epsilon}{2} \right) h_g^S + \left(\frac{1-\epsilon}{2} \right) h_f^S \right] \Gamma_w + Q_{wf} + DISS_f . \end{aligned} \quad 2.1.1-50$$

2.1.1.3. Horizontal Stratified Flow

Flow at low velocity in a horizontal passage can be stratified as a result of buoyancy forces caused by density differences between vapor and liquid. When the flow is stratified, the area average pressures are affected by nonuniform transverse distribution of the phases. Appropriate modifications to the basic field equations when stratified flow exists are obtained by considering separate area average pressures for the vapor and liquid phases, and the interfacial pressure between them. Using this model, the pressure gradient force terms of Equations 2.1.1-5 and 2.1.1-6 become

$$- \alpha_g A \left[\frac{\partial P}{\partial x} \right] + - \alpha_g A \left[\frac{\partial P_g}{\partial x} \right] + (P_I - P_g) A \left[\frac{\partial \alpha_g}{\partial x} \right] \quad 2.1.1-51$$

and

$$- \alpha_f A \left[\frac{\partial P}{\partial x} \right] + - \alpha_f A \left[\frac{\partial P_f}{\partial x} \right] + (P_I - P_f) A \left[\frac{\partial \alpha_f}{\partial x} \right] . \quad 2.1.1-52$$

The area average pressure for the entire cross section of the flow is expressed in terms of the phasic area average pressures by

$$P = \alpha_g P_g + \alpha_f P_f \quad . \quad 2.1.1-53$$

With these definitions, the sum of the phasic momentum equations, written in terms of the cross section average pressure (Equation 2.1.1-42) remains unchanged. However, the difference of the phasic momentum equations (Equation 2.1.1-43), contains on the right side the following additional terms

$$[\rho / (\alpha_g \alpha_f \rho_g \rho_f)] [-\alpha_f \partial (\alpha_g P_g) / \partial x + \alpha_g \partial (\alpha_f P_f) / \partial x + P_I (\partial \alpha_g / \partial x)] \quad . \quad 2.1.1-54$$

The interface and phasic cross-sectional average pressures, P_I , P_g , and P_f , can be found by means of the assumption of a transverse hydrostatic pressure in a round pipe. For a pipe having diameter D , pressures P_I , P_g , and P_f are given by

$$P_g = P_I - \rho_g B_Y D [\sin^3 \theta / (3\pi \alpha_g) - \cos \theta / 2] \quad . \quad 2.1.1-55$$

and

$$P_f = P_I + \rho_f B_Y D [\sin^3 \theta / (3\pi \alpha_f) + \cos \theta / 2] \quad . \quad 2.1.1-56$$

The angle, θ , is defined by the void fraction as illustrated in Figure 2.1.1-1. The algebraic relationship between α_g and θ is

$$\alpha_g \pi = (\theta - \sin \theta \cos \theta) \quad . \quad 2.1.1-57$$

The additional term in the momentum difference equation (Equation 2.1.1-54) can be simplified using Equations 2.1.1-55, 2.1.1-56, and 2.1.1-57 to obtain

$$- [\rho / (\rho_g \rho_f)] (\rho_f - \rho_g) \pi D B_y / (4 \sin \theta) (\partial \alpha_g / \partial x) \quad 2.1.1-58$$

where θ is related to the void fraction using Equation 2.1.1-57.

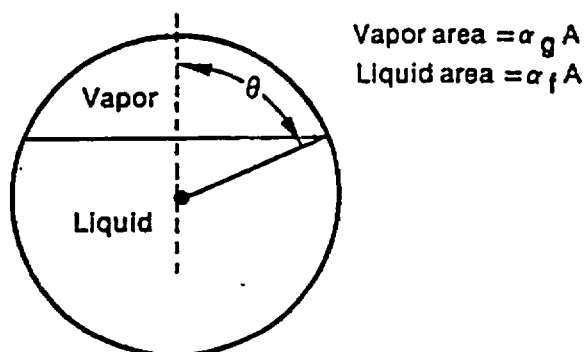


Figure 2.1.1-1. Relation of Central Angle θ to Void Fraction α_g .

The additional force term that arises for a stratified flow geometry in horizontal pipes is added to the basic equation when the flow is established to be stratified from flow regime considerations.

2.1.1.4. Semi-Implicit Scheme Difference Equations

The semi-implicit numerical solution scheme is based on replacing the system of differential equations with a system of finite-difference equations partially implicit in time. The terms evaluated implicitly are identified as the scheme is developed. In all cases, the implicit terms are formulated to be

linear in the dependent variables at new time. This results in a linear time-advancement matrix that is solved by direct inversion using a sparse matrix routine.¹⁹ An additional feature of the scheme is that implicitness is selected such that the field equations can be reduced to a single difference equation per fluid control volume or mesh cell, which is in terms of the hydrodynamic pressure. Thus, only an $N \times N$ system of the difference equations must be solved simultaneously at each time step (N is the total number of control volumes used to simulate the fluid system).

A well-posed numerical problem is obtained by several means. These include the selective implicit evaluation of spatial gradient terms at the new time, donor formulations for the mass and energy flux terms, and use of a donor-like formulation for the momentum flux terms. The term, donor-like, is used because the momentum flux formulation consists of a centered formulation for the spatial velocity gradient plus a numerical viscosity term similar to the form obtained when the momentum flux terms are donored with the conservative form of the momentum equations.

The difference equations are based on the concept of a control volume (or mesh cell) in which mass and energy are conserved by equating accumulation to rate of influx through the cell boundaries. This model results in defining mass and energy volume average properties and requiring knowledge of velocities at the volume boundaries. The velocities at boundaries are most conveniently defined through use of momentum control volumes (cells) centered on the mass and energy cell boundaries. This approach results in a numerical scheme having a staggered spatial mesh. The scalar properties (pressure, energies, and void fraction) of the flow are defined at cell centers, and vector quantities (velocities) are defined on the cell boundaries. The resulting one-dimensional spatial noding is illustrated in Figure

2.1.1-2. The term, cell, means an increment in the spatial variable, x , corresponding to the mass and energy control volume. The difference equations for each cell are obtained by integrating the mass and energy equations (Equations 2.1.1-38, 2.1.1-40, 2.1.1-41, 2.1.1-45, and 2.1.1-47) with respect to the spatial variable, x , from the junction at x_j to x_{j+1} . The momentum equations (Equations 2.1.1-42 and 2.1.1-43) are integrated with respect to the spatial variable from cell center to adjoining cell center (x_K to x_L , Figure 2.1.1-2). The equations are listed for the case of a pipe with no branching.

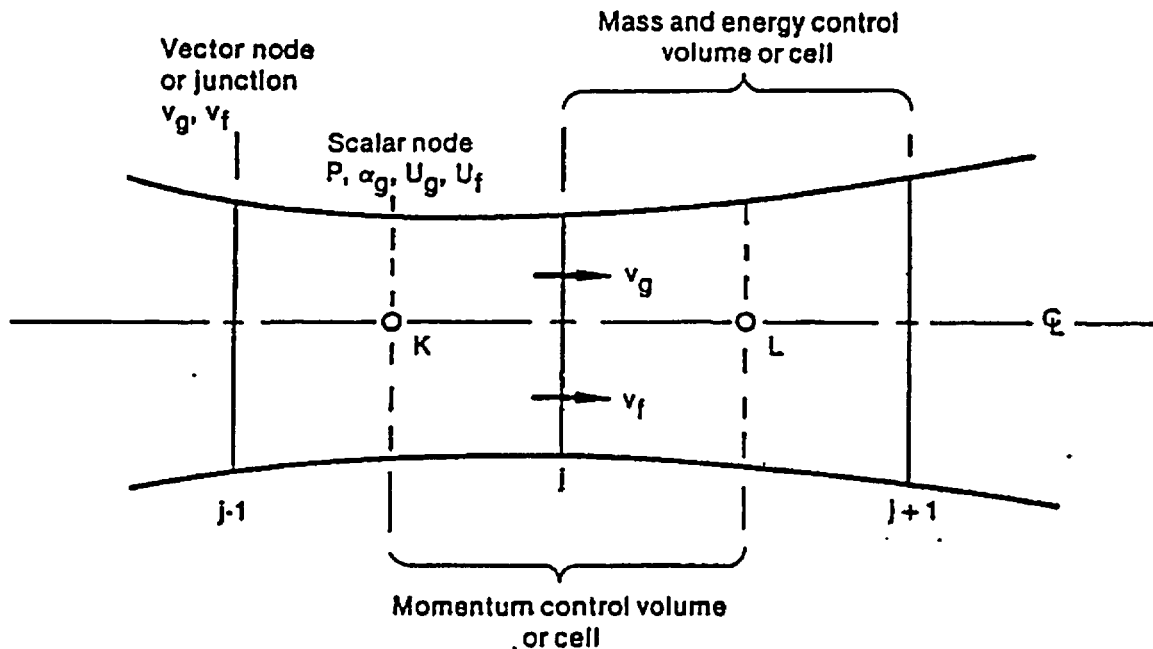


Figure 2.1.1-2. Difference Equation Nodalization Schematic.

When the mass and energy equations (Equations 2.1.1-38, 2.1.1-40, 2.1.1-41, 2.1.1-45, and 2.1.1-47) are integrated with respect to the spatial variable from junction j to $j+1$, differential equations in terms of cell-average properties and cell boundary fluxes are obtained. The development and form of

these finite-difference equations is described in detail in NUREG/CR-4312¹, section 3.1.1.4. The advancement techniques are also given in NUREG/CR-4312, section 3.1.1.6.

2.1.1.5. Volume-Average Velocities

Volume-average velocities are required for the momentum flux calculation, evaluation of the frictional forces and the Courant time step limit. In a simple constant area passage, the arithmetic-average between the inlet and outlet is a satisfactory approximation. However, at branch volumes with multiple inlets and/or outlets, or for volumes with abrupt area change, use of the arithmetic average results in nonphysical behavior.

The RELAP5 volume-average velocity formulas have the form

$$\begin{aligned}
 (v_f)_L^n &= \frac{\left[\sum_j (\alpha_f \rho_f v_f)_j^n A_j \cdot \sum_j A_j \right] \text{ inlets}}{\left[\sum_j (\alpha_f \rho_f)_j^n A_j \cdot A_L \right] \text{ inlets and outlets}} \\
 &+ \frac{\left[\sum_j (\alpha_f \rho_f v_f)_j^n A_j \cdot \sum_j A_j \right] \text{ outlets}}{\left[\sum_j (\alpha_f \rho_f)_j^n A_j \cdot A_L \right] \text{ inlets and outlets}}
 \end{aligned}
 \tag{2.1.1-59}$$

and

$$\begin{aligned}
 (v_g)_L^n &= \frac{\left[\sum_j (\alpha_g \rho_g v_g)_j^n A_j \cdot \sum_j A_j \right] \text{ inlets}}{\left[\sum_j (\alpha_g \rho_g)_j^n A_j \cdot A_L \right] \text{ inlets and outlets}} \\
 &+ \frac{\left[\sum_j (\alpha_g \rho_g v_g)_j^n A_j \cdot \sum_j A_j \right] \text{ outlets}}{\left[\sum_j (\alpha_g \rho_g)_j^n A_j \cdot A_L \right] \text{ inlets and outlets}}
 \end{aligned}
 \tag{2.1.1-60}$$

2.1.1.6. Nearly-Implicit Scheme Difference Equations and Time Advancement

For problems where the flow is expected to change very slowly with time, it is possible to obtain adequate information from an approximate solution based on very large time steps. This would be advantageous if a reliable and efficient means could be found for solving difference equations treating all terms--phase exchanges, pressure propagation, and convection--by implicit differences. Unfortunately, the state-of-the-art is less satisfactory here than in the case of semi-implicit (convection-explicit) schemes. A fully-implicit scheme for the six equation model of a 100 cell problem would require the solution of 600 coupled algebraic equations. If these equations were linearized for a straight pipe, inversion of a block tri-diagonal 600 x 600 matrix with 6 x 6 blocks would be required. This would yield a matrix of bandwidth 23 containing 13,800 nonzero elements, resulting in an extremely costly time advancement scheme.

To reduce the number of calculations required for solving fully implicit difference schemes, fractional step (sometimes called multiple step) methods have been tried. The equations can be split into fractional steps based upon physical phenomena. This is the basic idea in the nearly-implicit scheme. Fractional step methods for two-phase flow problems have been developed in References 24 and 25. These earlier efforts have been used to guide the development of the nearly-implicit scheme. The fractional step method described here differs significantly from prior efforts in the reduced number of steps used to evaluate the momentum equations.

The nearly-implicit scheme consists of a first step that solves all seven conservation equations treating all interphase exchange processes, the pressure propagation process, and the momentum convection process implicitly. These finite difference equations

are exactly the expanded ones solved in the semi-implicit scheme with one major change. The convective terms in the momentum equations are evaluated implicitly (in a linearized form) instead of in an explicit donored fashion as is done in the semi-implicit scheme. Development of this technique is given in NUREG-4312, Reference 1, section 3.1.1.7.

2.1.2. State Relationships

The six equation model with an additional equation for the noncondensable gas component has five independent state variables. The independent variables are chosen to be P , α_g , U_g , U_f , and X_n . All the remaining thermodynamic variables (temperatures, densities, partial pressures, qualities, etc.) are expressed as functions of these five independent properties. In addition to these properties several state derivatives are needed because of the linearization used in the numerical scheme. This section contains three parts. The first discusses the state property derivatives needed in the numerical scheme. The second section develops the appropriate derivative formulas for the single component case and the third section does the same for the two-phase, two-component case.

The values of thermodynamic state variables are stored in tabular form within a controlled environmental library which is attached by the code. The environmental library was received from EG&G with the base RELAP5 code version.

2.1.2.1. State Equations

To expand the time derivatives of the phasic densities in terms of these dependent variables using two-term Taylor series expansions, the following derivatives of the phasic densities are needed:

$$\left(\frac{\partial \rho_g}{\partial P}\right)_{U_g, X_n}, \quad \left(\frac{\partial \rho_g}{\partial U_g}\right)_{P, X_n}, \quad \left(\frac{\partial \rho_g}{\partial X_n}\right)_{P, U_g}, \quad \left(\frac{\partial \rho_f}{\partial P}\right)_{U_f}, \quad \text{and} \quad \left(\frac{\partial \rho_f}{\partial U_f}\right)_P.$$

The interphase mass and heat transfer requires an implicit (linearized) evaluation of the interphase temperature potentials

$T_f - T_I$ and $T_g - T_I$. T_I is the temperature that exists at the phase interface. For a single component mixture,

$$T_I = T^S(P) , \quad 2.1.2-1$$

where the superscript s denotes a saturation value. In the presence of a noncondensable mixed with the steam,

$$T_I = T^S(P_s) , \quad 2.1.2-2$$

where P_s is the partial pressure of the steam in the gaseous phase. The gaseous phase properties for a two-component mixture can be described with three independent properties. In particular, the steam partial pressure, P_s , can be expressed as

$$P_s = P_s(P, X_n, U_g) . \quad 2.1.2-3$$

Substituting Equation 2.1.2-3 into Equation 2.1.2-2 gives the interface temperature, T_I , as the desired function of P , X_n , and U_g .^a The implicit evaluation of the temperature potential in the numerical scheme requires the following derivatives of the phasic and interface temperatures, such as

$$\left(\frac{\partial T_g}{\partial P} \right)_{U_g, X_n} , \quad \left(\frac{\partial T_g}{\partial U_g} \right)_{P, X_n} , \quad \left(\frac{\partial T_g}{\partial X_n} \right)_{P, U_g} ,$$

$$\left(\frac{\partial T_f}{\partial P} \right)_{U_f} , \quad \left(\frac{\partial T_f}{\partial U_f} \right)_P , \quad \left(\frac{\partial T^S}{\partial P} \right)_{U_g, X_n} , \quad \left(\frac{\partial T^S}{\partial U_g} \right)_{P, X_n} , \text{ and } \left(\frac{\partial T^S}{\partial X_n} \right)_{P, U_g} .$$

^a ρ_g and T_g could have initially been written with P_s , X_n , U_f as the independent arguments. Equation 2.1.2-3 would then be used to write ρ_g and T_g with P , X_n , and U_g as the independent variables.

For a single component mixture the X_N derivatives are zero and

$$\left(\frac{\partial T^S}{\partial U_g}\right)_P = 0 ; \quad 2.1.2-4$$

since T^S is only a function of P for this case.

In addition to these derivatives, the basic phasic properties as functions of P , α_g , U_g , U_f , and X_N are needed along with the homogeneous equilibrium sound speed for the critical flow model.

The basic properties are obtained from steam tables that tabulate for each phase the phasic properties and three phasic derivatives: the isobaric thermal expansion coefficient (β), the isothermal compressibility (κ), and the specific heat at constant pressure (C_p).

2.1.2.2. Single Component Two-Phase Mixture

For the purposes of this discussion, a single component two-phase mixture will be referred to as Case 1. Case 1 is straight forward. Liquid properties are obtained from the steam tables given P and U_f . All the desired density and temperature derivatives can then be obtained from κ_f , β_f , and C_{pf} . The desired derivatives are given as

$$\left(\frac{\partial \rho_f}{\partial U_f}\right)_P = - \left[\frac{V_f \beta_f}{C_{pf} - V_f \beta_f P} \right] / V_f^2 , \quad 2.1.2-5$$

$$\left(\frac{\partial T_f}{\partial U_f}\right)_P = \frac{1}{C_{pf} - V_f \beta_f P} , \quad 2.1.2-6$$

$$\left(\frac{\partial \rho_f}{\partial P}\right)_{U_f} = \left[\frac{C_{pf} V_f \kappa_f - T_f (V_f \beta_f)^2}{C_{pf} - V_f \beta_f P} \right] / V_f^2, \text{ and} \quad 2.1.2-7$$

$$\left(\frac{\partial T_f}{\partial P}\right)_{U_f} = - \left[\frac{P V_f \kappa_f - T V_f \beta_f}{C_{pf} - V_f \beta_f P} \right]. \quad 2.1.2-8$$

Parallel formulas hold for the vapor phase with P and U_g as the independent variables.

The only nonstandard feature involved in the evaluation of the formulas in Equation 2.1.2-8 is the calculation of V , T , κ , β , and C_p if the steam is subcooled or the liquid is superheated, that is, metastable states. The extrapolation used for these cases is a constant pressure extrapolation from the saturation state for the temperature and specific volume. Using the first two terms of a Taylor series gives

$$T = T(P) + \frac{1}{C_p(P) - P V(P) \beta(P)} [U - U(P)] \quad 2.1.2-9$$

and

$$V = V(P) + V(P) \beta(P) [T - T(P)] \quad 2.1.2-10$$

In Equations 2.1.2-9 and 2.1.2-10 the argument P indicates a saturation value.

To obtain the β , κ , and C_p corresponding to the extrapolated V and T , the extrapolation formulas are differentiated. Taking the appropriate derivatives of Equations 2.1.2-9 and 2.1.2-10 gives

$$C_p(P, T) \triangleq \left(\frac{\partial h}{\partial T}\right)_P = \left(\frac{\partial U}{\partial T}\right)_P + P \left(\frac{\partial V}{\partial T}\right)_P = C_p(P), \quad 2.1.2-11$$

$$\beta(P, T) \triangleq \frac{1}{V} \left(\frac{\partial V}{\partial T}\right)_P = \frac{V(P) \beta(P)}{V(P, T)}, \text{ and} \quad 2.1.2-12$$

$$\kappa(P, T) \triangleq = - \frac{1}{V} \left(\frac{\partial V}{\partial P} \right)_T = \{ V(P) + [T - T(P)] V(P) \beta(P) \} \frac{\kappa(P)}{V(P, T)} \\ - [T - T(P)] V(P) \left[\frac{d\beta(P)}{dP} + \beta^2(P) \frac{dT}{dP}(P) \right] / V(P, T).$$

2.1.2-13

Equation 2.1.2-11 shows that a consistently extrapolated C_p is just the saturation value $C_p(P)$. Equation 2.1.2-12 gives the extrapolated β as a function of the saturation properties and the extrapolated V . Equation 2.1.2-13 gives the consistently extrapolated κ as a function of the extrapolated and saturation properties. The extrapolated κ in Equation 2.1.2-13 involves a change of saturation properties along the saturation line. In particular, $\frac{d\beta}{dP}(P)$ involves a second derivative of specific volume. Since no second-order derivatives are available from the steam property tables, this term was approximated for the vapor phase by assuming the fluid behaves as an ideal gas. With this assumption the appropriate formula for the vapor phase κ is

$$\kappa_g(P, T) = \{ V_g(P) + [T_g - T(P)] V_g(P) \beta_g(P) \} \kappa_g(P) / V_g(P, T).$$

2.1.2-14

For the liquid phase extrapolation (superheated liquid) only the specific volume correction factor in Equation 2.1.2-13 was retained, that is,

$$\kappa_f(P, T) = \frac{V_f(P) \kappa_f(P)}{V_f(P, T)}.$$

2.1.2-15

The homogeneous equilibrium sound speed is calculated from standard formulas using the saturation κ 's, β 's, and C_p 's. The sound speed formula

$$a^2 = v^2 \left(\frac{dp^s}{dT} \right)^2 \left\{ x \left[\frac{C_{pg}}{T_g} + v_g \frac{dp^s}{dT} \left(\kappa_g \frac{dp^s}{dT} - 2\beta_g \right) \right] + (1-x) \left[\frac{C_{pf}}{T_f} + v_f \frac{dp^s}{dT} \left(\kappa_f \frac{dp^s}{dT} - 2\beta_f \right) \right] \right\} \quad 2.1.2-16$$

is used, where from the Clapeyron equation

$$\frac{dp^s}{dT} = \frac{h_g^s - h_f^s}{T^s (v_g^s - v_f^s)} \quad , \quad 2.1.2-17$$

and X is the steam quality based on the mixture mass.

2.1.2.3. Two Component, Two-Phase Mixture

This case is referred to as Case 2. The liquid phasic properties and derivatives are calculated in exactly the same manner as described in Case 1 (see section 2.1.2.2), assuming the noncondensable component is present only in the gaseous phase.

The properties for the gaseous phase are calculated assuming a Gibbs-Dalton mixture of steam and an ideal noncondensable gas. A Gibbs-Dalton mixture is based upon the following assumptions:

1. $P = P_n + P_s \quad , \quad 2.1.2-18$

2. $U_g = X_n U_n + (1 - X_n) U_s \quad , \quad \text{and} \quad 2.1.2-19$

$$3. \quad X_n V_n = (1 - X_n) V_s = V_g, \quad 2.1.2-20$$

where P_s and P_n are the partial pressures of the steam and noncondensable components, respectively. The internal energies U_s , U_n , and the specific volumes V_s , V_n are evaluated at the gas temperature and the respective partial pressures. The vapor properties are obtained from the steam tables and the noncondensable state equations are^a

$$P_n V_n = R_n T_g \quad \text{and} \quad 2.1.2-21$$

$$U_n = \begin{cases} C_o T_g + U_o & T_g < T_o \\ C_o T_g + \frac{1}{2} D_o (T_g - T_o)^2 + U_o & T_g \geq T_o \end{cases} \quad 2.1.2-22$$

Given P , U_g , and X_n , Equations 2.1.2-18 through 2.1.2-20 are solved implicitly to find the state of the gaseous phase. If Equation 2.1.2-18 is used to eliminate P_n and Equation 2.1.2-21 is used for V_n , Equations 2.1.2-19 and 2.1.2-20 can be written as

$$(1 - X_n) U_s + X_n U_n \left[T_g(U_s, P_s) \right] - U_g = 0 \quad 2.1.2-23$$

and

$$(1 - X_n) \left[\frac{V_s(U_s, P_s) P_s}{T_g(U_s, P_s)} \right] (P - P_s) - X_n R_n P_s = 0. \quad 2.1.2-24$$

Given P , U_g , and X_n , Equations 2.1.2-23 and 2.1.2-24 implicitly determine U_s and P_s . (Equation 2.1.2-20 was divided by the temperature and multiplied by the partial pressures to obtain Equation 2.1.2-24.)

^aThe code input permits selection of any one of six noncondensable gases. The constants used to represent air are in SI units: $T_o = 250.0$ K, $C_o = 715.0$ J/(kg/K), $U_o = 158990.52$ J/kg, $D_o = 0.10329$ J/(kg K²), and $R_n = 287.066$ N m/(kg K).

To obtain the derivatives needed in the numerical scheme, the derivatives of U_s and P_s are taken with respect to P , U_g , and X_n . These derivatives can be obtained from Equations 2.1.2-23 and 2.1.2-24 by the use of the chain rule and implicit differentiation. For example, taking the derivative of Equations 2.1.2-23 and 2.1.2-24 with respect to P [recall that $P_s = P_s(P, U_g, X_n)$ and $U_s = U_s(P, U_g, X_n)$] yields

$$\begin{bmatrix} X_n \left[\frac{dU_n}{dT_g} \right] \left[\frac{\partial T_g}{\partial P_s} \right] & 1 - X_n + X_n \left[\frac{\delta U_n}{dT_g} \right] \left[\frac{\partial T_g}{\partial U_s} \right] \\ -X_n R_n - (1 - X_n) R_s & 0 + \text{TERM2} \\ + R_s + \text{TERM1} & \end{bmatrix} \times \begin{bmatrix} \left[\frac{\partial P_s}{\partial P} \right]_{U_g, X_n} \\ \left[\frac{\partial U_s}{\partial P} \right]_{U_g, X_n} \end{bmatrix} = \begin{bmatrix} 0 \\ (1 - X_n) R_s \end{bmatrix} \quad 2.1.2-25$$

as a linear system of two equations determining

$$\left[\frac{\partial P_s}{\partial P} \right]_{U_g, X_n} \quad \text{and} \quad \left[\frac{\partial U_s}{\partial P} \right]_{U_g, X_n}$$

In Equation 2.1.2-25

$$R_s = \frac{P_s V_s}{T_g} \quad 2.1.2-26$$

is the equivalent gas constant for the steam vapor,

$$\text{TERM1} = (1 - X_n) P_n R_s \left[\frac{1}{P_s} + \frac{1}{V_s} \left[\frac{\partial V_s}{\partial P_s} \right]_{U_s} - \frac{1}{T_g} \left[\frac{\partial T_g}{\partial P_s} \right]_{U_s} \right] \quad 2.1.2-27$$

and

$$\text{TERM2} = (1 - X_n) P_n R_s \left[\frac{1}{V_s} \left(\frac{\partial V_s}{\partial U_s} \right)_{P_s} - \frac{1}{T_g} \left(\frac{\partial T_g}{\partial U_s} \right)_{P_s} \right] \quad 2.1.2-28$$

The TERM factors have been singled out as they are treated in a special manner in the numerical scheme. To obtain the derivatives P_s and U_s with respect to U_g and X_n the above development is repeated, taking derivatives of Equations 2.1.2-23 and 2.1.2-24 with respect to U_g and X_n . In each case, linear equations parallel to those in Equation 2.1.2-25 are obtained. In fact, the left side matrix is exactly the same, only the right side vector changes.

Having obtained all the derivatives of P_s and U_s , it is relatively easy to obtain the derivatives needed for the gaseous phase. From the chain rule,

$$\left(\frac{\partial T_g}{\partial P} \right)_{U_g, X_n} = \left(\frac{\partial T_g}{\partial P_s} \right)_{U_s} \left(\frac{\partial P_s}{\partial P} \right)_{U_g, X_n} + \left(\frac{\partial T_g}{\partial U_s} \right)_{P_s} \left(\frac{\partial U_s}{\partial P} \right)_{U_g, X_n} \quad 2.1.2-29$$

$$\left(\frac{\partial T_g}{\partial U_g} \right)_{P, X_n} = \left(\frac{\partial T_g}{\partial P_s} \right)_{U_s} \left(\frac{\partial P_s}{\partial U_g} \right)_{P_g, X_n} + \left(\frac{\partial T_g}{\partial U_s} \right)_{P_s} \left(\frac{\partial U_s}{\partial U_g} \right)_{P, X_n} \quad \text{, and} \quad 2.1.2-30$$

$$\left(\frac{\partial T_g}{\partial X_n} \right)_{P, U_g} = \left(\frac{\partial T_g}{\partial P_s} \right)_{U_s} \left(\frac{\partial P_s}{\partial X_n} \right)_{P, U_g} + \left(\frac{\partial T_g}{\partial U_s} \right)_{P_s} \left(\frac{\partial U_s}{\partial X_n} \right)_{P, U_g} \quad 2.1.2-31$$

where

$$\left(\frac{\partial T_g}{\partial P_s}\right)_{U_s} \quad \text{and} \quad \left(\frac{\partial T_g}{\partial U_s}\right)_{P_s}$$

are the standard phasic derivatives for the vapor phase. Equations 2.1.2-29 through 2.1.2-31 give all the desired gaseous temperature derivatives. The interface temperature derivatives are obtained from the Clapeyron equation and the known P_s derivatives, that is,

$$\left(\frac{\partial T_i}{\partial P}\right)_{U_g, X_n} = \frac{dT_i}{dP_s} \left(\frac{\partial P_s}{\partial P}\right)_{U_s, X_n} \quad 2.1.2-32$$

$$\left(\frac{\partial T_i}{\partial U_g}\right)_{P, X_n} = \frac{dT_i}{dP_s} \left(\frac{\partial P_s}{\partial U_g}\right)_{P, X_n}, \quad \text{and} \quad 2.1.2-33$$

$$\left(\frac{\partial T_i}{\partial X_n}\right)_{P, U_g} = \frac{dT_i}{dP_s} \left(\frac{\partial P_s}{\partial X_n}\right)_{P, U_g} \quad 2.1.2-34$$

where dT_i/dP_s is given by the reciprocal of Equation 2.1.2-17.

The density derivatives can be obtained from $V_g = X_n V_n$ or $V_g = (1 - X_n)V_s$ as these two formulas for the gaseous specific volume are equivalent (see Equation 2.1.2-20). A symmetric formula can be obtained by eliminating X_n from the above two formulas giving

$$V_g = \frac{V_s V_n}{V_s + V_n} \quad 2.1.2-35$$

Using Equation 2.1.2-35 the ρ_g derivatives with respect to P are obtained

$$\left(\frac{\partial \rho_g}{\partial P}\right)_{U_g, X_n} = -\frac{1}{V_n^2} \left(\frac{\partial V_n}{\partial P}\right)_{U_g, X_n} - \frac{1}{V_s^2} \left(\frac{\partial V_s}{\partial P}\right)_{U_g, X_n} \quad 2.1.2-36$$

Parallel formulas are obtained when U_g or X_n is the independent variable. The partial derivatives on the right side of Equation 2.1.2-36 are obtained from formulas exactly parallel to those in Equations 2.1.2-29 through 2.1.2-31 with T_g replaced by V_s or V_n . When taking the derivatives of V_n ,

$$V_n = \frac{R_n T_g(P_s, V_s)}{P - P_s} \quad 2.1.2-37$$

Hence, an additional term appears in Equation 2.1.2-29 due to the direct dependence of V_n on P.

The homogeneous equilibrium sound speed for a noncondensable-steam-water mixture is derived in Reference 113.

The sound speed formula in Reference 113 is

$$\begin{aligned} a^2 = & V^2 (P'_s)^2 / \left\{ \left[-\hat{X}_n V_n P'_s \beta_n - \hat{X}_f V_f P'_s (\beta_f - P'_s \kappa_f) \right] \right. \\ & + \left\{ \hat{X}_s P'_s \left[\frac{C_{ps}}{T_s} + P'_s V_s (-2\beta_s + \kappa_s P'_s) \right] + \hat{X}_n P'_s \left[\frac{C_{pn}}{T_s} + P'_s V_n \beta_n \right] \right. \\ & \left. \left. + \hat{X}_f P'_s \left[\frac{C_{pf}}{T_s} - P'_s V_s \beta_s \right] \right\} \left(\frac{\partial T}{\partial P} \right)_{S, X_n} \right\} \quad 2.1.2-38 \end{aligned}$$

where

$$p'_s = \frac{dp^s}{dT} = \frac{h_s^s - h_f^s}{T^s(v_s^s - v_f^s)} \quad 2.1.2-39$$

and

$$\left(\frac{\partial T}{\partial P}\right)_{S, X_n} = \left\{ 1 + \left[\hat{X}_n v_n \beta_n + X_f v_f \beta_f \right] / \left[\hat{X}_s \kappa_n (S_s - S_f) \right] \right\} /$$

$$\left\{ p'_s + \left(\frac{\kappa_s}{\kappa_n} \right) \left\{ p'_s + \left(\frac{\beta_n - \beta_s}{\kappa_s} \right) + \left[\left(\hat{X}_n v_n \beta_n - \hat{X}_s v_s \beta_s \right) p'_s + \left(\hat{X}_n c_{pn} + \hat{X}_s c_{ps} + \hat{X}_f c_{pf} \right) / T^s \right] / \left[\hat{X}_s \kappa_s (S_s - S_f) \right] \right\} \right\} .$$

2.1.2-40

In the above formulas \hat{X}_s , \hat{X}_n , and \hat{X}_f are mass qualities based on the total mixture mass.

Evaluation of the sound speed formulas at the saturated equilibrium state requires a second iteration. To avoid this extra iteration the sound speed formulas were evaluated using the nonequilibrium state properties.

The liquid properties and derivatives are obtained as above for Case 1. To obtain the gaseous properties, Equations 2.1.2-23 and 2.1.2-24 must be solved iteratively. A standard Newton iteration in two variables is used. The iteration variables are P_s and U_s . The steam table Subroutine STH2X6 is called once during each iteration to obtain all the needed steam vapor properties and Equations 2.1.2-21 and 2.1.2-22 are used to obtain the air properties. To save calculation time only an approximate

Jacobian is used inside the iteration loop. From Equation 2.1.2-24, it is clear that if the steam behaves as an ideal gas, that is, $R_s = (V_s P_s / T_g)$ is constant, then Equation 2.1.2-24 is a simple linear equation determining P_s directly in terms of P and X_n . It simplifies the iteration to neglect the derivatives of R_s in the Jacobian, making it equal the left side matrix in Equation 2.1.2-25, with TERM1 and TERM2 terms absent. This iteration has been tested with P_s ranging from 2000 Pa to P and has always converged. The iteration is terminated when $|\Delta P_s|/P$ and $|\Delta V_s|/V_g$ are both <0.0005 . Hand calculations have been performed to compare both the properties and derivatives with the code calculations. In all cases the scheme converged in 4 iterations or less.

Once the iteration has converged the gaseous properties are determined from the formulas in this section. In the evaluations of all these derivatives the full matrix in Equation 2.1.2-25 is used including TERM1 and TERM2.

2.1.3. Constitutive Models

The constitutive relations include models for defining flow regimes and flow regime related models for interphase drag, wall friction, heat transfer, interphase heat and mass transfer, horizontal and vertical stratification, and water packing mitigation.

2.1.3.1. Flow Regime Maps

In RELAP5 the constitutive relations include flow regime effects for which simplified mapping techniques have been developed to control the use of constitutive relation correlations. Three flow regime maps are utilized. They are vertical and horizontal maps for flow in pipes, and a high mixing map for flow in pumps. The flow regime maps are based on the work of Taitel and Dukler^{27,28} and Ishii.²⁹⁻³¹

Taitel and Dukler have simplified flow regime classification and developed semi-empirical relations to describe flow regime transitions. However, some of their transition criteria are complex and further simplification has been carried out in order to apply these criteria efficiently in RELAP5. In addition, post-CHF regimes as suggested by Ishii²⁹ are included.

Vertical Flow Regime Map

The vertical flow regime map is modeled as seven regimes, three of which are for pre-CHF heat transfer, three of which are for post-CHF heat transfer, and one of which is for vertical stratification. For pre-CHF heat transfer, the regimes modeled are the bubbly, slug, and annular mist regimes. Formulations for these three regimes were utilized by Vince and Lahey³² to analyze their data. For post-CHF heat transfer, the bubbly, slug, and annular mist regimes are transformed to the inverted annular,

inverted slug, and mist regimes, respectively, as suggested by Ishii.²⁹ Unheated components are also modeled utilizing the pre-CHF map. A schematic representing the pre- and post-CHF regimes of the vertical flow regime map is shown in Figure 2.1.3-1. The vertically stratified regime may exist at low flow conditions and a schematic showing its relationship in the vertical flow regime map is given in Figure 2.1.3-2. The criteria for defining the boundaries for transition from one regime to another are given by the following correlations.

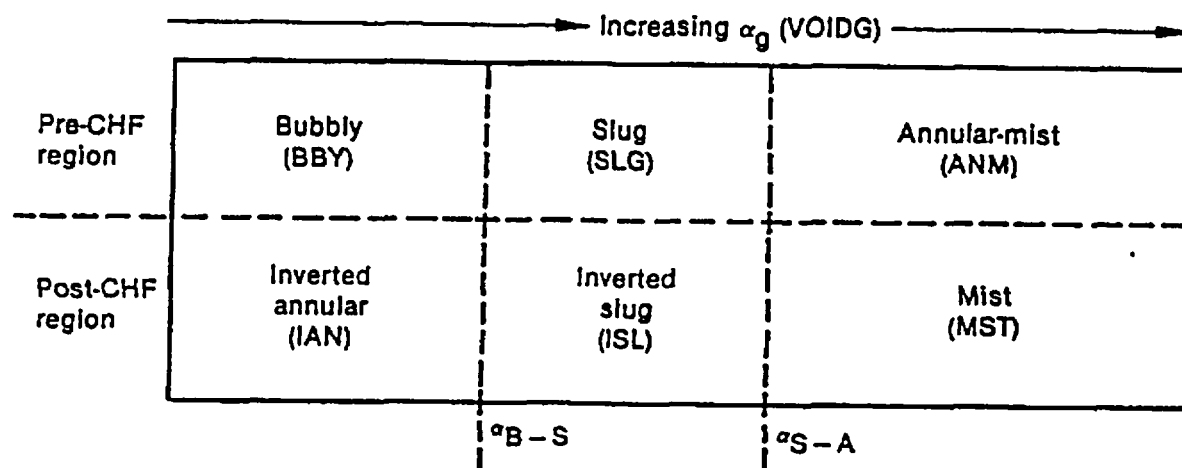


Figure 2.1.3-1. Sketch of Vertical Flow Regime Map.

For the bubbly to slug transition, Taitel and Dukler^{27,28} suggested that bubbly flow may not exist in tubes of small diameter where the rise velocity of small bubbles exceeds that of Taylor bubbles. The small bubble rise velocity is given by the correlation²⁸

$$v_{sb} = 1.53 \left[g(\rho_f - \rho_g)\sigma/\rho_f^2 \right]^{1/4} \quad 2.1.3-1$$

and the Taylor bubble rise velocity is given by the correlation¹¹

$$V_{Tb} = 0.35 \left[gD(\rho_f - \rho_g)/\rho_f \right]^{1/2} \quad 2.1.3-2$$

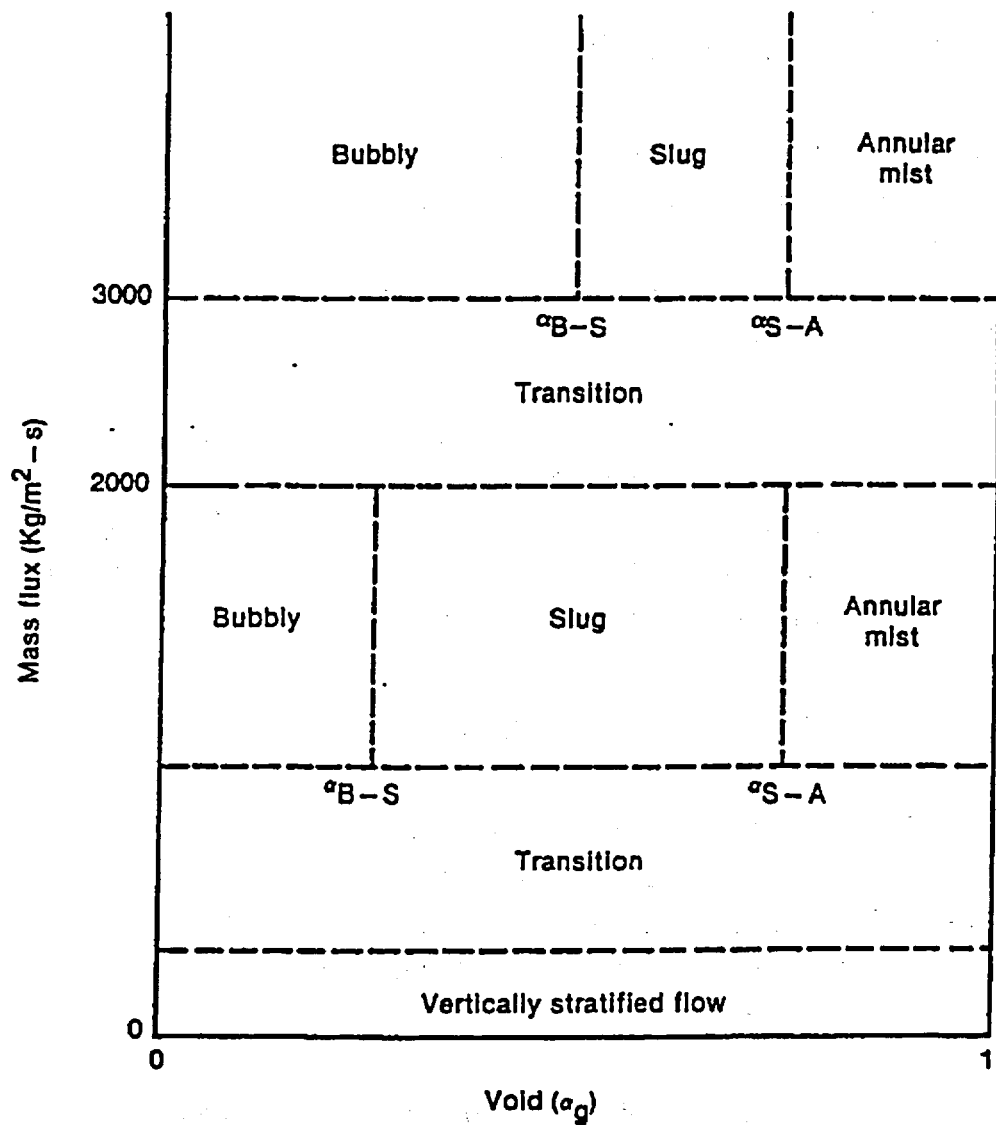


Figure 2.1.3-2. Vertical Flow Regime Map Including the Vertically Stratified Regime.

(Note: in Reference 28, $\rho_f - \rho_g$ is approximated as ρ_f , see also References 30 and 33). Accordingly, the limiting tube diameter allowing the presence of bubbly flow is

$$D^* \geq 19 , \quad 2.1.3-3$$

where D^* is the dimensionless tube diameter,

$$D^* = D[g(\rho_f - \rho_g)/\sigma]^{1/2} . \quad 2.1.3-4$$

Equation 2.1.3-2 is the dimensionless ratio of tube diameter to film thickness times the Deryagin number, where the Deryagin number is the ratio of film thickness to capillary length. Also, in the limit, as the fluid properties approach the thermodynamic critical pressure, $D^* = D$.

For tubes with diameters satisfying the condition of Equation 2.1.3-3 the bubble-slug transition occurs at a void fraction $\alpha_g = 0.25$ for low mass fluxes of $G \leq 2000 \text{ kg/m}^2\text{s}$. By combining this void criterion with Equation 2.1.3-3 the bubble-slug transition criterion can be defined such that

$$\alpha_L = 0.25 \text{ MIN } [1.0, (D^*/19)^8] . \quad 2.1.3-5$$

Hence, if the local void fraction, α_g^v , exceeds the criterion of Equation 2.1.3-5 then bubbly flow cannot exist since the rise velocity of small bubbles exceeds that of Taylor bubbles. The exponential power of 8 is used to provide a smooth variation of α_L as D^* decreases.

At high mass fluxes of $G \geq 3000 \text{ kg/m}^2\text{s}$, bubbly flow with finely-dispersed bubbles can exist up to a void fraction, α_g , of 0.5. Then, if the criterion is linearly interpolated between the upper

and lower void limits, the bubbly-slug transition criterion can be written as

$$\alpha_{B-S} = \alpha_L \quad 2.1.3-6$$

for mass fluxes of $G \leq 2000 \text{ kg/m}^2\text{s}$,

$$\alpha_{B-S} = \alpha_L + 0.001 (G - 2000) (0.5 - \alpha_L) \quad 2.1.3-7$$

for mass fluxes of $2000 < G < 3000 \text{ kg/m}^2\text{s}$, and

$$\alpha_{B-S} = 0.5 \quad 2.1.3-8$$

for mass fluxes of $G \geq 3000 \text{ kg/m}^2\text{s}$. The flow regime can therefore be in the bubbly regime if $\alpha_g < \alpha_{B-S}$ and in the slug regime if $\alpha_g \geq \alpha_{B-S}$.

The bubble-slug transition defined by Equations 2.1.3-6 to 2.1.3-8 is similar to that given by Taitel and Dukler,²⁸ except that the void fraction relation is converted into a form based on liquid and vapor superficial velocities and finely dispersed bubbles are also distinguished from ordinary bubbles.

For the slug to annular flow transition, Taitel and Dukler²⁸ developed a criterion based on the critical vapor velocity required to suspend a liquid droplet. The critical velocity, u_c , is written as

$$u_c = 3.1[\sigma g(\rho_f - \rho_g)]^{1/4} / \rho_g^{1/2} = (\alpha_g v_g)_c \quad 2.1.3-9$$

The value 3.1 for the numerical coefficient is somewhat larger than the value of 1.4 reported by Wallis³⁴ but is a better fit to the data reported by Vince and Lahey.³² In comparing RELAP5 code results to data, however, the coefficient value of 1.4 gives better results. The void fraction must also be greater than 0.75

in order to get good comparisons between code results and data. Hence, solving Equation 2.1.3-9 for void fraction and imposing a lower void limit of 0.75 yields the slug to annular transition criterion for which

$$\alpha_{S-A} = \text{MAX} \left[0.75, 1.4 [\sigma g (\rho_f - \rho_g)]^{1/4} / (v_g \rho_g^{1/2}) \right], \quad 2.1.3-10$$

where the flow regime is said to be in the slug regime if

$\alpha_g \leq \alpha_{S-A}$ and in the annular-mist regime if $\alpha_g > \alpha_{S-A}$.

For post-CHF heat transfer the same formulations are used to define the inverted flow regime transition criteria in that Equations 2.1.3-6 through 2.1.3-8 also define the inverted slug regime transition and Equation 2.1.3-10 defines the inverted slug to mist regime transition.

At low mass fluxes the possibility exists for vertically stratified conditions. In RELAP5 vertical flow in a volume cell is considered to be stratified if the difference in void fraction of the volumes above and below is greater than 0.5 and if the magnitude of the volume average mixture mass flux is less than the Taylor bubble rise velocity mass flux. The Taylor bubble criterion is based on the Taylor bubble velocity given by Equation 2.1.3-2 such that

$$|G| < \rho v_{Tb} \quad , \quad 2.1.3-11$$

where v_{Tb} is the Taylor bubble velocity and

$$|G| = |\alpha_g \rho_g v_g + \alpha_f \rho_f v_f| \quad . \quad 2.1.3-12$$

Hence, if Equation 2.1.3-11 is true, then transition to vertical stratification exists and if Equation 2.1.3-11 is false, then transition to vertical stratification does not exist.

Horizontal Flow Regime Map

The horizontal flow regime map is similar to the vertical flow regime map except that the post-CHF regimes are not included and a horizontal stratification regime is modeled that replaces the vertical stratification regime. The horizontal flow regime map therefore consists of horizontally stratified, bubbly, slug and annular mist regimes. The criteria for the bubbly to slug and the slug to annular mist regimes are also similar to those for the vertical map except that the bubbly to slug transition criterion is a constant

$$\alpha_{B-S} = \alpha_L = 0.25. \quad 2.1.3-13$$

The slug to annular mist transition criterion is also a constant

$$\alpha_{S-A} = 0.8. \quad 2.1.3-14$$

The criterion defining the horizontally stratified regime is one developed by Taitel and Dukler.²⁷

According to Taitel and Dukler, the flow field is horizontally stratified if the vapor velocity satisfies the condition that

$$v_g < v_{gL}, \quad 2.1.3-15$$

where

$$v_{gL} = \frac{1}{2} \left[\frac{(\rho_f - \rho_g) g a A}{\rho_g D \sin \theta} \right]^{1/2} (1 - \cos \theta). \quad 2.1.3-16$$

The angle θ is related to the liquid level, ll , and the void fraction, α_g , by the relationships

$$ll = D (1 + \cos\theta)/2 \quad 2.1.3-17$$

and

$$\alpha_g \pi = \theta - \sin\theta \cos\theta \quad 2.1.3-18$$

If the horizontal stratification condition of Equation 2.1.3-15 is met, then the flow field undergoes a transition to horizontally stratified. If the condition of Equation 2.1.3-15 is not met, then the flow field undergoes a transition to the bubbly, slug, or annular mist flow regime.

High Mixing Flow Regime Map

The high mixing flow regime map is based on vapor void fraction, α_g , and consists of a bubbly regime for $\alpha_g \leq 0.5$, a mist regime for $\alpha_g \geq 0.95$, and a transition regime for $0.5 < \alpha_g < 0.95$. The transition regime is modeled as a mixture of bubbles dispersed in liquid and droplets dispersed in vapor.

2.1.3.2. Interphase Drag

The interphase drag force per unit volume expressed in terms of relative phasic velocity is

$$F_{I_{gf}} = - f_{gf} |v_g - v_f| (v_g - v_f) \quad , \quad 2.1.3-19$$

with

$$f_{gf} = \rho_c S_F a_{gf} C_D / 8 \quad , \quad 2.1.3-20$$

where

- ρ_c = density of the continuous phase,
- C_D = drag coefficient,
- a_{gf} = interfacial area per unit volume, and
- S_F = shape factor.

The shape factor³⁰, S_F , is assumed to be unity (1.0). The evaluation of a_{gf} and C_D for different flow regimes is covered in the following discussion.

Dispersed Flow

The bubbly and mist flow regimes are both considered as dispersed flow. According to Wallis³⁴ and Shapiro,³⁵ the dispersed bubbles or droplets can be assumed to be spherical particles with a size distribution of the Nukiyama-Tanasawa form. The Nukiyama-Tanasawa distribution function in nondimensional form is

$$p^* = 4d^{*2} e^{-2d^*} \quad , \quad 2.1.3-21$$

where $d^* = d/d'$; d' is the most probable particle diameter, and p^* is the probability of particles with a nondimensional diameter of d^* . With this distribution, it can be shown that the average particle diameter $d_0 = 1.5 d'$, and the surface area per unit volume is

$$a_{gf} = \frac{6\bar{\alpha}}{d'} \left\{ \frac{\int d^{*2} p^* dd^*}{\int d^{*3} p^* dd^*} \right\} = \frac{2.4\bar{\alpha}}{d'} \quad , \quad 2.1.3-22$$

where $\bar{\alpha} = \alpha_g$ for bubbles and $\bar{\alpha} = \alpha_f$ for droplets. In terms of the average diameter, d_o , the interfacial area per unit volume, a_{gf} , is

$$a_{gf} = 3.6\bar{\alpha}/d_o \quad . \quad 2.1.3-23$$

The average diameter d_o is obtained by assuming that $d_o = 1/2 d_{max}$. The maximum diameter, d_{max} , is related to the critical Weber number, We , by

$$We = d_{max} \rho_c (v_g - v_f)^2 / \sigma \quad . \quad 2.1.3-24$$

The values for We are presently taken as $We = 10$ for bubbles and $We = 3.0$ for droplets.

The drag coefficient is given by Ishii and Chawla³⁰ for the viscous regime as

$$C_D = 24(1 + 0.1 Re_p^{0.75}) / Re_p \quad , \quad 2.1.3-25$$

where the particle Reynolds number Re_p is defined as

$$Re_p = |v_g - v_f| d_o \rho_c / \mu_m \quad . \quad 2.1.3-26$$

The mixture viscosity, μ_m , is $\mu_m = \mu_f / \alpha_f$ for bubbles and $\mu_m = \mu_g / (\alpha_g)^{2.5}$ for droplets.

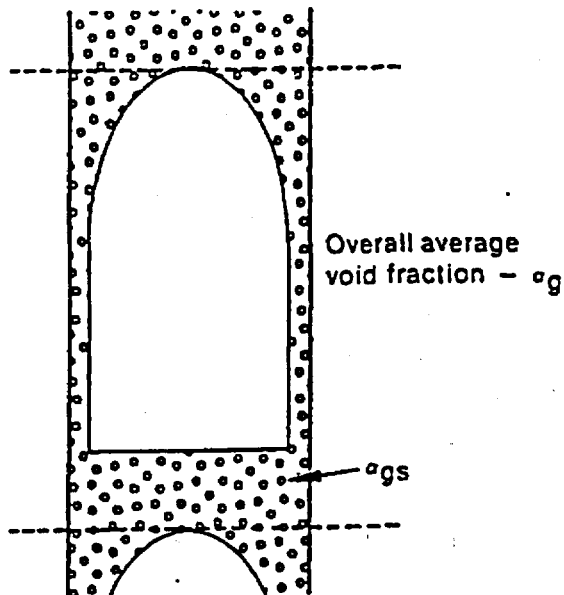


Figure 2.1.3-3. Slug Flow Pattern

Slug Flow

Slug flow is modeled as a series of Taylor bubbles separated by liquid slugs containing small bubbles. A sketch of a slug flow pattern is shown in Figure 2.1.3-3. The Taylor bubble has a diameter nearly equal to the pipe diameter and a length varying from one to one hundred pipe diameters.

The total drag in slug flow is partitioned into small bubble and Taylor bubble drag components:

$$f_{gf} = (f_{gf})_{sb} + (f_{gf})_T \quad 2.1.3-26.1$$

The interphasic friction term for small bubbles, $(f_{gf})_{sb}$, is of the form given in Equation 2.1.3-20 and is determined with the a_{gf} and C_D derived for dispersed flow (Equations 2.1.3-23 and 2.1.3-25).

The void fraction of a single Taylor bubble, α_b , in the total mixture is

$$\alpha_b = (\alpha_g - \alpha_{gs}) / (1 - \alpha_{gs}) \quad . \quad 2.1.3-27$$

where α_{gs} is the average void fraction in the liquid film and slug region.

To provide a smooth transition into and out of slug flow, α_{gs} , in Equation 2.1.3-27, is considered as a free parameter varying from the void fraction (α_{B-S}) at the bubbly to slug flow regime transition to nearly zero at the slug to annular mist flow regime transition. The variation is represented by the exponential expression

$$\alpha_{gs} = \alpha_{B-S} \exp[-10(\alpha_g - \alpha_{B-S}) / (\alpha_{S-A} - \alpha_{B-S})] \quad . \quad 2.1.3-28$$

Three options are available for computing the Taylor bubble interphase drag in slug flow: the base INEL drag, the Wilson drag, and the B&W modified slug-drag model. The Wilson drag is based on the Wilson bubble rise velocity in a vertical pipe.¹³⁵ The BWNT modified slug-drag model uses coefficients that are a function of pressure and void fraction to adjust the INEL drag model. The default is the INEL model.

INEL Drag Model

By approximating the ratio of the Taylor bubble diameter to the tube diameter and the diameter-to-length ratio of a Taylor bubble, Ishii and Mishima³¹ obtained the surface-to-volume ratio of a Taylor bubble as $4.5/D$. In the INEL drag model, this is used to obtain the interfacial area per unit volume, a_{gf} , for slug flow:

$$a_{gf} = (4.5 C_t/D)\alpha_b + (3.6 \alpha_{gs}/d_o)(1 - \alpha_b) , \quad 2.1.3-29$$

in which the first term pertains to Taylor bubbles and the second term to small bubbles. C_t is a roughness parameter that is introduced to account for irregularities in the surface of large Taylor bubbles. At the present time, C_t is assumed to be unity (1.0).

The INEL model drag coefficient for Taylor bubbles is given by Ishii and Chawla³⁰ as

$$(C_D)_T = 9.8 (1 - \alpha_b)^3 , \quad 2.1.3-30$$

where α_b is given by combining Equations 2.1.3-27 and 2.1.3-28.

The Wilson Drag Model

The Wilson drag model was first derived for reflood applications using BEACH¹³⁶ and is now applied to non-reflood conditions in RELAP5/MOD2-B&W.

b,c,d,e

b,c,d,e

The estimate of the phasic slip, Δv , is obtained from a modified set of the Wilson¹³⁵ bubble rise model:

b,c,d,e

The coefficients a_j and b_j for $j = 1$ and 2 are from the original correlation. The third set ($j = 3$), however, was added to obtain a better match to the original data at high α_g^* (greater than about 6.526). As implemented in RELAP5/MOD2-B&W, the bubble velocity is multiplied by a user-defined multiplier, C_{WB} :

$$v_{bub} = C_{WB} \Delta v.$$

2.1.3-30.6

b,c,d,e

where C_{WSL} is a user-defined multiplier for slug flow conditions which, at the present time, is set equal to one.

In RELAP5, an interphase drag for each volume is calculated and then the drag for the junctions between connecting volumes are determined. RELAP5 uses several techniques to smooth the void behavior across the junction. One of these smoothing techniques is used when the difference between the void fractions of adjoining volumes is greater than 0.001. For some situations (for example, in RSG PWR small break LOCA, during the hot leg draining period and during the period preceding core uncover), it is expected that discontinuous void behavior will occur at the core-upper plenum boundary. The unmodified junction drag logic calculates void behavior reasonably well. However, because RELAP5 smooths the void behavior across the junction when the difference between connecting nodes is greater than 0.001, a flat

void profile is calculated for some cases as illustrated in Figure 2.1.3-3.1. Therefore, as an option to the Wilson drag model, the void difference threshold for curve smoothing is increased to 0.5.

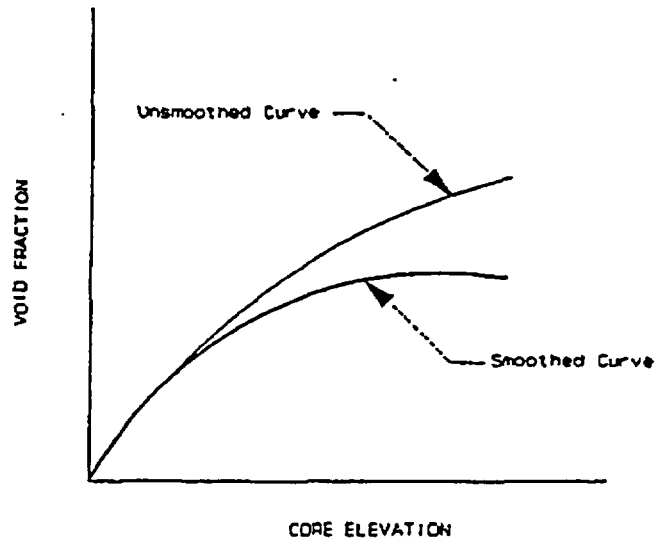


Figure 2.1.3-3.1. Typical RELAP5 Void Profile: Smoothed and Unsmoothed Curves.

BWNT has added an option to adjust the slug interphase drag for non-reflood applications via coefficients added to Equation 2.1.3-26.1. The adjustments, based on numerous benchmarks, are functions of pressure and void fraction as shown in the following equations.

$$f_{gf} = M_{st} [(f_{gf})_{sb} + M_s (f_{gf})_T] \quad , \quad 2.1.3-30.7.1$$

where

$$\left[\quad \quad \quad b, c, d, e \quad \quad \quad \right]$$

b,c,d,e

The values given in parentheses are the default coefficients. These are selected by the user through input of a control volume flag which refers back to a tabular default table number containing the five coefficients that are listed. A different set of coefficients may be specified by the user on input. Use of the default drag adjustments are appropriate for two-phase applications in heated tube bundles and small diameter pipes during non-reflood calculations.

Annular Mist Flow

Annular mist flow is characterized by a liquid film along the wall and a vapor core containing entrained liquid droplets. The INEL drag is the sum of the annular vapor and liquid droplet drag components

$$f_{gf} = (f_{gf})_{ann} + (f_{gf})_{drp} \quad 2.1.3-30.8$$

Let α_{ff} be the average liquid volume fraction of the liquid film along the wall. Then, from simple geometric considerations, the interfacial area per unit volume can be shown to be

$$\alpha_{gf} = (4C_{an}/D)(1 - \alpha_{ff})^{1/2} + (3.6\alpha_{fd}/d_o)(1 - \alpha_{ff}), \quad 2.1.3-31$$

where C_{an} is a roughness parameter introduced to account for waves in the liquid wall film and α_{fd} is the average liquid volume fraction in the vapor core, for which

$$\alpha_{fd} = (\alpha_f - \alpha_{ff}) / (1 - \alpha_{ff}) \quad . \quad 2.1.3-32$$

A simple relation based on the flow regime transition criterion and liquid Reynolds number is used to correlate the average liquid film volume fraction. For vertical flow regimes, the entrainment relation is

$$\alpha_{ff} = \alpha_f C_f \exp \left\{ -7.5 \cdot 10^{-5} (\alpha_g v_g / u_c)^6 \right\}, \quad 2.1.3-33$$

where u_c is the entrainment critical velocity given by Equation 2.1.3-9 with the coefficient 3.1 replaced by 1.4. For horizontal flow regimes, the entrainment relation is

$$\alpha_{ff} = \alpha_f C_f \exp \left\{ -4.0 \cdot 10^{-5} (v_g / v_{gl})^6 \right\}, \quad 2.1.3-34$$

where v_{gl} is the horizontal stratification critical velocity given by Equation 2.1.3-16. The term C_f is expressed as

$$C_f = 10^{-4} \rho_f \alpha_f v_f D / \mu_f \quad .$$

The interfacial friction factor, f_i , for the liquid film takes the place of C_D in Equation 2.1.3-20, and is described by a correlation obtained by Bharathan et al.³⁶ for which

$$f_i = 4 \left(0.005 + A(\delta^*)^B \right), \quad \dots \quad 2.1.3-35$$

where

$$\log_{10} A = -0.56 + 9.07/D^*, \quad \dots \quad 2.1.3-36$$

$$B = 1.63 + 4.74/D^*, \text{ and} \quad \dots \quad 2.1.3-37$$

$$\delta^* = \delta \left\{ \frac{(\rho_f - \rho_g) g}{\sigma} \right\}^{1/2} \quad \dots \quad 2.1.3-38$$

The term δ^* is the liquid wall film Deryagin number for which δ is the film thickness, and D^* is the dimensionless diameter given by Equation 2.1.3-5.

BWNT has added an option to include a multiplicative coefficient on the overall drag computed for control volumes in an annular mist flow regime. This coefficient is available for non-reflood applications. The default coefficient, x_{ms} , is 1.0; however, it may be changed on input specified by the user. The coefficient is applied as follows

$$f_{gf} = x_{ms} [(f_{gf})_{ann} + (f_{gf})_{drp}] \quad \dots \quad 2.1.3-38.1$$

Vertical Stratified Flow

For vertically stratified flow the previously discussed interphase drag relationships are applied except that a low interphase drag coefficient of $0.1 \text{ N-s}^2/\text{m}^5$ is imposed for the junction above the vertically stratified volume.

Horizontal Stratified Flow

By simple geometric consideration, one can show that the interfacial area per unit volume is

$$a_{gf} = 4C_{st} \sin \theta (\pi D) , \quad 2.1.3-39$$

where C_{st} is a roughness parameter introduced to account for surface waves and is set to 1 at the present time.

The interface Reynolds number is defined with the vapor properties and regarding liquid as the continuous phase for which

$$Re_i = D_i \rho_g | v_g - v_f | \mu_g , \quad 2.1.3-40$$

where the equivalent wetted diameter, D_i , for the interface is

$$D_i = \alpha \pi D / (\theta + \sin \theta) . \quad 2.1.3-41$$

The interfacial friction factor, f_i , replaces C_D in Equation 2.1.3-20 and is obtained by assuming typical friction factor relationships for which

$$f_i = 64/Re_i \quad 2.1.3-42$$

for laminar flow, where $Re_i \leq 1187$,

$$f_i = 0.3164/Re_i^{0.25} \quad 2.1.3-43$$

for turbulent flow, where $Re_i \geq 4000$, and

$$f_i = 0.0539 \quad 2.1.3-44$$

for the laminar to turbulent transition where $1187 < Re_i < 4000$.

Inverted Flow Regimes

The interphase drag relationships for post-CHF inverted flow regimes are treated in a similar fashion to the corresponding pre-CHF flow regimes except that the roles of vapor and liquid are interchanged.

2.1.3.3. Wall Friction

In RELAP5, the wall friction force terms include only wall shear effects. Losses due to abrupt area change are calculated using mechanistic form loss models. Other losses due to elbows or complicated flow passage geometry are modeled using energy loss coefficients that must be input by the user.

In the development of the RELAP5/MOD2 wall friction model, emphasis was placed on obtaining reasonable values for wall friction in all flow regimes. The flow regime models are discussed in section 2.1.3.1.

The wall friction model is based on a two-phase multiplier approach in which the two-phase multiplier is calculated from the Heat Transfer and Fluid Flow Service (HTFS) modified Baroczy correlation.³⁷ The individual phasic wall friction components are calculated by apportioning the two-phase friction between the

phases using a technique derived from the Lockhart-Martinelli³⁸ model. The model is based on the assumption that the frictional pressure drop may be calculated using a quasi-steady form of the momentum equation.

The Two-Phase Friction Multiplier Approach

The overall friction pressure drop can be expressed in terms of the liquid-alone wall friction pressure drop

$$\left(\frac{\partial P}{\partial x}\right)_{2\phi} = \phi_f^2 \left(\frac{\partial P}{\partial x}\right)_f \quad 2.1.3-45$$

or the vapor-alone wall friction pressure drop

$$\left(\frac{\partial P}{\partial x}\right)_{2\phi} = \phi_g^2 \left(\frac{\partial P}{\partial x}\right)_g \quad 2.1.3-46$$

where ϕ_f and ϕ_g are the liquid-alone and vapor-alone two-phase friction multipliers, respectively. The phasic wall friction pressure gradients are expressed as

$$\left(\frac{\partial P}{\partial x}\right)_f = \frac{\lambda'_f M_f^2}{2D\rho_f A^2} \quad 2.1.3-47$$

for the liquid-alone, and

$$\left(\frac{\partial P}{\partial x}\right)_g = \frac{\lambda'_g M_g^2}{2D\rho_g A^2} \quad 2.1.3-48$$

for the vapor-alone, where the prime indicates the liquid and vapor-alone friction factors, respectively, calculated at the respective Reynolds numbers

$$Re'_f = \frac{\alpha_f \rho_f |v_f| D}{\mu_f} \quad 2.1.3-49$$

and

$$Re'_g = \frac{\alpha_g \rho_g |v_g| D}{\mu_g} \quad 2.1.3-50$$

The liquid and vapor mass flow rates, respectively, are defined as

$$M_f = \alpha_f \rho_f v_f A \quad 2.1.3-51$$

and

$$M_g = \alpha_g \rho_g v_g A \quad 2.1.3-52$$

Throughout the current literature the overall two-phase friction pressure gradient is calculated using two-phase friction multiplier correlations. However, regardless of the correlation used, the multipliers may be interrelated using Equations 2.1.3-45 through 2.1.3-48 and the Lockhart-Martinelli³⁸ ratio defined as

$$x^2 = \frac{\left(\frac{dP}{dx}\right)_f}{\left(\frac{dP}{dx}\right)_g} = \frac{\phi_g^2}{\phi_f^2} \quad 2.1.3-53$$

In RELAP5 these equations are used to apportion the overall wall friction into liquid and vapor wall friction coefficients.

Flow Regime Effects

Two-phase friction can be modeled in terms of two-phase friction multipliers and known friction factors using the method developed by Lockhart-Martinelli.³⁹ Chisholm³⁸ also developed a theoretical basis for the Lockhart-Martinelli model that provides a rationale for relating the equations to empirical results.

From the theoretical basis developed by Chisholm, irrespective of flow regime, the quasi-steady phasic momentum equations can be expressed in scalar form as

$$\alpha_f A \left(\frac{\partial P}{\partial x} \right)_{2\phi} - \tau_f p_f - S_{FI} = 0 \quad 2.1.3-54$$

for the liquid, and

$$\alpha_g A \left(\frac{\partial P}{\partial x} \right)_{2\phi} - \tau_g p_g - S_{FI} = 0 \quad 2.1.3-55$$

for the vapor, where τ_f and τ_g are the liquid and vapor wall shear stresses, respectively, p_f and p_g are the liquid and vapor wetted wall perimeter, respectively, and S_{FI} is a stress gradient due to interphase friction. These equations can be expressed in terms of Darcy friction factors and simplified so that

$$\left(\frac{dP}{dx} \right)_{2\phi} \left[1 + S_R \frac{\alpha_g}{\alpha_f} \right] = \frac{\lambda_f^p \rho_f v_f^2}{2D} \left(\frac{\alpha_{fw}}{\alpha_f} \right) \quad 2.1.3-56$$

for the liquid, and,

$$\left(\frac{dP}{dx}\right)_{2\phi} (1 + S_R) = \frac{\lambda_g \rho_g v_g^2}{2D} \left(\frac{\alpha_{gw}}{\alpha_g}\right) \quad 2.1.3-57$$

for the vapor, where the interphase friction term, S_R , is defined as

$$S_R = \frac{S_{FI}}{\alpha_g A \left(\frac{\partial P}{\partial x}\right)_{2\phi}} \quad 2.1.3-58$$

The terms α_{fw} and α_{gw} are the liquid and vapor volume fractions, respectively, at the wall, and α_f and α_g are the overall liquid and vapor volume fractions, respectively. Taking the ratio of Equation 2.1.3-56 to 2.1.3-57 gives

$$z^2 = \frac{\lambda_f \rho_f v_f^2 \left(\frac{\alpha_{fw}}{\alpha_f}\right)}{\lambda_g \rho_g v_g^2 \left(\frac{\alpha_{gw}}{\alpha_g}\right)} = \frac{1 + S_R \frac{\alpha_g}{\alpha_f}}{(1 - S_R)} \quad 2.1.3-59$$

Consider the pure liquid case where $\alpha_g = 0$ and $\alpha_{fw} = \alpha_f$ and for which Equation 2.1.3-56 reduces to

$$\left(\frac{\partial P}{\partial x}\right)_{2\phi} = \left(\frac{\partial P}{\partial x}\right)_f = \frac{\lambda_f \rho_f v_f^2}{2D} \quad 2.1.3-60$$

For this case, the friction factor, λ_f , can be precisely calculated based on a Reynolds number expressed in terms of D .

Similarly, for the two-phase case, liquid and vapor friction factors can be calculated based on Reynolds number of

$$R_f = \frac{\rho_f \left(\frac{\alpha_f}{\alpha_{fw}} \right) D |v_f|}{\mu_f} \quad \text{and} \quad 2.1.3-61$$

$$R_g = \frac{\rho_g \left(\frac{\alpha_g}{\alpha_{gw}} \right) D |v_g|}{\mu_g} \quad 2.1.3-62$$

for the liquid and vapor, respectively. These terms have the property that, as one phase or the other disappears, the friction factors calculated reduce to their single-phase formulations.

Equations 2.1.3-56 and 2.1.3-57 can be rewritten as

$$\left(\frac{dp}{dx} \right)_{2\phi} \left(\frac{z^2}{\alpha_g + \alpha_f z^2} \right) = \frac{\lambda_f \rho_f v_f^2}{2D} \left(\frac{\alpha_{fw}}{\alpha_f} \right) \quad 2.1.3-63$$

and

$$\left(\frac{dp}{dx} \right)_{2\phi} \left(\frac{1}{\alpha_g + \alpha_f z^2} \right) = \frac{\lambda_g \rho_g v_g^2}{2D} \left(\frac{\alpha_{gw}}{\alpha_g} \right) \quad 2.1.3-64$$

for the liquid and vapor, respectively. However, these equations are now flow regime dependent since knowledge of the wetted wall and overall void fractions is required in order to calculate the friction factors. The term z^2 can also be considered as a correlating factor relating the overall two-phase friction pressure gradient to the known phasic friction factors.

The quasi-steady phasic momentum equations similar to Equations 2.1.3-63 and 2.1.3-64 can also be written in terms of the RELAP5 friction coefficient, where

$$\alpha_f \left(\frac{dP}{dx} \right)_{2\phi} \left[\frac{z^2}{\alpha_g + \alpha_f z^2} \right] = FWF(\alpha_f \rho_f v_f) \quad 2.1.3-65$$

for the liquid, and

$$\alpha_g \left(\frac{dP}{dx} \right)_{2\phi} \left[\frac{1}{\alpha_g + \alpha_f z^2} \right] = FWG(\alpha_g \rho_g v_g) \quad 2.1.3-66$$

for the vapor. Taking the sum of these two equations gives the overall quasi-steady two-phase pressure gradient as

$$\left(\frac{dP}{dx} \right)_{2\phi} = FWF(\alpha_f \rho_f v_f) + FWG(\alpha_g \rho_g v_g) \quad 2.1.3-67$$

It should be noted that the calculation of the phasic friction factors using the Reynolds numbers given by Equation 2.1.3-61 and the assumption that two-phase flows behave similarly to single-phase flows in the laminar, transition, and turbulent regimes provides the rationale relating Equations 2.1.3-63 and 2.1.3-64 to empirical data. It is this same rationale that allows expressing the correlating term, z^2 , in terms of friction factors that are independent of interphase friction as given by Equation 2.1.3-59. It is this equation that forms the basis for apportioning the overall two-phase wall friction between the phases.

Apportioning Wall Friction

Overall two-phase wall friction can be apportioned into phasic components by combining Equations 2.1.3-65 and 2.1.3-66 with

Equations 2.1.3-45 through 2.1.3-48 and 2.1.3-59, 2.1.3-62, and 2.1.3-64 which results in

$$\phi_f^2 \frac{\lambda'_{f\rho_f} (\alpha_f v_f)^2}{2D} \frac{\alpha_{fw} \lambda'_{f\rho_f} v_f^2}{\alpha_{gw} \lambda'_{g\rho_g} v_g^2 + \alpha_{fw} \lambda'_{f\rho_f} v_f^2} = FWF(\alpha_f \rho_f v_f) \quad 2.1.3-68$$

for the liquid, and

$$\phi_g^2 \frac{\lambda'_{g\rho_g} (\alpha_g v_g)^2}{2D} \frac{\alpha_{gw} \lambda'_{g\rho_g} v_g^2}{\alpha_{gw} \lambda'_{g\rho_g} v_g^2 + \alpha_{fw} \lambda'_{f\rho_f} v_f^2} = FWG(\alpha_g \rho_g v_g) \quad 2.1.3-69$$

for the vapor, where the two-phase multiplier terms are calculated using a two-phase friction multiplier correlation. Flow regime effects are also included in the relationships between wetted wall and overall void fractions and their effect in calculating the friction factor terms.

The H.T.F.S. Two-Phase Friction Multiplier Correlation

In RELAP5 only the H.T.F.S. correlation³⁷ is used to calculate two-phase friction multipliers. This correlation was chosen because it is correlated to empirical data over very broad ranges of phasic volume fractions, phasic flowrates and flow regimes. The correlation has also been shown to give good agreement with empirical data.

The H.T.F.S. correlation for two-phase friction multiplier³⁷ is expressed as

$$\phi_f^2 = 1 + \frac{C}{x} + \frac{1}{x^2} \quad 2.1.3-70$$

for the liquid-alone multiplier, or

$$\phi_g^2 = x^2 + Cx + 1 \quad 2.1.3-71$$

for the vapor-alone multiplier, where C is the correlation term and x is the Lockhart-Martinelli ratio given by Equation 2.1.3-53. The correlation term is expressed in terms of scalar mass flux, G, and the Baroczy dimensionless property index, Λ , such that

$$2 \leq C = -2 + f_1(G) T_1, \quad 2.1.3-72$$

where

$$f_1(G) = 28 - 0.3 G^{0.5}, \quad 2.1.3-73$$

$$T_1 = \exp - \left[\frac{(\log_{10} \Lambda + 2.5)^2}{2.4 - G(10^{-4})} \right], \quad 2.1.3-74$$

$$\Lambda = \frac{\rho_g}{\rho_f} \left[\frac{\mu_f}{\mu_g} \right]^{0.2}, \text{ and} \quad 2.1.3-75$$

$$G = \alpha_f \rho_f v_f + \alpha_g \rho_g v_g \quad 2.1.3-76$$

The terms ρ , μ , α and v denote the density, viscosity, volume fraction and velocity, respectively.

If the H.T.F.S. correlation is combined with the wall friction formulations by combining Equations 2.1.3-45 through 2.1.3-48, 2.1.3-51 through 2.1.3-53, 2.1.3-70, and 2.1.3-71, then

$$\begin{aligned} \left(\frac{dP}{dx}\right)_{2\phi} &= \phi_f^2 \left(\frac{dP}{dx}\right)_f = \phi_g^2 \left(\frac{dP}{dx}\right)_g \\ &= \frac{1}{2D} \left(\lambda'_f \rho_f (\alpha_f v_f)^2 + C \left[\lambda'_f \rho_f (\alpha_f v_f)^2 \lambda'_g \rho_g (\alpha_g v_g)^2 \right]^{0.5} \right. \\ &\quad \left. + \lambda'_g \rho_g (\alpha_g v_g)^2 \right). \end{aligned} \quad 2.1.3-77$$

This equation can then be combined with Equation 2.1.3-68 and 2.1.3-69 and simplified such that

$$\begin{aligned} FWF(\alpha_f \rho_f) &= \alpha_{fw} \frac{\rho_f \lambda_f |v_f|}{2D} (\lambda'_f \rho_f (\alpha_f v_f)^2 \\ &\quad + C \left[\lambda'_f \rho_f (\alpha_f v_f)^2 \lambda'_g \rho_g (\alpha_g v_g)^2 \right]^{0.5} \\ &\quad + \lambda'_g \rho_g (\alpha_g v_g)^2) / \left[\alpha_{gw} \lambda_g \rho_g v_g^2 + \alpha_{fw} \lambda_f \rho_f v_f^2 \right] \end{aligned} \quad 2.1.3-78$$

for the liquid, and

$$\begin{aligned} FWG(\alpha_g \rho_g) &= \alpha_{gw} \frac{\rho_g \lambda_g |v_g|}{2D} (\lambda'_f \rho_f (\alpha_f v_f)^2 \\ &\quad + C \left[\lambda'_f \rho_f (\alpha_f v_f)^2 \lambda'_g \rho_g (\alpha_g v_g)^2 \right] \\ &\quad + \lambda'_g \rho_g (\alpha_g v_g)^2) / \left[\alpha_{gw} \lambda_g \rho_g v_g^2 + \alpha_{fw} \lambda_f \rho_f v_f^2 \right] \end{aligned} \quad 2.1.3-79$$

for the vapor.

In RELAP5 the friction factor and velocity terms are calculated in such a manner that as the velocity terms disappear the equations give the correct limits. For example, the friction factor terms are evaluated such that

$$\lim_{\left| \frac{\alpha_f}{\alpha_{fw}} v_f \right| \rightarrow 0} \left[\lambda_f \left| \frac{\alpha_f}{\alpha_{fw}} v_f \right| \right] = \frac{64\mu_f}{D\rho_f} = \lim_{|\alpha_f v_f| \rightarrow 0} (\lambda'_f |\alpha_f v_f|),$$

$$\lim_{\left| \frac{\alpha_g}{\alpha_{gw}} v_g \right| \rightarrow 0} \left[\lambda_g \left| \frac{\alpha_g}{\alpha_{gw}} v_g \right| \right] = \frac{64\mu_g}{D\rho_g} = \lim_{|\alpha_g v_g| \rightarrow 0} (\lambda'_g |\alpha_g v_g|),$$

2.1.3-80

and the velocity terms are evaluated such that

$$\lim_{|v_f| \rightarrow 0} |v_f| = \epsilon = \lim_{|v_g| \rightarrow 0} |v_g|.$$

2.1.3-81

Hence, for stagnant flow or single-phase conditions, a positive and finite friction coefficient is always calculated. Thus, the numerical possibility of an infinite or negative friction coefficient is eliminated.

In Equations 2.1.3-78 and 2.1.3-79, flow regime effects are included in the terms (α_{fw}/α_f) and (α_{gw}/α_g) for the liquid and vapor, respectively. These terms are such that

$$\alpha_{fw} = 1 - \alpha_{gw}$$

2.1.3-82

and

$$\alpha_f = 1 - \alpha_g.$$

2.1.3-83

Equations 2.1.3-80 and 2.1.3-83 are restricted such that as overall phasic volume fraction disappears its corresponding wall film volume fraction disappears so that

$$\lim_{\alpha_f \rightarrow 0} \left(\frac{\alpha_{fw}}{\alpha_f} \right) = 1 \quad \text{and} \quad \lim_{\alpha_f \rightarrow 0} \left(\frac{\alpha_{gw}}{\alpha_g} \right) = 1, \quad 2.1.3-84$$

and similarly,

$$\lim_{\alpha_g \rightarrow 0} \left(\frac{\alpha_{gw}}{\alpha_g} \right) = 1 \quad \text{and} \quad \lim_{\alpha_g \rightarrow 0} \left(\frac{\alpha_{fw}}{\alpha_f} \right) = 1. \quad 2.1.3-85$$

Flow Regime Factors for Phasic Wall Friction

Phasic wall friction is expressed in terms of wall shear stress, which in turn requires knowledge of the surface area wetted by each phase. From the flow regime model discussed in section 2.1.3.1, expressions for the wall film phasic volume fractions can be derived. Using these expressions, the phasic wall friction factors that appear in Equations 2.1.3-56 and 2.1.3-57 may then be completed.

In the flow regime map, seven flow regimes are modeled, which are: for pre-CHF heat transfer, the bubbly, slug, and annular mist; for post-CHF heat transfer, the inverted-annular, inverted-slug and mist; and for stratified flow, the vertically and horizontally stratified. For the transition regime between pre- and post-CHF heat transfer, an interpolation scheme is also implemented in the code.

To implement flow regime effects in the two-phase wall friction model, first consider the wall liquid and vapor volume fractions.

These terms are

$$\frac{p_f}{p} = \alpha_{fw} \quad , \quad 2.1.3-86$$

which represents the liquid volume fraction in the wall film, and

$$\frac{p_g}{p} = \alpha_{gw} \quad , \quad 2.1.3-87$$

which represents the vapor volume fraction in the wall film where the terms p_f , p_g , and p are the perimeters wetted by the liquid, vapor, and mixture, respectively. Then, from the flow regime model these are formulated for all of the flow regimes as follows:

For the bubbly regime

$$\alpha_{fw} = \alpha_f \quad \text{and} \quad \alpha_{gw} = \alpha_g \quad , \quad 2.1.3-88$$

where α_f , α_g are the overall liquid and vapor volume fraction, respectively.

For the slug regime

$$\alpha_{fw} = 1 - \alpha_{gs} \quad \text{and} \quad \alpha_{gw} = \alpha_{gs} \quad , \quad 2.1.3-89$$

where α_{gs} is given by Equation 2.1.3-29.

For the annular-mist regime

$$\alpha_{fw} = (\alpha_{ff})^{\frac{1}{4}} \quad \text{and} \quad \alpha_{gw} = 1 - (\alpha_{ff})^{\frac{1}{4}} \quad , \quad 2.1.3-90$$

where α_{ff} is given by Equation 2.1.3-34.

For the inverted-annular regime

$$\alpha_{gw} = (\alpha_{gg})^{\frac{1}{4}} \quad \text{and} \quad \alpha_{fw} = 1 - (\alpha_{gg})^{\frac{1}{4}}, \quad 2.1.3-91$$

where α_{gg} is the inverted form of Equation 2.1.3-34.

For the inverted-slug regime

$$\alpha_{fw} = \alpha_{fs} \quad \text{and} \quad \alpha_{gw} = 1 - \alpha_{fs}, \quad 2.1.3-92$$

where α_{fs} is the inverted form of Equation 2.1.3-29.

For the mist regime

$$\alpha_{fw} = \alpha_f \quad \text{and} \quad \alpha_{gw} = \alpha_g, \quad 2.1.3-93$$

which is similar to the bubbly regime.

For the vertically stratified regime

$$\alpha_{fw} = \alpha_f \quad \text{and} \quad \alpha_{gw} = \alpha_g. \quad 2.1.3-94$$

For the horizontally stratified regime

$$\alpha_{fw} = 1 - \frac{\theta}{\pi} \quad \text{and} \quad \alpha_{gw} = \frac{\theta}{\pi}, \quad 2.1.3-95$$

where θ results from the solution of Equations 2.1.3-17 and 2.1.3-18.

The Friction Factor Model

In RELAP5, the friction factor is computed using a high speed calculational scheme representing an engineering approximation to the Colebrook correlation.³⁹

The friction factor model is simply an interpolation scheme linking the laminar, laminar-turbulent transition, and turbulent-full turbulent transition regimes. The laminar friction factor is calculated as

$$\lambda_L = \frac{64}{R} \quad 0 \leq R \leq 2000, \quad 2.1.3-96$$

where R is the Reynolds number. The laminar-turbulent friction factor is interpolated as

$$\lambda_{L,T} = 5.285 \left[1.189 - \left(\frac{4000}{R} \right)^{0.25} \right] (\lambda_{t,4000} - \lambda_{L,2000}) + \lambda_{L,2000} \quad 2000 < R < 4000, \quad 2.1.3-97$$

where $\lambda_{L,2000}$ is the laminar factor at a Reynolds number of 2000 and where $\lambda_{t,4000}$ is the turbulent friction factor at a Reynolds number of 4000. The interpolation factor is defined such that

$$0 \leq 5.285 \left[1.189 - \left(\frac{4000}{R} \right)^{0.25} \right] \leq 1.0 \quad 2.1.3-98$$

The turbulent-full turbulent friction factor is interpolated as

$$\lambda_{t,tt} = \frac{\left[1 - \left(\frac{4000}{R} \right)^{0.25} \right]}{\left[1 - \left(\frac{4000}{R_c} \right)^{0.25} \right]} (\lambda_{tt} - \lambda_{t,4000}) + \lambda_{t,4000} \quad 4000 \leq R \leq R_c, \quad 2.1.3-99$$

where the interpolation factor is defined such that

$$0 \leq \frac{\left[1 - \left(\frac{4000}{R}\right)^{0.25}\right]}{\left[1 - \left(\frac{4000}{R_c}\right)^{0.25}\right]} \leq 1 \quad 2.1.3-100$$

and R_c is the critical Reynolds number at which the Colebrook equation gives a constant friction factor of

$$\lambda_{tt} = [1.74 - 2\text{Log}_{10}(2\epsilon/D)]^{-2}, \quad 2.1.3-101$$

and where ϵ is the surface roughness.

The critical Reynolds number is given as

$$R_c = \frac{378.3}{\frac{2\epsilon}{D} \lambda_{tt}^{0.5}}, \quad 2.1.3-102$$

where $2\epsilon/D \geq 10^{-9}$.

If precise values for $\lambda_{t,4000}$ are used, Equations 2.1.3-96 and 2.1.3-97 are identical to the formulations used in the Colebrook friction factor model for the laminar and transition regimes. Equation 2.1.3-101 is also identical to the solution of the Colebrook model for Reynolds numbers greater than the critical Reynolds number. Therefore, the interpolation scheme in the friction factor model lies in the formulation of Equation 2.1.3-99, which is linear in $(1/R)^{0.25}$. The maximum deviation between the friction factor calculated using Equation 2.1.3-99 and that calculated using the Colebrook correlation is within the third significant figure for a moderate ϵ/D of 0.0003, and as ϵ/D increases the deviation decreases until at an ϵ/D such that $R_c <$

4000 the value given by Equation 2.1.3-99 is precisely that of Equation 2.1.3-101. In any case, the results calculated using Equation 2.1.3-99 are negligibly different from those calculated by the Colebrook equation. This accuracy is achieved using a good estimate for $\lambda_{t,4000}$ given by

$$\lambda_{t,4000} \approx \lambda_0 + K(\lambda_{tt} - \lambda_1) , \quad 2.1.3-103$$

where λ_0 is a constant evaluated from the Blasius smooth pipe formula at a Reynolds number of 4000, such that

$$\lambda_0 = 0.0398. \quad 2.1.3-104$$

The coefficients have been evaluated as

$$K = 0.558 \quad \text{and} \quad \lambda_1 = 0.0158 \quad 2.1.3-105$$

by the method of least squares.

In calculational schemes, it is desirable to evaluate the friction factor in terms of $\lambda|\psi v|$ so that the limiting terms will be correctly calculated as defined by Equations 2.1.3-80. For this case, the Reynolds number must be defined as

$$R = \frac{\rho D}{\mu} |\psi v| \quad 2.1.3-106$$

and Equation 2.1.3-97 can be rewritten as

$$\lambda|\psi v| = \lambda_L^* + L[5.285(1.189 - R^*)](L[(1 - R^*)/(1 - R_C^*)]) \cdot (\lambda_{tt} - \lambda_{t,4000})|\psi v| + \lambda_{t,4000}|\psi v| - \lambda_L^* , \quad 2.1.3-107$$

where $L(y)$ denotes a general limit function such that

$$0 \leq L(y) \leq 1 \quad , \quad 2.1.3-108$$

$$R^* = (4000/R)^{.25} \quad \text{and} \quad R_c^* = (4000/R_c)^{.25} \quad , \quad \text{and} \quad 2.1.3-109$$

$$R \geq 2000 \quad \text{and} \quad R_c \geq 4000 \quad , \quad 2.1.3-110$$

and where the laminar term is

$$\lambda_L^* = \frac{64\mu}{\rho D} \quad . \quad 2.1.3-111$$

The accuracy of the improved friction factor model can be observed in Figure 2.1.3-4, which is a plot of results calculated by Equation 2.1.3-107 compared to similar results calculated by the Colebrook equation. Four curves are plotted for each model representing roughness to diameter ratios of $2\epsilon/D = 0.0, 0.0006, 0.02, \text{ and } 0.1$, respectively. Equation 2.1.3-107 results are plotted and labeled as INTERP in the plot legend. Colebrook equation results are plotted and labeled as COLBRK in the plot legend. The axes of the plot are scaled logarithmically.

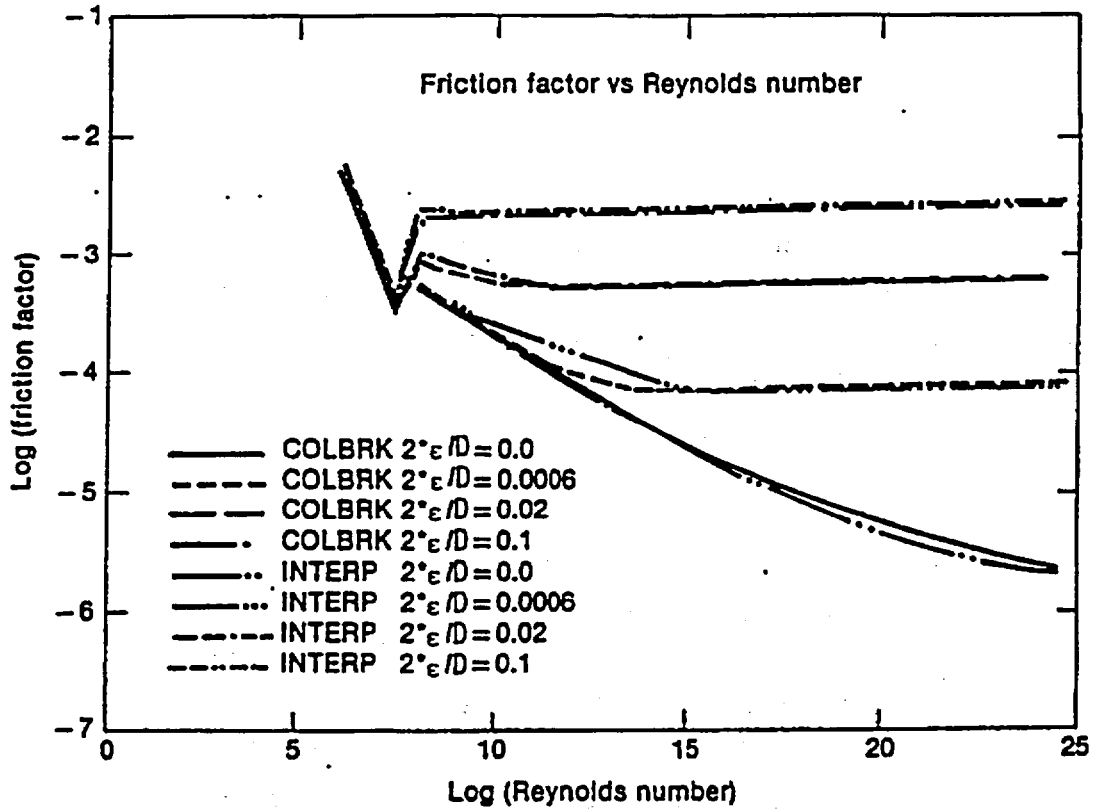


Figure 2.1.3-4. Comparison of Friction Factor for the Colebrook and the Improved RELAP5 Friction Factor Models.

2.1.3.4. Interphase Heat and Mass Transfer

The interface mass transfer is modeled according to the thermodynamic process, interphase heat transfer regime, and flow regime. After the thermodynamic process is decided, the flow regime map discussed in section 2.1.3.1 is used to determine the phasic interfacial area and to select the interphase heat transfer correlation.

The mass transfer model is formulated so that the net interfacial mass transfer rate is composed of two components which are the mass transfer rate at the wall and the mass transfer rate in the bulk fluid, which is expressed as

$$\Gamma_g = \Gamma_w + \Gamma_{ig}$$

2.1.3-112

For system components in which wall heat transfer is modeled, mass transfer at the wall is calculated according to the wall heat transfer model and mass transfer to the bulk fluid is calculated according to the interphase heat transfer regime and flow regime. For system components in which wall heat transfer is not modeled, mass transfer at the wall is ignored and mass transfer in the bulk fluid is modeled according to the interphase heat transfer regime and flow regime.

For components modeling wall heat transfer processes, the interfacial mass transfer at the wall is calculated from the total wall-to-liquid heat transfer minus the wall-to-liquid convective heat transfer. For these processes, the heat transfer model developed by Chen, as discussed in section 2.2.2.1, is used to model the total wall to liquid heat transfer. The Chen model assumes that the total wall-to-liquid heat transfer is composed of boiling and convective heat transfer and that the interfacial mass transfer at the wall is mainly due to boiling heat transfer. Consequently, the contribution due to convective heat transfer must be subtracted from the total wall to liquid heat transfer in

order to calculate the interfacial mass transfer at the wall. Correlations used to calculate interfacial mass transfer at the wall for different heat transfer regimes are discussed in section 2.2.2.

For components not modeling wall heat transfer and for the general bulk mass transfer processes, the interfacial mass transfer in the bulk fluid is modeled according to the flow regime. In the bubbly flow regime, for the liquid side, interfacial mass transfer is the larger of either the model for bubble growth developed by Plesset and Zwick⁴⁷ or the model for convective heat transfer for a spherical bubble,⁴⁸ and for the vapor side, an interphase heat transfer coefficient is assumed that is high enough to drive the vapor temperature toward saturation. Analogously, in the annular mist regime, for the vapor side, a convective heat transfer model for a spherical droplet is used for the interphase heat transfer coefficient, and for the liquid side, an interphase heat transfer coefficient is assumed that is high enough to drive the liquid temperature toward saturation. Correlations used to calculate interfacial mass transfer in the bulk fluid are summarized in Table 2.1.3-1.

For condensation processes, the interfacial mass transfer in the bulk fluid, for the liquid side, is calculated by the Unal bubble collapse model⁴⁹ in the bubbly flow regime and by the Theofanous interfacial condensation model⁵¹ in the annular mist flow regime and for the vapor side, a large interphase heat transfer coefficient is assumed in order to drive the vapor temperature toward saturation.

Table 2.1.3-1. RELAP/MOD2 Interfacial Mass Transfer in Bulk Fluid.

Depressurization Process ($T_f > T_{sat}$)

1. Bubbly Flow Regimes:

$$Q_{if} = H_{if} (T_s - T_f) \cdot \cdot$$

where

$$H_{if} = \text{MAX} \left[\begin{array}{l} \frac{12}{\pi d_b^2} \Delta T_{sat} \frac{\rho_f (C_p) k_f}{\rho_g h_{fg}} \quad (\text{Plesset-Zwick})^{47} \quad (\text{w/m}^3\text{-K}) \\ \frac{6\alpha_g K_f}{d_b^2} (2 + 0.74 \text{Re}_b^{0.5} \text{Pr}_f^{0.333}) \quad (\text{Force convection for single bubble}),^{42} \end{array} \right.$$

$$\text{Re}_b = \frac{\rho_f d_b |v_g - v_f|}{\mu_f} \quad (\text{Bubble Reynolds number}),$$

d_b = bubble diameter (m),

$$Q_{ig} = H_{ig} (T_s - T_g), \text{ and}$$

where

$$H_{ig} = \frac{6\alpha_g}{d_b} k_g \text{Nu}_{ib} \quad \text{and}$$

$$\text{Nu}_{ib} = 10^4 \cdot \cdot$$

2. Annular-Mist Regime:

$$Q_{if} = H_{if} (T_s - T_f),$$

Table 2.1.3-1. (Continued)

where

$$H_{if} = \frac{6 (1-\alpha_g)}{d_b^2} k_f Nu_{id} ,$$

$$Nu_{id} = 10^5, \text{ and}$$

$$Q_{ig} = H_{ig} (T_s - T_g),$$

where

$$H_{ig} = \frac{6(1-\alpha_g)}{d_d^2} \cdot k_g (2. + 0.74 Re_d^{0.5} Pr_g^{0.33}) \\ + 0.0023 (Re)_g^{0.8} \cdot k_g \cdot \frac{(\alpha_g)^{0.5}}{D_e^2} ,$$

$$Re_d = \frac{\rho_g d_d |v_g - v_f|}{\mu_g} \text{ (Droplet Reynolds number), and}$$

d_d = drop diameter (m).

Heat Transfer Process ($T_f \leq T_{sat}$)

1. Bubbly Flow Regime:

$$Q_{if} = H_{if} (T_s - T_f) ,$$

Table 2.1.3-1. (Continued)

where

$$H_{if} = \frac{3\phi C h_{fg} \alpha_g}{\frac{1}{\rho_g} - \frac{1}{\rho_f}} \quad (\text{Unal's correlation}),^{49} \quad \text{and}$$

where

$$\phi = \begin{cases} 1 & v_f \leq 0.61 \text{ (m/s)} \\ [1.639 v_f]^{0.47} & v_f > 0.61 \text{ (m/s)} \end{cases}$$

$$C = \begin{cases} 61 - 6.489 \cdot 10^{-5} (P - 1.7 \cdot 10^5) & P \leq 10^6 \text{ (Pa)} \\ 2.3 \cdot 10^9 / P^{1.418} & P > 10^6 \text{ (Pa)} \end{cases}$$

P = pressure (Pa), and

$$Q_{ig} = H_{ig} (T_s - T_g),$$

where

$$H_{ig} = \frac{6\alpha_g}{d_b^2} k_g \text{Nu}_{ib} \quad \text{and}$$

$$\text{Nu}_{ib} = 10^4.$$

Table 2.1.3-1. (Continued)

2. Annular-Mist Flow Regime:

Similar to the depressurization process.

Condensation Process

1. Bubbly Flow Regime:

Similar to the heat transfer process.

2. Annular-Mist Flow Regime:

$$Q_{if} = H_{if} (T_s - T_f),$$

where

$$H_{if} = 6 \left[2. + \frac{8. (T_s - T_f)}{T_m - T_f} \right] k_f (1 - \alpha_g) / d_d^2 \\ + 10^{-3} \cdot \rho_f \cdot v_f \cdot C_{pf} \cdot A_{film},$$

A_{film} = area of film per unit volume, and

$$T_m = \frac{T_s - T_f}{1 + C_{pg}(T_g - T_s)/h_{fg}}$$

The first term on the right side uses the condensation of a single droplet in superheated steam model developed by Brown.⁵⁰

Table 2.1.3-1. (Continued)

The second term on the right side uses the film condensation model developed by Theofanous.⁵¹

$$Q_{ig} = H_{ig} (T_s - T_f) ,$$

where

$$H_{ig} = \frac{6 \cdot (1-\alpha)}{d_d^2} k_g \cdot Nu_{id} \text{ and}$$

$$Nu_{id} = 10^5 .$$

2.1.3.5. Horizontal Stratification Entrainment Model

Under stratified conditions in horizontal components, the void fraction of flow through a junction may be different from the upstream volume void fraction. Consequently, the regular donoring scheme for junction void fraction is no longer appropriate because vapor may be pulled through the junction and liquid may also be entrained and pulled through the junction. The correlations describing the onset of vapor pull through and liquid entrainment for various geometrical conditions were summarized by Zuber.⁷³

The incipient liquid entrainment is determined by the criterion that

$$v_g \geq v_{ge} \quad , \quad 2.1.3-113$$

where v_{ge} is given by the expressions

$$v_{ge} = 5.7 \left[\frac{D-ll}{d} \right]^{3/2} \left[\frac{B_y (\rho_f - \rho_g) (D-ll)}{\rho_g} \right]^{1/2} \quad 2.1.3-114$$

for an upwardly oriented junction⁷³, and

$$v_{ge} = 3.25 \left[\frac{D/2-ll}{d} \right]^2 \left[\frac{B_y (\rho_f - \rho_g) (D/2-ll)}{\rho_g} \right]^{1/2} \quad 2.1.3-115$$

for a centrally oriented junction,^{74,75} where d is the junction diameter and ll is the liquid level.

The condition for the onset of vapor pull-through is determined by the criterion

$$v_f > v_{fp} \quad , \quad 2.1.3-116$$

where

$$v_{fp} = 3.25 \left[\frac{12 - D_c/2}{d} \right]^{5/2} \left[\frac{B_y (\rho_f - \rho_g) d}{\rho_f} \right]^{1/2}, \quad 2.1.3-117$$

and where

$$c = \begin{cases} 1 & \text{for a centrally located or side junction} \\ 0 & \text{for downward oriented junction.}^{76,77} \end{cases}$$

Equations 2.1.3-113 through 2.1.3-117 together with the horizontal stratification criterion (Equation 2.1.3-15) from section 2.1.3.1, form the basis for calculating the junction void fraction under stratification conditions.

For liquid entrainment, the junction liquid fraction, $\alpha_{f,j}$, is related to the donor volume liquid fraction, $\alpha_{f,K}$, by the expression

$$\alpha_{f,j} = \alpha_{f,k} \left[1 - \exp(-C_1 v_g/v_{ge} - 10v_g^2/v_{gL}^2) \right], \quad 2.1.3-118$$

where v_{gL} is from Equation 2.1.3-16. For vapor pull-through, the junction void fraction, $\alpha_{g,j}$, is given by the expression

$$\alpha_{g,j} = \alpha_{g,k} \left[1 - \exp(-C_2 v_f/v_{fp} - 10v_g^2/v_{gL}^2) \right]. \quad 2.1.3-119$$

The constants C_1 and C_2 for Equations 2.1.3-118 and 2.1.3-119 are obtained by comparisons of code calculations with experimental data.⁷⁸⁻⁸⁰

2.1.3.6. Vertical Stratification Model

The vertical stratification model has been installed so that the nonequilibrium modeling capability can include repressurization transients in which subcooled liquid and superheated vapor may coexist in the pressurizer and/or other locations in the primary coolant system. A version⁸⁸ of this model has been modified, and this modified version is described in this section.

For this model, a vertically stratified flow regime is included in the vertical flow regime map as shown in Figure 2.1.3-2. A vertical volume is detected as being vertically stratified when the difference between the void fraction in the volume above and that in the volume below is greater than 0.50.

The criterion is based on the Taylor bubble velocity in Reference 28. The factor F is calculated first.

$$F = \left[\frac{v_g}{0.35 [gD(\rho_f - \rho_g)/\rho_f]^{1/2}} \right]^3 \quad 2.1.3-120$$

If $F \leq 1$, then the vertical stratification model is not used and the normal vertical flow regime map is used. If $F > 1$, then a linear interpolation is used between the normal flow regime values for the interphase mass transfer, wall heat transfer, and the interphase drag coefficients.

For a vertically stratified volume, the interphase mass transfer, wall heat transfer, and interphase drag coefficients are modified. The interphase mass transfer is given in terms of the interphase heat transfer. The interphase heat transfer rate per unit volume (neglecting contribution from the wall) is given as

$$Q_{if} = h_{if} \frac{A_c}{V} (T^S - T_f) \quad 2.1.3-121$$

and

$$Q_{ig} = h_{ig} \frac{A_c}{V} (T^s - T_g), \quad 2.1.3-122$$

where h_{if} and h_{ig} are the liquid side and vapor side interface heat transfer coefficients, A_c is the cross-sectional flow area (equal to the interfacial area when stratified), and V is the volume. A value of $10 \text{ w/m}^2\text{-K}$ is used for both h_{if} and h_{ig} in the vertical stratification model. The wall heat transfer coefficients h_{wf} and h_{wg} are partitioned with respect to their corresponding vapor and liquid fractions (α_f and α_g) when vertical stratification occurs. For the junction above the vertically stratified volume, an interphase drag coefficient of $10^{-1} \text{ N-s}^2/\text{m}^5$ is used.

There is no specific edit information output for a vertically stratified volume.

2.1.3.7. Water Packing Mitigation Scheme

Large pressure spikes that cannot be explained by known physical phenomena are at times encountered when Eulerian type codes are used to analyze integral systems tests or reactor accidents. These spikes usually do not affect overall transient behavior, but in some cases may affect important localized behavior (e.g. delivery of coolant to the reactor core). A water packing scheme has been installed to mitigate these spikes.

The water packing scheme closely follows the method used in the TRAC code.^{89,90} It involves a detection scheme to determine when a pressure change occurs in a volume containing mostly liquid. It then imposes changes to the momentum equations, followed by a recalculation of the pressure solution using the sparse matrix solver.

The detection logic used in the water packing scheme evolved from experience gained in running a vertical fill problem.⁹¹ The scheme requires a pressure increase of 0.23% or more, a void fraction (α_g) less than or equal to 0.12, the liquid temperature (T_f) to be less than the saturation temperature (T^S), the volume to be flagged as vertically stratified, and the volume above to be highly voided. Thus a legitimate water hammer would not be detected in the water packing scheme.

The next part of the scheme involves altering the momentum equations so that only small pressure changes will occur in the volume that fills with water. The scheme involves modifying the coefficient that multiplies the pressure change in the filling volume. The modification multiplies this coefficient by 10^6 . This is discussed in more detail in the next paragraph. Since the pressure solution is rejected when water packing occurs, the pressure calculation is repeated using the sparse matrix solver.

The finite difference form of the phasic momentum equations used can be written

$$v_{f,j}^{n+1} = v_{f,j}^{n,exp} - (VFDP)_j^n \left[(P_L^{n+1} - P_L^n) - (P_K^{n+1} - P_K^n) \right] \quad 2.1.3-123$$

and

$$v_{g,j}^{n+1} = v_{g,j}^{n,exp} - (VGDP)_j^n \left[(P_L^{n+1} - P_L^n) - (P_K^{n+1} - P_K^n) \right], \quad 2.1.3-124$$

where $v_{f,j}^{n,exp}$ and $v_{g,j}^{n,exp}$ contain all the old time terms and $(VFDP)_j^n$ and $(VGDP)_j^n$ contain all the terms that multiply the pressure change. Consider the filling example in Figure 2.1.3-5 where volume K is full of liquid and volume L is full of steam. The change to the momentum equations is to multiply the $(P_K^{n+1} - P_K^n)$ terms by 10^6 , which forces P_K^{n+1} to be approximately the

same as P_K^n . Thus, the water filled K volume will not show a pressure spike. The momentum equations then have the form

$$v_{f,j}^{n+1} = v_{f,j}^{n,exp} - (VFDP)_j^n (P_L^{n+1} - P_L^n) + (VFDP)_j^n (10^6) (P_K^{n+1} - P_K^n)$$

2.1.3-125

and

$$v_{g,j}^{n+1} = v_{g,j}^{n,exp} - (VGDP)_j^n (P_L^{n+1} - P_L^n) + (VGDP)_j^n (10^6) (P_K^{n+1} - P_K^n).$$

2.1.3-126

In addition to the modification of the momentum equation, the interphase drag is reduced to $10^{-1} (N - s^2)/m^5$ for junction j.

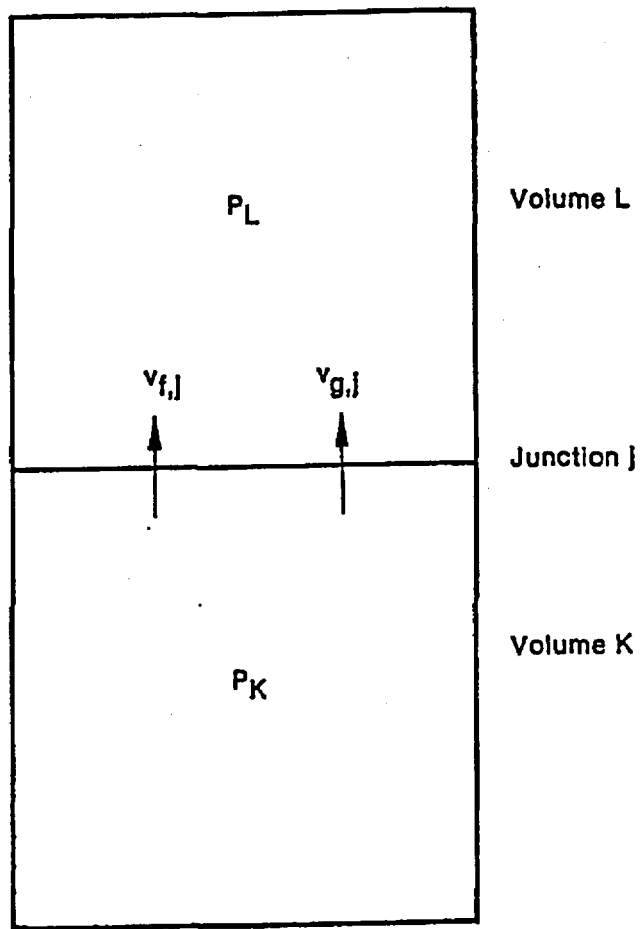


Figure 2.1.3-5. Two Vertical Vapor/Liquid Volumes.

2.1.4. Special Process Models

Certain models in RELAP5/MOD2 have been developed to simulate special processes. These models, described in the following subsections, include: choked flow, abrupt area change, crossflow junction, and branch models.

2.1.4.1. Choked Flow Models

Two mutually exclusive models are available for calculating choked flow in RELAP5/MOD2. The first option uses the original built-in Ransom-Trapp method. The second option uses a table interpolation with any of the four following critical mass flux tables: Extended Henry-Fauske, Moody, HEM, or Murdock-Bauman.

Ransom-Trapp Choked Model

A choked flow model developed by Ransom and Trapp^{62,18} is included in RELAP5 primarily for calculation of the mass discharge from the system at a pipe break or a nozzle. Generally, the flow at the break or nozzle is choked until the system pressure nears the containment pressure. The choked flow model is used to predict if the flow is choked at the break or nozzle and, if it is, to establish the discharge boundary condition. In addition, the choked flow model can be used to predict existence of and calculate choked flow at internal points in the system.

Choking is defined as the condition wherein the mass flow rate becomes independent of the downstream conditions (that point at which further reduction in the downstream pressure does not change the mass flow rate). The fundamental reason that choking occurs is that acoustic signals can no longer propagate upstream. This occurs when the fluid velocity equals or exceeds the propagation velocity. The choked flow model is based on a definition that is established by a characteristic analysis using time-dependent differential equations.

Consider a system of n first-order quasi-linear, partial differential equations of the form

$$A(U) (\partial U / \partial t) + B(U) (\partial U / \partial x) + C(U) = 0 \quad . \quad 2.1.4-1$$

The characteristic directions (or characterization velocities) of the system are defined^{63,64} as the roots, $\lambda_i (i \leq n)$, of the characteristic polynomial

$$(A\lambda - B) = 0 \quad . \quad 2.1.4-2$$

The real part of any root, λ_i , give the velocity of signal propagation along the corresponding characteristic path in the space/time plane. An imaginary part of any complex root, λ_i , gives the rate of growth or decay of the signal propagating along the respective path. For a hyperbolic system in which all the roots of Equation 2.1.4-2 are real and nonzero, the number of boundary conditions required at any boundary point equals the number of characteristic lines entering the solution region as time increases. If we consider the system (Equation 2.1.4-1) for a particular region $0 \leq x \leq L$, and examine the boundary conditions at $x = L$, as long as any λ_i is less than zero, we must supply some boundary information to obtain the solution. If λ_i is greater than or equal to zero, no boundary conditions are needed at $x = L$, and the interior solution is unaffected by conditions beyond this boundary.

A choked condition exists when no information can propagate into the solution region from the exterior. Such a condition exists at the boundary point, $x = L$, when

$$\lambda_j \geq 0 \text{ for all } j \leq n \quad . \quad 2.1.4-3$$

These are the mathematical conditions satisfied by the equations of motion for a flowing fluid when reduction in downstream

pressure ceases to result in increased flow rate. It is well-known⁶⁵ that the choked condition for single-phase flow occurs when the fluid velocity just equals the local sound speed. For this case, one of the λ_j 's is just equal to zero. For the two-phase case, it is possible for all λ_j 's to be greater than zero under special conditions which can exist during discharge of a subcooled liquid.

During the course of the RELAP5 development, extensive investigation was carried out to determine two-phase choked flow criterion under two assumed conditions:^a (a) thermal equilibrium between phases, and (b) adiabatic phases without phase change (frozen).⁶⁶ The frozen assumption was in poor agreement with data, compared to the thermal equilibrium assumption. Therefore, the thermal equilibrium assumption with slip is used as the basis for the RELAP5 choked flow criterion. In the following paragraphs, theoretical aspects of choked flow are discussed.

Ransom-Trapp Model Choking Criterion for Nonhomogeneous, Equilibrium Two-Phase Flow

The two-fluid model for the conditions of thermal equilibrium (equilibrium interphase mass transfer) is described by the overall mass continuity equation, two phasic momentum equations, and the mixture entropy equation. This system of equations is

$$\partial(\alpha_g \rho_g + \alpha_f \rho_f) / \partial t + \partial(\alpha_g \rho_g v_g + \alpha_f \rho_f v_f) / \partial x = 0, \quad 2.1.4-4$$

$$\begin{aligned} \alpha_g \rho_g [\partial v_g / \partial t + v_g (\partial v_g / \partial x)] + \alpha_g (\partial P / \partial x) \\ + C \alpha_g \alpha_f \rho (\partial v_g / \partial t - \partial v_f / \partial t) = 0, \quad 2.1.4-5.. \end{aligned}$$

^aThe hydrodynamic model is not based on either of these assumptions; however, the purpose of this analysis is simply to establish a criterion for choked flow and thus, there is no conflict with the basic hydrodynamic model.

$$\alpha_f \rho_f [\partial v_f / \partial t + v_f (\partial v_f / \partial x)] + \alpha_f (\partial P / \partial x) + C \alpha_f \alpha_g \rho (\partial v_f / \partial t - \partial v_g / \partial t) = 0, \quad 2.1.4-6$$

and

$$\partial (\alpha_g \rho_g S_g + \alpha_f \rho_f S_f) / \partial t + \partial (\alpha_g \rho_g S_g v_g + \alpha_f \rho_f S_f v_f) / \partial x = 0. \quad 2.1.4-7$$

The momentum equations include the interphase force terms due to relative acceleration.¹⁶ These force terms have a significant effect on wave propagation velocity and consequently on the choked flow velocity. The particular form chosen is frame invariant and symmetrical, and the coefficient of virtual mass, $C \alpha_g \alpha_f \rho$, is chosen to ensure a smooth transition between pure vapor and pure liquid. For a dispersed flow, the constant, C , has a theoretical value of 0.5, whereas for a separated flow, the value may approach zero. The energy equation is written in terms of mixture entropy, which is constant for adiabatic flow (the energy dissipation associated with interphase mass transfer and relative phase acceleration is neglected).

The nondifferential source terms, $C(U)$, in Equation 2.1.4-1 do not enter into the characteristic analysis or affect the propagation velocities. For this reason, the source terms associated with wall friction, interphase drag, and heat transfer are omitted for brevity in Equations 2.1.4-4 through 2.1.4-7.

In the thermal equilibrium case, ρ_g , ρ_f , S_g , and S_f are known functions of the pressure only (the vapor and liquid values along the saturation curve). The derivatives of these variables are designated by an asterisk as follows

$$\rho_f^* = d\rho_f^S / dP \text{ and } \rho_g^* = d\rho_g^S / dP, \quad 2.1.4-8$$

and

$$S_f^* = dS_f^S/dP \text{ and } S_g^* = dS_g^S/dP \quad . \quad 2.1.4-9$$

The system of governing equations (Equations 2.1.4-4 through 2.1.4-7) can be written in terms of the four dependent variables, α_g , P , v_g , and v_f , by application of the chain rule and the property derivatives (Equations 2.1.4-8 and 2.1.4-9). Thus, the system of equations can be written in the form of Equation 2.1.4-1 where the A and B are fourth-order square coefficient matrices.

The characteristic polynomial that results is fourth-order in λ and factorization can only be carried out approximately to obtain the roots for λ , and establish the choking criterion. The first two roots are

$$\lambda_{1,2} = \frac{\left[\begin{array}{l} \left\{ \alpha_{fg} \rho_g + \rho C/2 \pm \left[(\rho C/2)^2 - \alpha_g \alpha_{fg} \rho_g \rho_f \right]^{1/2} \right\} v_g \\ + \left\{ \alpha_g \rho_f + \rho C/2 + \left[(\rho C/2)^2 - \alpha_g \alpha_{fg} \rho_g \rho_f \right]^{1/2} \right\} v_f \end{array} \right]}{(\alpha_{fg} \rho_g + \rho C/2) + (\alpha_g \rho_f + \rho C/2)}$$

2.1.4-10

These two roots are obtained by neglecting the fourth-order factors relative to the second-order factors in $(\lambda - v_g)$ and $(\lambda - v_f)$. There are no first- or third-order factors. Inspection of Equation 2.1.4-10 shows that $\lambda_{1,2}$ have values between v_g and v_f ; thus, the fourth-order factors $(\lambda - v_g)$ and $(\lambda - v_f)$ are small (i.e., neglecting these terms is justified). The values for $\lambda_{1,2}$ may be real or complex depending on the sign of the quantity $[(\rho C/2)^2 - \alpha_g \alpha_{fg} \rho_g \rho_f]$.

The remaining two roots are obtained by dividing out the quadratic factor containing $\lambda_{1,2}$, neglecting the remainder, and subsequent factorization of the remaining quadratic terms. [This procedure can be shown to be analogous to neglecting the second- and higher-order terms in the relative velocity, $(v_g - v_f)$.] The remaining roots are

$$\lambda_{3,4} = v + D(v_g - v_f) \pm a, \quad 2.1.4-11$$

where

$$v = (\alpha_g \rho_g v_g + \alpha_f \rho_f v_f) / \rho, \quad 2.1.4-12$$

$$a = a_{HE} \left\{ \left[C\rho^2 + \rho(\alpha_g \rho_f + \alpha_f \rho_g) \right] / (C\rho^2 + \rho_g \rho_f) \right\}^{1/2}, \quad 2.1.4-13$$

and

$$D = 0.5 \left[\frac{(\alpha_g \rho_f - \alpha_f \rho_g)}{(\rho C + \alpha_f \rho_g + \alpha_g \rho_f)} + \frac{\rho_g \rho_f (\alpha_f \rho_f - \alpha_g \rho_g)}{\rho (\rho_g \rho_f + C\rho^2)} - a_{HE}^2 \frac{\rho [\alpha_g \rho_g^2 S_g^* + \alpha_f \rho_f^2 S_f^*]}{\rho_g \rho_f (S_g - S_f)} \right]. \quad 2.1.4-14$$

The quantity, a_{HE} , is the homogeneous equilibrium speed of sound. The roots, $\lambda_{3,4}$, have only real values.

The general nature and significance of these roots is revealed by applying the characteristic considerations. The speed of propagation of small disturbances is related to the values of the characteristic roots. In general, the velocity of propagation corresponds to the real part of a root and the growth or attenuation is associated with the complex part of the root.

Choking will occur when the signal, which propagates with the largest velocity relative to the fluid, is just stationary, that is,

$$\lambda^R = 0 \text{ for } j \leq 4 \quad 2.1.4-15$$

and

$$\lambda^R \geq 0 \text{ for all } i \neq j \quad 2.1.4-16$$

The existence of complex roots for $\lambda_{1,2}$ makes the initial boundary value problem ill-posed. This problem has been discussed by many investigators^{13,20} and the addition of any small, second-order viscous effects renders the problem well-posed.^{13,21} The whole phenomenon of systems with mixed orders of derivatives and a first-order system with the addition of a small, second-order term, has been discussed and analyzed by Whitham.⁶⁴ He has shown that the second-order viscous terms give infinite characteristic velocities. However, very little information is propagated along these characteristic lines and the bulk of the information is propagated along characteristic lines defined by the first-order system. We conclude that the ill-posed nature of Equations 2.1.4-4 through 2.1.4-7 can be removed by the addition of small, second-order viscous terms that have little effect upon the propagation of information. Therefore, the choking criterion for the two-phase flow system analyzed here is established from Equation 2.1.4-15.

The explicit character of the choking criterion for the two-phase flow model defined by Equations 2.1.4-4 through 2.1.4-7 is examined. Since the two roots, $\lambda_{1,2}$, are between the phase velocities, v_f and v_g , the choking criterion is established from the roots, $\lambda_{3,4}$, and Equation 2.1.4-15. The choking criterion is

$$v + D(v_g - v_f) = ia. \quad 2.1.4-17$$

The choking criterion can be rewritten in terms of the mass mean and relative Mach numbers

$$M_V = v/a \text{ and } M_R = (v_g - v_f)/a \quad 2.1.4-18$$

as

$$M_V + DM_R = 1. \quad 2.1.4-19$$

This relation is similar to the choking criterion for single-phase flow where only the mass average Mach number appears and choking corresponds to a Mach number of unity.

The choking criterion (Equation 2.1.4-19) is a function of the two parameters, D and a . In Figure 2.1.4-1, a is plotted as a function of the void fraction, α_g , for a typical steam/water system at 7.5 MPa with C equal to zero (the stratified equilibrium sound speed), C equal to 0.5 (the typical value for a dispersed flow model), and in the limiting case when C become infinite (homogeneous equilibrium sound speed). From Figure 2.1.4-1 it is evident that the virtual mass coefficient has a

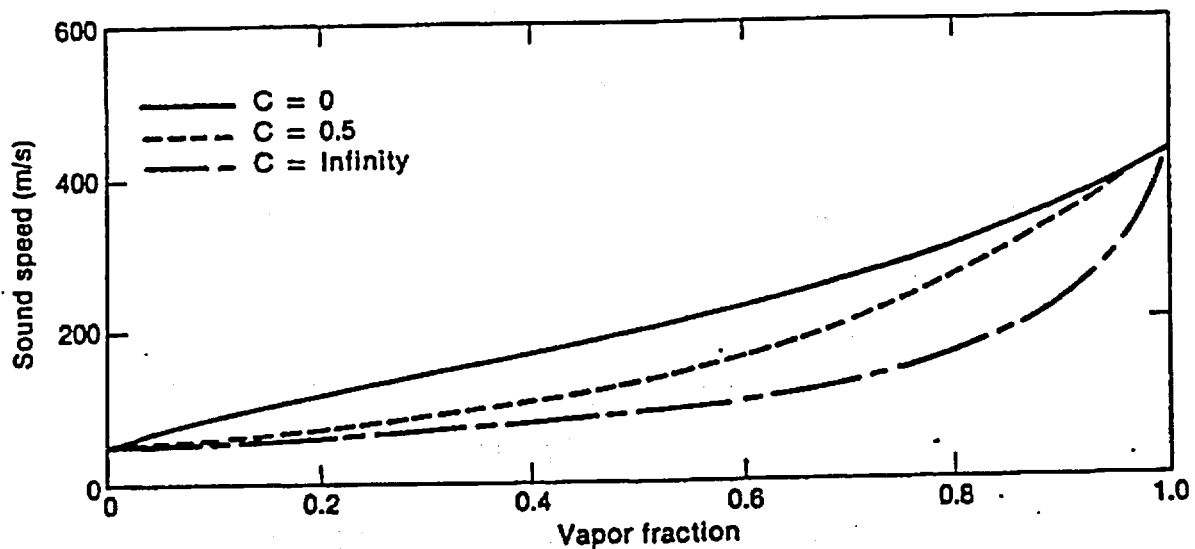


Figure 2.1.4-1. Equilibrium Speed of Sound as a Function of Void Fraction and Virtual Mass Coefficient.

significant effect upon the choked two-phase flow dynamics.¹⁴

To establish the actual choked flow rate for two-phase flow with slip, the relative velocity term in Equation 2.1.4-19 must also be considered. The relative Mach number coefficient, D , is shown in Figure 2.1.4-2 for values of C equal to 0, 0.5, and ∞ . It is evident from these results that the choked flow velocity can differ appreciably from the mass mean velocity when slip occurs. It is significant that the variation of the choked flow criterion from the homogeneous result is entirely due to velocity nonequilibrium, since these results have been obtained under the assumption of thermal equilibrium. The particular values of

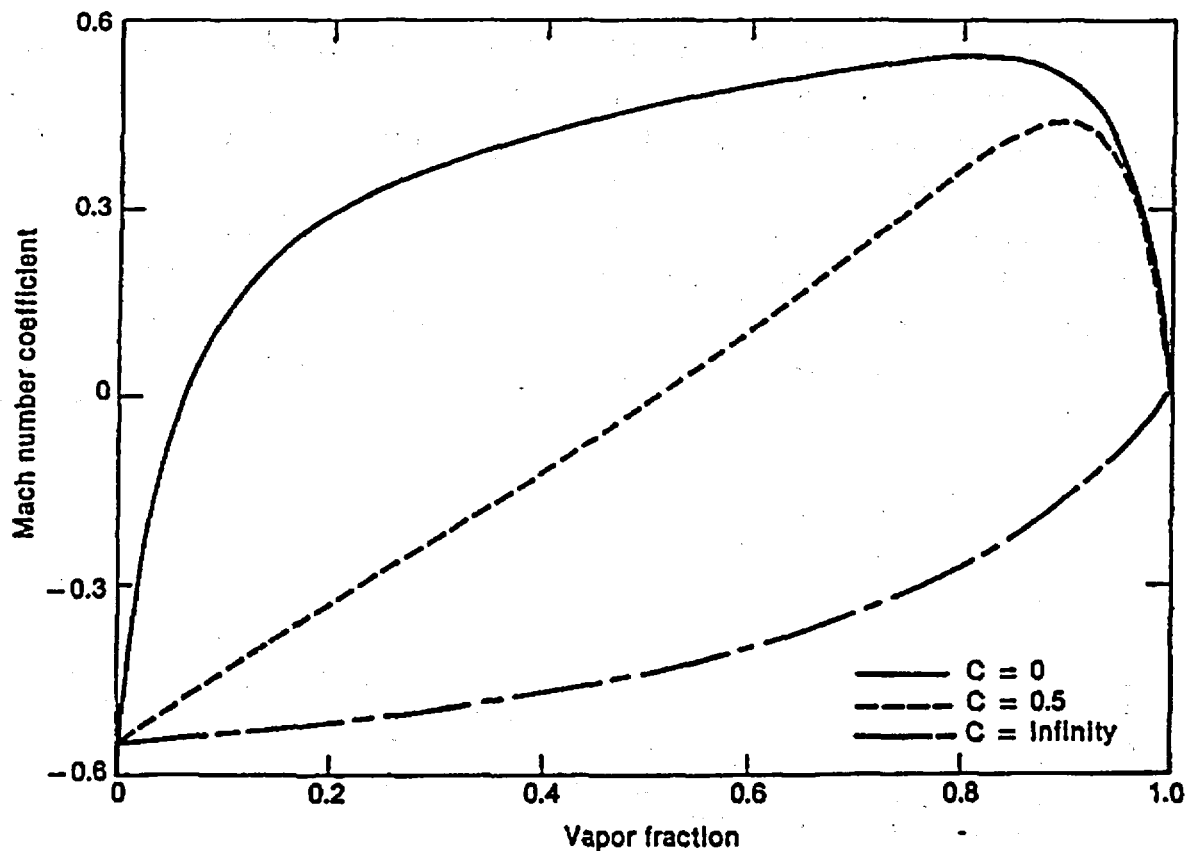


Figure 2.1.4-2. Coefficient of Relative Mach Number for Thermal Equilibrium Flow as a Function of Void Fraction and Virtual Mass Coefficient.

these parameters used in the model are discussed later in this section.

Ransom-Trapp Subcooled Choking Criterion

The previous analysis assumes two-phase conditions exist throughout the break flow process. However, initially and in the early phase of blowdown, the flow approaching the break or break nozzle will be subcooled liquid. Under most conditions of interest in LWR systems, the fluid undergoes a phase change at the break. The transition from single- to two-phase flow is accompanied by a discontinuous change in the fluid bulk modulus. This is especially true for the liquid-to-liquid/vapor transition. For example, at 600 KPa, the ratio of the single- to two-phase sound speed at the liquid boundary is 339.4. Thus, considerable care must be exercised when analyzing a flow having transitions to or from a pure phase (a discontinuity is also present at the vapor boundary, but the ratio is only 1.069).

To understand the physical process that occurs for subcooled upstream conditions, consider the flow through a converging/diverging nozzle connected to an upstream plenum with subcooled water at a high pressure. For a downstream pressure only slightly lower than the upstream pressure, subcooled liquid flow will exist throughout the nozzle. Under these conditions the flow can be analyzed using Bernoulli's equation, which predicts a minimum pressure, P_t , at the throat.^a As the downstream pressure is lowered further, a point is reached where the throat pressure equals the local saturation pressure, P_{sat} . If the downstream pressure is lowered further, vaporization will take place at the throat.^b When this happens, the fluid sound

^aFor all practical cases of choking, the subcooled water can be considered incompressible with infinite sound speed.

^bAn idealized one-dimensional homogeneous equilibrium model is assumed in the example.

speed lowers drastically, but continuity considerations dictate that the velocity, v_t , of the two-phase mixture (at the point of minuscule void fraction) just equals the velocity of the subcooled water slightly upstream of the throat. When this occurs, v_t in the subcooled region is less than the water sound speed, but in the two-phase region, v_t can be greater than the two-phase sound speed. Hence, the subcooled water has a Mach number (M) less than one, whereas the two-phase mixture at the throat has a Mach number greater than one. Under these conditions (Mach numbers greater than one in the two-phase region), downstream pressure effects are not propagated upstream and the flow is choked. In particular, the supersonic two-phase fluid at the throat must increase in velocity and the pressure drop as it expands in the diverging section^a (transition back to

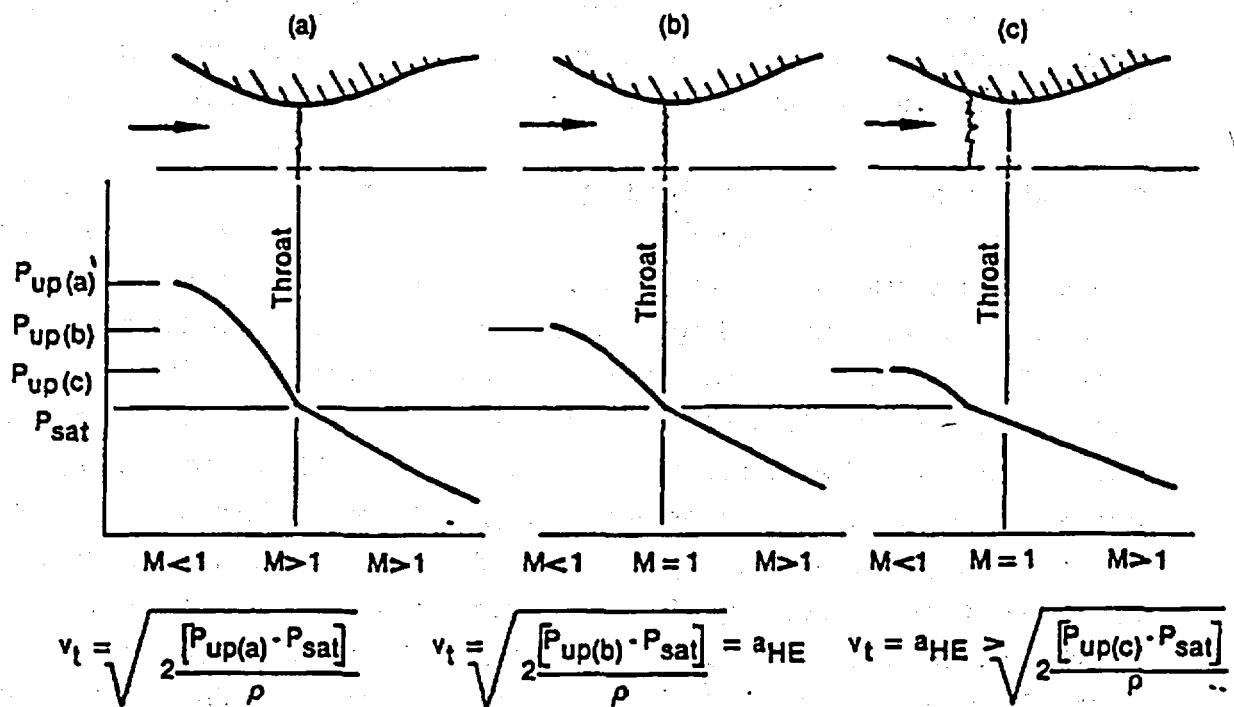


Figure 2.1.4-3. Subcooled Choking Process.

^aIn a supersonic flow, a diverging nozzle implies an increase in velocity.

subsonic flow can occur in the nozzle as a result of a shock wave). The choked condition is shown in Figure 2.1.4-3(a).

Contrary to the usual single-phase choked flow in a converging/diverging nozzle, there is no point in the flow field where $M = 1$. This is because in the homogeneous equilibrium model the fluid undergoes a discontinuous change in sound speed from single-phase subcooled conditions to two-phase conditions, although the fluid properties are continuous through the transition point.

When this condition prevails, the flow rate can be established from application of Bernoulli's equation ($1/2 \rho v_t^2 = P_{up} - P_{sat}$). For a further decrease in the downstream pressure, no further increase in upstream fluid velocity will occur as long as the upstream conditions are maintained constant.

Now consider the process where a subcooled choked flow, as described above, initially exists (with a very low downstream pressure) and the upstream pressure is lowered. As the upstream pressure decreases, the pressure at the throat will remain at P_{sat} and Bernoulli's equation will give a smaller subcooled water velocity (v_t) at the throat. As P_{up} is lowered further, a point is reached where $v_t = a_{HE}$ and $M = 1$ on the two-phase side of the throat (the Mach number in the subcooled portion upstream of the throat is much less than one). This situation is shown schematically in Figure 2.1.4-3(b).

As the upstream pressure is lowered further, the point where the pressure reaches P_{sat} must move upstream of the throat [see... Figure 2.1.4-3(c)]. The subcooled water velocity at the P_{sat} location is smaller than the two-phase sound speed and the flow is subsonic. In the two-phase region between the point at which P_{sat} is reached and the throat, the Mach number is less than 1, but increases to $M = 1$ at the throat, that is, the two-phase

sonic velocity is reached at the throat (as in the case of choked flow having a continuous variation of sound speed with pressure). As P_{up} is lowered still further, the P_{sat} point moves upstream until the flow becomes completely two-phase.

The homogeneous assumption applied in the above subcooled choking description is very close to the real situation when vapor is first formed. However, nonequilibrium can result in a superheated liquid state at a throat pressure, P_t , much lower than the saturation pressure, P_{sat} . The onset of vaporization occurs at P_t instead of P_{sat} .

The pressure undershoot, $P_{sat} - P_t$, can be described by the Alamgir-Lienhard-Jones correlation⁶⁷⁻⁶⁹

$$P_{sat} - P_t = \text{MAX} (\Delta P, 0) , \quad 2.1.4-20$$

with

$$\Delta P = 0.258 \sigma^{3/2} T^{13.76} \left[1 + 13.25 \sum'^{0.8} \right]^{1/2} / \left[(k_B T_C)^{1/2} (1 - v_f v_g) \right] - 0.07^2 (A_t/A) \left[\rho v_C^2 / 2 \right] . \quad 2.1.4-21$$

The first term in ΔP represents the static depressurization effect and is derived by Alamgir and Lienhard⁶⁸ based on classical nucleation theory. For steady flow in a nozzle, the depressurization rate, Σ' , can be shown to be

$$\Sigma' = \left[\rho v_C^3 / A_t \right] (dA/dx)_t . \quad 2.1.4-22$$

Note that in Equation 2.1.4-21 Σ' is in units of Matm/s, but in Equation 2.1.4-22, Σ' is in units of Pa/s. Here, $(dA/dx)_t$ is the variation of area with respect to axial length and is to be

evaluated at the throat. The second term in ΔP (Equation 2.1.4-21) represents the turbulence effect and is developed by Jones.⁶⁹

The choking velocity, based upon the process shown in Figure 2.1.4-3(a), can be calculated by applying Bernoulli's equation

$$v_c = \left[v_{up}^2 + 2 (P_{up} - P_t) / \rho \right]^{1/2}, \quad 2.1.4-23$$

where P_t is to be computed from Equation 2.1.4-20.

For the process shown in Figures 2.1.4-3(b) and (c)

$$v_c = a_{HE}, \quad 2.1.4-24$$

and the two-phase choking criterion applies.

To determine which of the above situations exists, both v_c 's are calculated and the larger is used as the choking velocity to be imposed at the throat. This velocity is imposed numerically at the throat in exactly the same manner as the choking criterion used for the two-phase condition described previously.

The subcooled choking model is very similar to models proposed by Burnell⁷⁰ and Moody;⁷¹ however, the criterion for transition from subcooled choking to two-phase choking is now better understood and is in agreement with the physics of two-phase flow. The model here is also in agreement with cavitating venturi experience (experimentally confirmed behavior).

Ransom-Trapp Horizontal Stratified Choked Flow

Under stratified conditions, the void fraction of the flow out of a small break may be quite different from the upstream void

fraction. The usual definition of the outlet void fraction as a donored void fraction is no longer applicable. A simple approach based on the height of the liquid level and a criterion for the stability of small disturbances is used to determine the junction void fraction for stratified break flow.

By balancing the upward pressure force due to the Bernoulli effect and the downward gravitational force acting on a small surface perturbation, Taitel and Dukler²⁷ developed the following criterion for transition from the stratified horizontal flow regime in a round pipe

$$v_g > \left[\frac{(\rho_f - \rho_g) B_v \alpha_g A}{\rho_g dA_f/dH_f} \right]^{1/2} \left(1 - \frac{H_f}{D} \right) \quad 2.1.4-25$$

In Equation 2.1.4-25, A_g and A_f are the flow areas of vapor and liquid, respectively. The right side of Equation 2.1.4-25 is the limiting vapor velocity designated by v_{gL} . The following geometrical relationships define H_g and H_f .

$$H_g = D (1 - \cos\theta)/2 \quad 2.1.4-26$$

and

$$H_f = D (1 + \cos\theta)/2, \quad 2.1.4-27$$

where θ is the central angle formed by a vertical cord and a radius to the liquid vapor interface. It can be shown that dA_f/dH_f equals $D \sin \theta$ and hence v_{gL} becomes

$$v_{gL} = 1/2 \left[\frac{(\rho_f - \rho_g) B_v \alpha_g A}{\rho_g D \sin\theta} \right]^{1/2} (1 - \cos\theta) \quad 2.1.4-28$$

Let D_t be the diameter of the break area. When the liquid level is above the break [i.e., $H_f > (D + D_t)/2$], the outlet void fraction, $\alpha_{g,j}$, which accounts for the pull-through of vapor, is defined as

$$\alpha_{g,j} = \alpha_{g,K} (v_g/v_{gL})^{1/2}, \quad 2.1.4-29$$

where $\alpha_{g,K}$ and v_g are the void fraction and vapor velocity upstream of the outlet. If the liquid level falls below the break [i.e., $H_f < (D - D_t)/2$], liquid entrainment is modeled by defining the outlet liquid fraction, $\alpha_{f,j}$, as

$$\alpha_{f,j} = \alpha_{f,K} (v_g/v_{gL})^{1/2}, \quad 2.1.4-30$$

where $\alpha_{f,K}$ is the liquid volume fraction upstream of the outlet. The equality, $\alpha_{g,j} + \alpha_{f,j} = 1$, is used to obtain $\alpha_{g,j}$ ($\alpha_{f,j}$), if $\alpha_{f,j}$ ($\alpha_{g,j}$) is known. When the liquid level lies within the outlet area [i.e., $(D + D_t)/2 > H_f > (D - D_t)/2$], the void fraction is obtained by interpolation of the two void fractions computed at the boundaries.

Implementation of the Ransom-Trapp Choked Flow Model

Ideally, the two-phase choking criterion (Equation 2.1.4-17) can be used as a boundary condition for obtaining flow solutions. However, the applicability of Equation 2.1.4-17 has not been fully explored. Instead, an approximate criterion

$$(\alpha_g \rho_f v_g + \alpha_f \rho_g v_f) / (\alpha_g \rho_f + \alpha_f \rho_g) = \pm a_{HE} \quad 2.1.4-31$$

has been applied extensively and has produced good code/data comparisons. Equation 2.1.4-31 can be derived from Equation 2.1.4-17 by neglecting the third term in D and setting $C = 0$ (stratified) on the right side of Equation 2.1.4-17 and $C = \infty$

(homogeneous) on the left side. Because of extensive experience with this approximate model, Equation 2.1.4-31 is currently used in RELAP5/MOD2 choked flow calculations.

At each time step and at each flow junction where two-phase cocurrent flow exists, the choking criterion (Equation 2.1.4-31) is checked using explicitly calculated values. When choking occurs, Equation 2.1.4-31 is solved semi-implicitly with the upstream vapor and liquid momentum equations for v_g , v_f , and P_t , throat pressure, at the point of flow choking (upstream is with reference to v_g and v_f). As P_t is not needed in system calculations, we can eliminate $\partial P/\partial x$ from the vapor and liquid momentum equations to obtain

$$\begin{aligned} & \rho_g \left[\partial v_g / \partial t + 1/2 \partial v_g^2 / \partial x \right] - \rho_f \left[\partial v_f / \partial t + 1/2 \partial v_f^2 / \partial x \right] \\ & = \rho_g - \rho_f B_x + \Gamma_g (v_I - \alpha_f v_g - \alpha_g v_f) / \alpha_f \alpha_g \\ & - \rho_g v_g^{FWG} + \rho_f v_f^{FWF} - \rho_f \rho_g (v_g - v_f) FI \\ & - C \rho \partial (v_g - v_f) / \partial t \end{aligned} \quad 2.1.4-32$$

The finite difference form of this equation is obtained by integrating with respect to the spatial variable from the upstream volume center to the junction. In this finite-difference equation, all junction velocities are evaluated implicitly; a_{HE}^{n+1} is approximated by

$$a_{HE}^{n+1} = a_{HE}^n + (\partial a_{HE} / \partial P) (P^{n+1} - P^n), \quad 2.1.4-33$$

where P is the upstream volume pressure. The finite-difference equations corresponding to Equations 2.1.4-31 and 2.1.4-32 can be solved for v_g^{n+1} and v_f^{n+1} in terms of P^{n+1} and old time values.

In the case of subcooled choking, the choking criterion (Equation 2.1.4-31) and the velocity equation (Equation 2.1.4-32) reduce to

$$v_f = v_g = \pm v_c . \quad 2.1.4-34$$

Here, v_c is determined according to the procedures described previously. The frictional pressure losses and gravity head, which do not appear in the ideal Equation 2.1.4-23 are properly taken into account in the actual calculation.

In general, there is a large drop in critical velocity when the fluid changes from a subcooled state to a two-phase state. This sudden change often leads to unrealistic velocity oscillations and causes the time step size to be reduced considerably. To provide a smooth transition from subcooled to two-phase, a transition region is defined as in the low void region. Within the transition region, an underrelaxation scheme,

$$v_g^{n+1} = v_g^n + 0.1 \left[v_g^{n+1} - v_g^n \right]$$

and

2.1.4-35

$$v_f^{n+1} = v_f^n + 0.1 \left[v_f^{n+1} - v_f^n \right]$$

is implemented. Experience with this scheme indicates that it works satisfactorily.

Tabular Choked Flow Models

The extended Henry-Fauske¹¹³, Moody¹¹⁴, HEM and Murdock-Bauman¹¹⁵ critical flow models are new options added for evaluation model calculations. Each of these models, extracted from the RELAP46D code, consist of tabular critical mass fluxes as functions of upstream volume stagnation pressure and enthalpy. These tables are listed in Appendix C.

$$G_C = f(P_0, h_0) ,$$

2.1.4-36

where

G_C = critical mass flux (lbm/ft²-s),

P_0 = upstream volume stagnation pressure (psia), and

h_0 = upstream volume stagnation enthalpy (Btu/lbm).

The user has the option to select static volume pressure and enthalpy or stagnation properties for the interpolation within these supplied models. The calculated critical mass flux will be compared with the mass flux calculated by the RELAP5 momentum equations at each time step. If the former is smaller than the latter, choking is assumed to occur and phasic velocities will be calculated based on the critical mass flux.

Since the RELAP5 code derives the total junction mass fluxes only in terms of the junction phasic velocities, the total mass flux from the tables must be translated into equivalent liquid and vapor velocities. The energy flux calculations must be separated similarly.

$$G_C = \alpha_g \rho_g V_g + \alpha_f \rho_f V_f$$

2.1.4-37

and

$$G_{Ch} = \alpha_g \rho_g V_{ghg} + \alpha_f \rho_f V_{fhf} ,$$

2.1.4-38

where

α = volume fraction,

ρ = density (lbm/ft³),

v = velocity (ft/s),

h = static upstream enthalpy (Btu/lbm),

and the subscripts denote

g = vapor phase and

f = liquid phase.

The phasic velocities are defined by the slip between the liquid and steam during two-phase conditions where the slip ratio, s , is defined as

$$s = V_g / V_f. \quad 2.1.4-39$$

There are several slip models available in the code. These models include homogeneous (no slip), constant slip, Moody's slip, RELAP5 momentum equation slip, and upstream volume equilibrium quality slip. They are described as follows:

1. Homogeneous

$$V_f = V_g. \quad 2.1.4-40$$

2. Constant slip ratio

s = user input constant .

3. Moody's slip ratio

$$s = (v_g / v_f)^{1/3}, \quad 2.1.4-41...$$

where

v_g = saturated steam specific volume and
 v_f = saturated liquid specific volume.

4. RELAP5 momentum equation slip ratio

$$s = V_g / V_f , \quad 2.1.4-42$$

where the phasic velocities are calculated by the momentum equation.

5. Equilibrium quality slip ratio

$$s = \begin{cases} X_e \rho_f \alpha_f / [(1 - X_e) \rho_g \alpha_g] & X_e \leq 0.5 \\ (1 - X_e) \rho_g \alpha_g / [X_e \rho_f \alpha_f] & X_e > 0.5 . \end{cases} \quad 2.1.4-43$$

Each slip model has the option to smooth the slip ratio and specify a minimum and maximum value. The smoothing is provided in the form

$$s^{n+1} = 0.1 s^{n+1} + 0.9 s^n . \quad 2.1.4-44$$

The slip ratio calculated by one of the above models will be used to determine the phasic velocity.

$$V_f = G_c / (\alpha_g \rho_g s + \alpha_f \rho_f) \quad 2.1.4-45$$

and

$$V_g = s V_f . \quad 2.1.4-46$$

Note that all these slip models may not be consistent with the tabular critical flow model formulations.

Some of the added critical flow models may have limitations imposed over which fluid conditions they can be applied. Table 2.1.4-1 shows the conditions over which the individual models may be applied. A discontinuity arises at the saturation boundaries

because two separate models without consistent end points meet. To prevent unreasonable time step size reductions and to provide a smooth transition from the subcooled region to the two-phase region, where the critical mass flux decreases significantly, the following smoothing options are available. Based on either a quality or void fraction criteria the smoothing

$$v^{n+1} = v^n + 0.1 (v^{n+1} - v^n) \quad 2.1.4-47$$

is applied if

$$0.0 < |(h_0 - h_{f0}) / h_{fg}| < e \quad \text{for quality, or}$$

$$\alpha_{gl} \leq \alpha_g \leq \alpha_{gu} \quad \text{for void fraction,}$$

where

h_{fg} = latent heat of vaporization at P_0 ,
 $n+1, n$ = time step,
 e = transition criteria (based on user input),
 α_{gl} = lower void fraction transition limit (input), and
 α_{gu} = upper void fraction transition limit (input).

Equation 2.1.4-47 is the same technique used in the original RELAP5 choked flow model.

The stagnation properties are the theoretical basis of the critical flow models described above. The stagnation pressure and enthalpy are calculated from the static upstream volume pressure and enthalpy assuming isentropic flow. The stagnation enthalpy is calculated from the kinetic energy relationship using a calculated fluid velocity.

$$h_0 = h_1 + V^2/2C, \quad 2.1.4-48$$

where

h_1 = upstream volume static enthalpy (Btu/lbm) and

C = conversion factor from (ft-lbm) to (Btu):

Applying the basic energy equation in differential form,

$$Tds = dh - v dP, \quad 2.1.4-49$$

and assuming an isentropic process ($ds = 0$),

$$dP = dh / v. \quad 2.1.4-50$$

Integrating Equation 2.1.4-50 over the change in enthalpy from static to stagnation limit gives

$$P_0 = P_1 + \int_{h_1}^{h_0} dh/v, \quad 2.1.4-51$$

where

P_1 = upstream volume static pressure (psia) and

v = specific volume (ft³/lbm).

Equation 2.4.1-51 is evaluated between the limits (h_1, P_1) and (h_0, P_0) by a fourth-order Runge-Kutta technique. The specific volume is obtained from the steam tables.

In order to minimize computational time, the stagnation property will not be calculated if the upstream volume phase is not liquid and at the same time the Mach number of the average volume flow is less than 0.3. Also if

$$(h_0 - h_1) / h_1 \leq \text{THDTH}, \quad 2.1.4-52$$

where

THDTH = user input criteria (defaulted to 0.001)

stagnation properties are not calculated.

Table 2.1.4-1. Critical Flow Logic.

		TWO PHASE MODEL	JCHOKE FLAGS			
			0	1	3	4
SUBCOOLED MODEL			ORIGINAL RANSOM TRAPP	EXTENDED HENRY-FAUSKE	MOODY	HOMOGENEOUS EQUILIBRIUM
			I C H O K E F L A G	0	ORIGINAL RANSOM TRAPP	
1	EXTENDED HENRY-FAUSKE			X		
3	MOODY	X		X	X	X
4	HOMOGENEOUS EQUILIBRIUM			X		

NOTES

X DENOTES IMPROPER MODEL COMBINATIONS

MURDOCK-BAUMAN IS CHOSEN BY SETTING JCHOKE TO -3 OR -4

THE |JCHOKE| THEN IS USED TO SELECT THE TWO PHASE MODE

2.1.4.2. Abrupt Area Change

The general reactor system contains piping networks with many sudden area changes and orifices. To apply the RELAP5 hydrodynamic model to such systems, analytical models for these components have been developed.⁸¹ The basic hydrodynamic model is formulated for slowly varying (continuous) flow area variations; therefore, special models are not required for this case.

The abrupt area change model discussed here and developed in detail in Reference 81, is based on the Bourda-Carnot⁸² formulation for a sudden enlargement and standard pipe flow relations, including the vena-contracta effect for a sudden contraction or an orifice or both. Quasi-steady continuity and momentum balances are employed at points of abrupt area change. The numerical implementation of these balances is such that hydrodynamic losses are independent of upstream and downstream nodalization. In effect, the quasi-steady balances are employed as jump conditions that couple fluid components having abrupt changes in cross-sectional area. This coupling process is achieved without change to the basic linear semi-implicit numerical time-advancement scheme.

Abrupt Area Change Modeling Assumptions

The basic assumption used for the transient calculation of two-phase flow in flow passages with points of abrupt area change is that the transient flow process can be approximated as a quasi-steady flow process that is instantaneously satisfied by the upstream and downstream conditions (i.e., transient inertia, mass, and energy storage are neglected at abrupt area changes). However, the upstream and downstream flows are treated as fully transient flows.

There are several bases for the above assumption. A primary consideration is that available loss correlations are based on data taken during steady flow processes; however, transient investigations⁸³ have verified the adequacy of the quasi-steady assumption. The volume of fluid and associated mass, energy, and inertia at points of abrupt area change is generally small compared with the volume of upstream and downstream fluid components. The transient mass, energy, and inertia effects are approximated by lumping them into upstream and downstream flow volumes. Finally, the quasi-steady approach is consistent with modeling of other important phenomena in transient codes (i.e., heat transfer, pumps, and valves).

Review of Single-Phase Abrupt Area Change Models

The modeling techniques used for dynamic pressure losses associated with abrupt area change in a single-phase flow are reviewed briefly before discussing the extension of these methods to two-phase flows. In a steady incompressible flow, losses at an area change are modeled by the inclusion of an appropriate dynamic head loss term, h_L , in the one-dimensional modified Bernoulli equation

$$(v^2/2 + P/\rho)_1 = (v^2/2 + P/\rho)_2 + h_L \quad 2.1.4-53$$

The particular form of the dynamic head loss is obtained by employing the Bourda-Carnot⁸² assumption for calculating losses associated with the expansion part of the flow process. Losses associated with the contracting part of the flow process are small relative to the expansion losses, and are neglected.

The most general case of an abrupt area change is a contraction with an orifice at the point of contraction. Such a configuration is shown in Figure 2.1.4-4. Three area ratios are used throughout this development. The first is the contraction

area ratio at the vena-contracta relative to the minimum physical area, $\epsilon_c = A_c/A_T$. The second is the ratio of the minimum physical area to the upstream flow area, $\epsilon_T = A_T/A_1$. The third is the ratio of the downstream to upstream area, $\epsilon = A_2/A_1$.

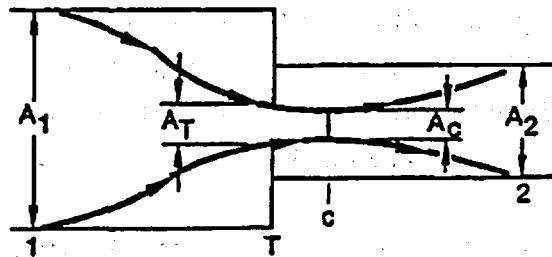


Figure 2.1.4-4. Orifice at Abrupt Area Change.

The loss associated with the contracting fluid stream from Station 1 to c (the point of vena-contracta) is neglected [measurements indicate that the contracting flow experiences a loss no larger than $\Delta P_f \approx 0.05 (1/2 \rho v_c^2)$ where v_c is the velocity at the vena-contracta] whereas the dynamic pressure loss associated with the expansion from the vena-contracta to the downstream section is given by

$$\Delta P_f = 1/2 \rho (1 - A_c/A_2)^2 v_c^2 \quad 2.1.4-54$$

The contraction ratio, $\epsilon_c = A_c/A_T$, is an empirical function of $\epsilon_T = A_T/A_1$. Using the continuity equation, $v_c = \frac{A_T v_T}{A_c} = v_T / \epsilon_c$, and $v_T = \frac{A_2 v_2}{A_T} = \frac{\epsilon}{\epsilon_T} v_2$, Equation 2.1.4-54 can be written as

$$\Delta P_f = 1/2 \rho \left[1 - \frac{\epsilon}{\epsilon_c \epsilon_T} \right]^2 v_2^2 \quad . \quad 2.1.4-55$$

Equation 2.1.4-55 is applicable to all the cases of interest. For a pure expansion, $\epsilon_T = 1$, $\epsilon_c = 1$, and $\epsilon > 1$; for a contraction, $\epsilon_T = \epsilon < 1$ and $\epsilon_c < 1$. Each of these is a special case of Equation 2.1.4-55. The two-phase dynamic pressure loss model is based on an adaptation of the general single-phase head loss given by this equation.

Two-Phase Abrupt Area Change Model

The two-phase flow through an abrupt area change is modeled in a manner very similar to that for single-phase flow by defining phasic flow areas. The two phases are coupled through the interphase drag, a common pressure gradient, and the requirement that the phases coexist in the flow passage.

The one-dimensional phasic stream-tube momentum equations are given in section 2.1.1.1. The flow at points of abrupt area change is assumed to be quasi-steady and incompressible. In addition, the terms in the momentum equations due to body force, wall friction, and mass transfer are assumed to be small in the region affected by the area change. The interphase drag terms are retained since the gradient in relative velocity can be large at points of abrupt area changes.

Equations 2.1.1-5 and 2.1.1-6 can be integrated approximately for a steady incompressible, smoothly varying flow to obtain modified Bernoulli-type equations.

$$\begin{aligned} \left[\frac{1}{2} \rho_f v_f^2 + P \right]_1 &= \left[\frac{1}{2} \rho_f v_f^2 + P \right]_2 + \left[\frac{FI'}{\alpha_f} \right]_1 (v_{f1} - v_{g1}) L_1 \\ &+ \left[\frac{FI'}{\alpha_f} \right]_2 (v_{f2} - v_{g2}) L_2 \end{aligned} \quad 2.1.4-56$$

and

$$\begin{aligned} \left[\frac{1}{2} \rho_g v_g^2 + P \right]_1 &= \left[\frac{1}{2} \rho_g v_g^2 + P \right]_2 + \left[\frac{FI'}{\alpha_f} \right]_1 (v_{g1} - v_{f1}) L_1 \\ &+ \left[\frac{FI'}{\alpha_f} \right]_2 (v_{g2} - v_{f2}) L_2, \end{aligned} \quad 2.1.4-57$$

where $FI' = \alpha_f \alpha_g \rho_f \rho_g FI$. The interphase drag is divided into two parts associated with the upstream and downstream parts of the flow affected by the area change.

General Model

Consider the application of Equations 2.1.4-56 and 2.1.4-57 to the flow of a two-phase fluid through a passage having a generalized abrupt area change (the flow passage shown in Figure 2.1.4-5).^a Here, the area A_T is the throat or minimum area associated with an orifice located at the point of the abrupt area change. Since each phase is governed by a modified Bernoulli-type equation, it is reasonable to assume that losses associated with changes in the phasic flow area can be modeled by separate dynamic pressure loss terms for both the liquid and gas phases. Hence, we assume that the liquid sustains a loss as if it alone (except for the interphase drag) were experiencing an area change from $\alpha_{f1} A_1$ to $\alpha_{fT} A_T$ to $\alpha_{f2} A_2$, and the gas phase

^aIn Figure 2.1.4-5, the flow is shown as a separated flow for clarity. The models developed are equally applicable to separated and dispersed flow regimes.

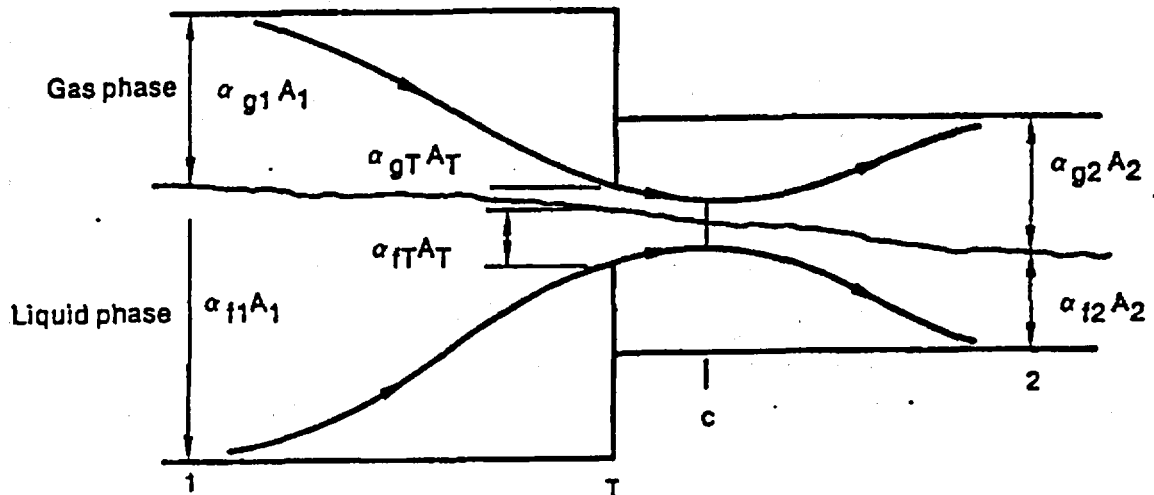


Figure 2.1.4-5. Schematic Flow of Two-Phase Mixture at Abrupt Area Change.

experiences a loss as if it alone were flowing through an area change from $\alpha_{g1} A_1$ to $\alpha_{gT} A_T$ to $\alpha_{g2} A_2$. The area changes for each phase are the phasic area changes (see Figure 2.1.4-5). When the losses for these respective area changes (based on the Bourda-Carnot model and given by Equation 2.1.4-55) are added to Equations 2.1.4-56 and 2.1.4-57, the following phasic momentum equations are obtained

$$\left[\frac{1}{2} \rho_f v_f^2 + P \right]_1 = \left[\frac{1}{2} \rho_f v_f^2 + P \right]_2 + \frac{1}{2} \rho_f \left[1 - \frac{\alpha_{f2} \epsilon}{\alpha_{fT} \epsilon_{fc} \epsilon_T} \right]^2 \cdot (v_{f2})^2 + \left[\frac{FI'}{\alpha_f} \right]_2 (v_{f1} - v_{g1}) L_1 + \left[\frac{FI'}{\alpha_f} \right]_2 (v_{f2} - v_{g2}) L_2$$

2.1.4-58

and

$$\left[\frac{1}{2} \rho_g v_g^2 + P \right]_1 = \left[\frac{1}{2} \rho_g v_g^2 + P \right]_2 + \frac{1}{2} \rho_g \left[1 - \frac{\alpha_{f2} \epsilon}{\alpha_{gT} \epsilon_{gc} \epsilon_T} \right]^2 \cdot (v_{g2})^2 + \left[\frac{FI'}{\alpha_g} \right]_2 (v_{g1} - v_{f1}) L_1 + \left[\frac{FI'}{\alpha_g} \right]_2 (v_{g2} - v_{f2}) L_2.$$

2.1.4-59

These phasic momentum equations are used across an abrupt area change. In Equations 2.1.4-58 and 2.1.4-59, ϵ_{fc} and ϵ_{gc} are the same tabular function of area ratio as in the single-phase case except that the area ratios used are the phasic area ratios

$$\epsilon_{fT} = (\alpha_{fT} / \alpha_{f1}) \epsilon_T$$

2.1.4-60

and

$$\epsilon_{gT} = (\alpha_{gT} / \alpha_{g1}) \epsilon_T$$

2.1.4-61

respectively. The area ratios, $\epsilon = A_2/A_1$ and $\epsilon_T = A_T/A_1$, are the same as for single-phase flow.

The interphase drag effects in Equations 2.1.4-58 and 2.1.4-59 are important. These terms govern the amount of slip induced by an abrupt area change, and if they are omitted, the model will always predict a slip at the area change appropriate to a completely separated flow situation and give erroneous results for a dispersed flow.

Model Application

A few remarks concerning the way Equations 2.1.4-58 and 2.1.4-59 are applied to expansions and contractions, both with and without an orifice, are necessary. In a single-phase steady flow situation, given the upstream conditions, v_1 and P_1 , using the

continuity equation ($v_1 A_1 = v_2 A_2$) and Equation 2.1.4-53 one can solve for v_2 and P_2 . Equations 2.1.4-58 and 2.1.4-59 along with the two phasic continuity equations can be used in a similar manner except now the downstream void fraction is an additional unknown which must be determined.

Expansion

For the purpose of explanation, consider the case of an expansion ($\alpha_{fT} = \alpha_{f1}$, $\epsilon > 0$, $\epsilon_T = 1$, $\epsilon_{fc} = \epsilon_{gc} = 1$, $FI'_1 = 0$, $L_1 = 0$) for which Equations 2.1.4-58 and 2.1.4-59 reduce to

$$\begin{aligned} \left[\frac{1}{2} \rho_f v_f^2 + P \right]_1 &= \left[\frac{1}{2} \rho_f v_f^2 + P \right]_2 + \frac{1}{2} \rho_f \left[1 - \frac{\alpha_{f2} \epsilon}{\alpha_{f1}} \right]^2 (v_{f2})^2 \\ &+ \left[\frac{FI'}{\alpha_f} \right]_2 (v_{f2} - v_{g2}) L_2 \end{aligned} \quad 2.1.4-62$$

and

$$\begin{aligned} \left[\frac{1}{2} \rho_g v_g^2 + P \right]_1 &= \left[\frac{1}{2} \rho_g v_g^2 + P \right]_2 + \frac{1}{2} \rho_g \left[1 - \frac{\alpha_{g2} \epsilon}{\alpha_{g1}} \right]^2 (v_{g2})^2 \\ &+ \left[\frac{FI'}{\alpha_g} \right]_2 (v_{g2} - v_{f2}) L_2 \end{aligned} \quad 2.1.4-63$$

These two equations with the incompressible continuity equations

$$\alpha_{f1} v_{f1} A_1 = \alpha_{f2} v_{f2} A_2 \quad 2.1.4-64$$

and

$$\alpha_{g1} v_{g1} A_1 = \alpha_{g2} v_{g2} A_2 \quad 2.1.4-65$$

are a system of four equations having four unknowns, α_{f2} ($\alpha_{g2} = 1 - \alpha_{f2}$), v_{f2} , v_{g2} , and P_2 , in terms of the upstream conditions, α_{f1} ($\alpha_{g1} = 1 - \alpha_{f1}$), v_{f1} , v_{g1} , and P_1 . (The

interphase drag, FI' , is a known function of the flow properties.) It is important to note that the downstream value of the liquid fraction (α_{f2}) is an additional unknown compared with the single-phase case and is determined (with the downstream velocities and pressure) by simultaneous solution of Equations 2.1.4-62 through 2.1.4-65 without additional assumptions. It is reassuring that by taking a proper linear combination of Equations 2.1.4-58 and 2.1.4-59 the usual overall momentum balance obtained using the Bourda-Carnot⁸² assumption can be obtained.⁸⁴⁻⁸⁵

If, as in the cited literature,⁸⁴⁻⁸⁷ only the overall momentum balance is used at an expansion, there will be an insufficient number of equations to determine all the downstream flow parameters, α_{f2} , v_{f2} , v_{g2} , and P_2 . The indeterminacy has been overcome in cited works by means of several different assumptions concerning the downstream void fraction.^a In the model developed here (Equations 2.1.4-62 and 2.1.4-63), division of the overall loss into liquid and gas parts, respectively, results in sufficient conditions to determine all downstream flow variables including α_{f2} . In addition, the present model includes force terms due to interphase drag in Equations 2.1.4-62 and 2.1.4-63, which are necessary to predict the proper amount of slip and void redistribution that occur at points of area change.

Contraction

Consider the application of Equations 2.1.4-61 and 2.1.4-62 to a contraction. To determine both the downstream conditions and throat conditions from the upstream values of α_{f1} (α_{g1}), v_{f1} , v_{g1} , and P_1 , an additional consideration needs to be made. To obtain

^aJ. G. Collier⁸⁴ mentions three different assumptions that have been used: (i) $\alpha_{f2} = \alpha_{f1}$, (ii) α_{f2} is given by a homogeneous model, and (iii) α_{f2} is given by the Hughmark void fraction correlation.

the throat values, apply the momentum equations valid for the contracting section of flow (here, the L_1 portion of the interphase force is associated with the contraction), that is,

$$\left[\frac{1}{2} \rho_f v_f^2 + P \right]_1 = \left[\frac{1}{2} \rho_f v_f^2 + P \right]_T + \left[\frac{FI'}{\alpha_f} \right]_1 (v_{f1} - v_{g1}) L_1, \quad 2.1.4-66$$

$$\left[\frac{1}{2} \rho_g v_g^2 + P \right]_1 = \left[\frac{1}{2} \rho_g v_g^2 + P \right]_T + \left[\frac{FI'}{\alpha_f} \right]_1 (v_{g1} - v_{f1}) L_1, \quad 2.1.4-67$$

$$\alpha_{f1} v_{f1} A_1 = \alpha_{fT} v_{fT} A_T, \quad 2.1.4-68$$

and

$$\alpha_{g1} v_{g1} A_1 = \alpha_{gT} v_{gT} A_T. \quad 2.1.4-69$$

These four equations are solved simultaneously for the values of α_{fT} (α_{gT}), v_{fT} , v_{gT} , and P_T at the throat section (the minimum physical area). No additional or special assumptions are made concerning the throat conditions since they follow as a direct consequence of the unique head loss models for each phase. After the throat values have been obtained, the conditions at the point of vena-contracta are established assuming the void fraction is the same as that at the throat. Thus, ϵ_{fc} and ϵ_{gc} are established using the tabular function in Appendix A of Reference 81 and the throat area ratios, ϵ_{fT} and ϵ_{gT} , defined by Equations 2.1.4-60 and 2.1.4-61. To determine the downstream values, Equations 2.1.4-58 and 2.1.4-59 can be applied directly from stations 1 to 2 with the throat values known or the expansion loss equations can be used from the throat section to station 2. Both approaches produce identical downstream solutions. As in the case of an expansion, because the proper upstream and

downstream interphase drag is included, this modeling approach establishes the phase slip and resulting void redistribution. An orifice at an abrupt area change is treated exactly as the contraction explained above (i.e., with two separate calculations to establish first the throat and then the downstream flow variables).

Countercurrent Flow

The preceding development implicitly assumed a cocurrent flow. For countercurrent flow, Equations 2.1.4-58 and 2.1.4-59 are applied exactly as in cocurrent flow except that the upstream sections for the respective phases are located on different sides of the abrupt area change. The difference appears in how the throat and downstream voids are determined. To determine the throat properties, equations similar to Equations 2.1.4-66 through 2.1.4-67 are used with the upstream values appropriate for each phase. These four equations are then solved for $\alpha_{fT}(\alpha_{gT})$, V_{fT} , V_{gT} , and P_T . To determine the downstream values for each phase, only the head loss terms are needed for the downstream voids (the downstream V_f , V_g , and P do not appear). For countercurrent flow, these voids are set such that the downstream void of each phase plus the upstream void of the opposite phase adds to one (both phases together must fill the flow channel). With the throat and downstream voids now known, Equations 2.1.4-58 and 2.1.4-59 can be used directly to determine the total loss for each phase at the abrupt area change.

2.1.4.3. Crossflow Junction

The RELAPS numerical scheme is generally formulated using one-dimensional elements. However, there are several applications where an approximate treatment of crossflow provides an improved physical simulation. Three different applications for a crossflow formulation are described in the following paragraphs.

The first application concerns a small crossflow between two essentially axial flow streams. This situation is typical of regions such as a reactor core or a steam generator because the component geometry provides a large resistance to crossflow and a small resistance to axial flow. Hence, simplified crossflow momentum equations can be used to couple a hot flow channel to a bulk flow channel.

The second application of a crossflow junction is to provide a tee model. In this case, the momentum flux in the side branch is assumed to be perpendicular to the main stream and thus the main stream momentum flux does not contribute to the crossflow momentum formulation.

The third application is modeling of leak flow paths. In this case, the flow is small and governed primarily by pressure differential, gravity, and flow resistance. Thus, the momentum flux terms can be neglected.

The vapor momentum finite difference equation used in the basic numerical scheme is

$$\begin{aligned}
 & \left(\alpha_g \rho_g \right)_j^n \left(v_g^{n+1} - v_g^n \right)_j \Delta x_j^n + \frac{1}{2} \left(\alpha_g \rho_g \right)_j^n \left[\left(v_g^2 \right)_L^n - \left(v_g^2 \right)_K^n \right] \Delta t + \text{VISCOUS TERMS} \\
 & = - \alpha_{g,j}^n \left(P_L^{n+1} - P_K^{n+1} \right) \Delta t \\
 & - \left(\alpha_g \rho_g \right)_j^n \left[\left(FWC_K^n + FWC_L^n \right) \Delta x_j + HLOSSG_j^n \right] v_{g,j}^{n+1} \Delta t \\
 & - \left(\alpha_g \rho_g \right)_j^n FIG_j^n \left(v_{g,j}^{n+1} - v_{f,j}^{n+1} \right) \Delta x_j \Delta t + \left(\alpha_g \rho_g \right)_j^n B_x \Delta x_j \Delta t \\
 & + \text{ADDED MASS} + \text{MASS TRANSFER MOMENTUM} \\
 & + \text{HORIZONTAL STRATIFIED PRESSURE GRADIENT EFFECT,}
 \end{aligned}$$

2.1.4-70

where

$$\Delta x_j = \frac{1}{2}(\Delta x_K + \Delta x_L) \quad . \quad 2.1.4-71$$

A parallel equation holds for the liquid phase. It should be noted that the momentum Equation 2.1.4-70 is in reality the sum of half the K cell momentum plus half the L cell momentum. This is the reason for Equation 2.1.4-71.

There are two areas in which the crossflow modeling affects the numerical scheme. One concerns the approximations made in the junction momentum equations; the other concerns the volume average velocities in a volume.

If the junction is to model crossflow perpendicular to the main or axial-flow direction then the volume average velocity in the K and L cells, which represent the axial flow velocity, should not include crossflow junction velocity components. For the simple leak flow situation shown in Figure 2.1.4-6, this requires that

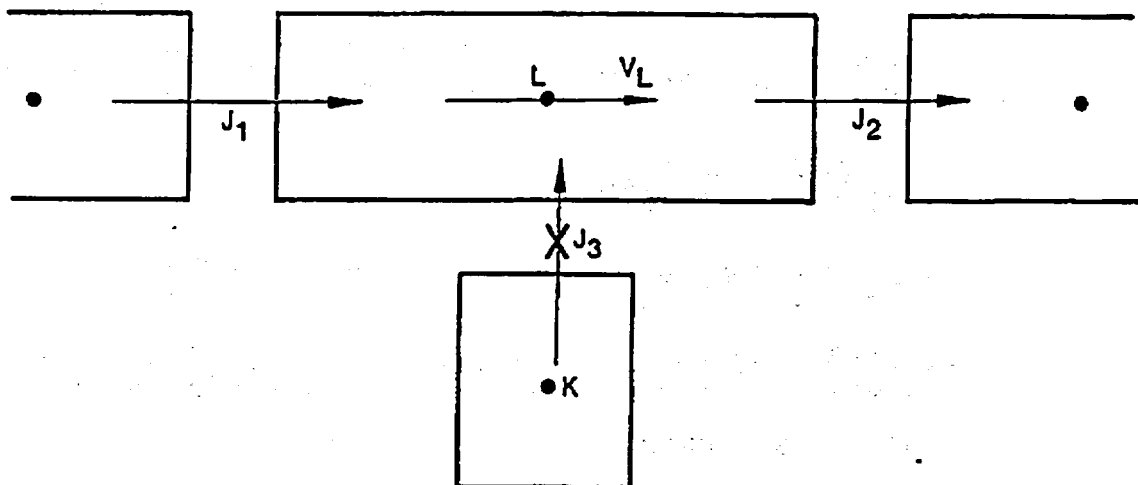


Figure 2.1.4-6. Simplified Tee Crossflow.

$v_{j,3}$ not be included in the volume average (axial) velocity calculation for cell L.

The second area of numerical modification relates to the reduced form of the momentum equations to be used at a crossflow junction. In crossflow junctions, the cross product momentum flux terms are neglected, that is, there is no x-direction transport of momentum due to the y velocity.

For the case of a small crossflow junction between two axial-flow streams (J_2 in Figure 2.1.4-7) all the geometric input (AVOL, DX, DZ) for both of the volumes relates to the axial flow direction as does the wall drag and code calculated form losses. Since the crossflow has a different flow geometry and resistance (for example, crossflow resistance in a rod bundle) the friction and form losses must be user input and must be appropriate for the crossflow direction geometry. For crossflow junctions the user input form losses should include all crossflow resistance (form losses and wall drag). The normal terms representing wall drag and abrupt area change losses are not included in the formulation of the momentum equation at a crossflow junction as these refer to the axial properties of the K and L volumes.

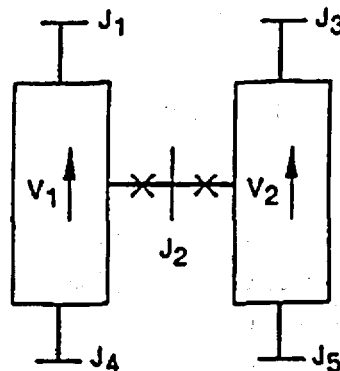


Figure 2.1.4-7. Modeling of Crossflows or Leak.

Since the connecting K and L volumes are assumed to be predominately axial-flow volumes, the crossflow junction momentum flux (related to the axial volume velocity in K and L) is neglected along with the associated numerical viscous term. In addition, the horizontal stratified pressure gradient is neglected.

All lengths and elevation changes in the one-dimensional representation are based upon the axial geometry of the K and L volumes and the crossflow junction is assumed to be perpendicular to the axial direction and of zero elevation change, thus, no gravity force term is included.

The resulting vapor momentum finite difference equation for a crossflow junction is

$$\begin{aligned} & \left(\alpha_g \rho_g \right)_j^n \left(v_g^{n+1} - v_g^n \right)_j \Delta x_j = - \alpha_{g,j}^n (P_L - P_K)^{n+1} \Delta t \\ & - \left(\alpha_g \rho_g \right)_j^n HLOSSG_j^n v_{g,j}^{n+1} \Delta t \\ & - \left(\alpha_g \rho_g \right)_j^n FIG_j^n \left(v_{g,j}^{n+1} - v_{f,j}^{n+1} \right) \Delta x_j \Delta t \end{aligned}$$

+ ADDED MASS + MASS TRANSFER MOMENTUM.

2.1.4-72

A similar equation can be written for the liquid phase. In Equation 2.1.4-72, $HLOSSG_j^n$ contains only the user-input crossflow resistance. The Δx_j term that is used to estimate the inertial length associated with crossflow is defined using the diameters of volumes K and L,

$$\Delta x_j = \frac{1}{2} [D(K) + D(L)] .$$

2.1.4-73

A special void-dependent form loss option of the full crossflow model has been added for certain multi-core channel applications. This option allows the user to alter the input constant form loss coefficient based on the void fraction in the upstream volume. The specific applications are possibly multi-channel core analyses such as SBLOCA scenarios with significant core uncovering or future multi-channel BEACH reflooding calculations. This model allows the regions of the core covered by a two-phase mixture or pool to have a resistance that is different from that in the uncovered or steam region. The crossflow resistance changes can alter the volume-average axial velocities that are used to determine the core surface heat transfer. Any cross flow is excluded from the volume average velocity used for heat transfer.

The model uses the input form loss coefficients whenever the upstream steam void fraction is less than a user-supplied minimum void fraction value given as $\alpha_{\text{min-Kcross}}$. The model allows user input of a forward, $M_{K\text{-forward}}$, and reverse, $M_{K\text{-reverse}}$, crossflow resistance multiplier when the upstream steam void fraction is greater than the maximum user-input void fraction, $\alpha_{\text{max-Kcross}}$. Linear interpolation is used to determine the multiplicative factor when the void fraction is between minimum and maximum input void fractions as indicated in the following equations. For the forward flow direction (from Volume K to Volume L),

If	$\alpha_v(K) < \alpha_{\text{min-Kcross}}$	$K_{\text{jun}} = K_{\text{jun forward}}$
If	$\alpha_{\text{max-Kcross}} \leq \alpha_v(K)$	$K_{\text{jun}} = K_{\text{jun forward}} * M_{K\text{-forward}}$
If	$\alpha_{\text{min-Kcross}} \leq \alpha_v(K) < \alpha_{\text{max-Kcross}}$	$K_{\text{jun}} = K_{\text{jun forward}} * M_{K\text{f interp}}$

2.1.4-73.1

where

$$M_{Kf \text{ interp}} = 1 - (1 - M_{K\text{-forward}}) * [\alpha_{\text{min-Kcross}} - \alpha_g(K)] / (\alpha_{\text{min-Kcross}} - \alpha_{\text{max-Kcross}})$$

and $K_{\text{jun forward}}$ is the user-supplied forward loss coefficient specified in this junction input.

The equation for the reverse flow direction (from Volume L to Volume K) is similar.

If $\alpha_g(L) < \alpha_{\text{min-Kcross}}$	$K_{\text{jun}} = K_{\text{jun reverse}}$
If $\alpha_{\text{max-Kcross}} \leq \alpha_g(L)$	$K_{\text{jun}} = K_{\text{jun reverse}} * M_{K\text{-reverse}}$
If $\alpha_{\text{min-Kcross}} \leq \alpha_g(L) < \alpha_{\text{max-Kcross}}$	$K_{\text{jun}} = K_{\text{jun reverse}} * M_{Kf \text{ interp}}$

2.1.4-73.2

where

$$M_{Kr \text{ interp}} = 1 - (1 - M_{K\text{-reverse}}) * [\alpha_{\text{min-Kcross}} - \alpha_g(L)] / (\alpha_{\text{min-Kcross}} - \alpha_{\text{max-Kcross}})$$

and $K_{\text{jun reverse}}$ is the user-supplied reverse loss coefficient specified in this junction input.

The code performs several input checks to ensure that the user input will not cause code failures. These checks include tests to see if the input form loss multipliers are greater than zero. The minimum void fraction must be greater than zero and less than the maximum void fraction input. The maximum void fraction must be less than or equal to one.

The crossflow option can be used with the crossflow junction perpendicular to the axial flow in Volume L (or K) but parallel

to the axial flow in volume K (or L) (see Figure 2.1.4-6). Here, the situation regarding the half cell momentum contribution associated with volume K is the same as for a normal junction. Hence, this crossflow junction has all the terms in Equation 2.1.4-70 except that; (a) wall friction, momentum flux, and gravity only include the K cell contribution, (b) the $HLOSS_j^n$ term is only the user input loss, and (c) the Δx cell in the inertial term and interphase drag includes the normal K cell contribution and a term of the form in Equation 2.1.4-73 for the L cell. This type of crossflow modeling can be used for a 90 degree tee simulation.

For leak flows and minor flow paths the modeling approach shown in Figure 2.1.4-8 is recommended. Here, J_3 is the normal flow path, whereas junction J_1 , volume M, and junction J_2 represent the leak flow path. Junctions J_1 and J_2 should be modeled as tee junctions described above. The only reason for using volume M is

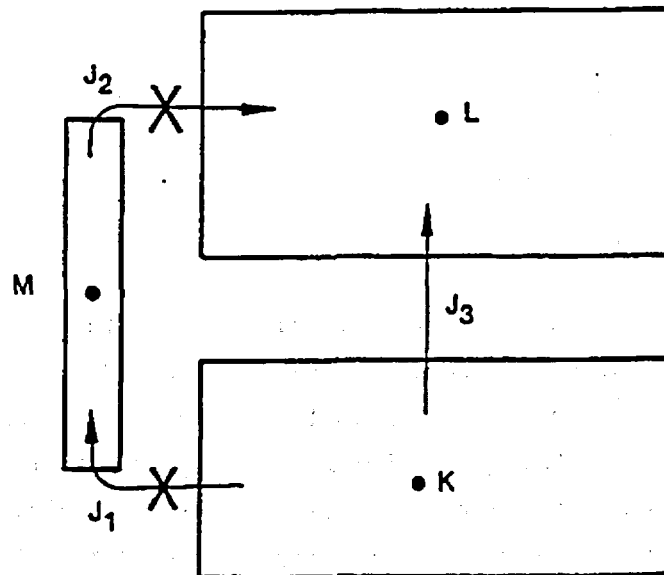


Figure 2.1.4-8. Leak Flow Modeling.

to obtain a correct representation of the gravity head from K to L. If a crossflow junction were modeled directly between volumes K and L then there would be no gravity head in the leak flow junction equation. Leak paths may also be modeled using a crossflow junction that is perpendicular to both the K and L volumes when the leak flow is between volumes having the same volume center elevation.

2.1.4.4. Branch

The branch component is a model designed for convenient interconnection of hydrodynamic components. The identical result can be obtained by using a single volume component and several single junction components. Thus the branch is a separate component only in the input processing scheme.

In RELAP5/MOD2 the crossflow junction has been added in which the junction velocities are assumed to be normal to the one-dimensional flow path of the hydrodynamic volume. Thus, the branch component can include multiple connections at the inlet, outlet, or in the crossflow direction.

Specialized modeling considerations are applied to any volume having multiple junctions connected at either volume end (the ends of a hydrodynamic volume are the inlet and outlet as defined in section 2.1.1.1).

These special calculations include both the method for calculating the volume average velocities and the method for partitioning the volume cross-sectional area between the multiple inlet or multiple outlet junctions. The partitioned volume areas are used both in the abrupt area change model to calculate kinetic loss factors and in the momentum equations to simulate the stream-tube area.

In applications, the multiple junction and crossflow models are used in three distinct ways to model branching flows. These are the one-dimensional branching, a tee branch, and a crossflow branch. Combination of the three basic branches may also occur. Each of the three basic models will be discussed in turn.

One-Dimensional Branching

This basic branch model is consistent with the one-dimensional approximation for a piping network and assumes that multidimensional effects at branches are small compared to system interaction effects. In the case of branched flows that occur in headers or plena, the model gives an accurate physical description of the flow division or merging process and the one-dimensional branch model is intended primarily for use in modeling such branched flows. Examples of such situations in LWR systems are flow division at the core inlet if parallel flow paths through the core are modeled, steam generator inlet and outlet plena when several parallel tube groups are modeled (for the effect of tube height and length), or at a wye connection.

The one-dimensional branch is illustrated in Figure 2.1.4-9 for a volume having two inlet junctions and one outlet junction. The junctions J_1 and J_2 are the inlet junctions and junction J_3 is the outlet junction. The multiple flows are assumed to merge in such a way that they come to the common velocity equal to the inlet volume average velocity for volume V_3 . The volume cross-sectional area is then divided in proportion to the volume flow of the respective inlet junctions. This method of apportioning volume cross-sectional area satisfies continuity but does not conserve momentum, particularly for high velocity differences between the merging streams (for flow splitting, however, the method does preserve momentum). For this reason the special jet mixer component was developed for merging flows having high relative velocities such as in a jet pump. The jet-mixer can be used for one-dimensional mixing, but is limited to two inlet

streams and a single outlet stream (see Appendix A for a reference to the jet-mixer model). The volume partitioned areas are calculated as follows

$$(A_K)_j = \frac{[|\alpha_f|_j^n |v_f|_j^n + |\alpha_g|_j^n |v_g|_j^n] A_j A_k}{\sum_{i=J_1}^{J_N} [|\alpha_f|_i^n |v_f|_i^n + |\alpha_g|_i^n |v_g|_i^n] A_i} \quad 2.1.4-74$$

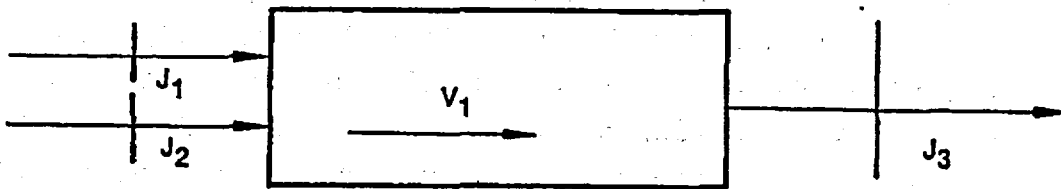


Figure 2.1.4-9. One-Dimensional Branch.

The apportioned volume areas for each junction are used with the abrupt area change model, section 2.1.4.2, to calculate energy loss coefficients for the liquid and vapor streams at each junction.

Ninety-Degree Tee Model

The crossflow junction (see section 2.1.4.3) is used to form a 90-degree tee as shown in Figure 2.1.4-6. In this particular application the side connection to the tee is modeled using a junction in which only one-half of the junction momentum equation has the crossflow form (the half of the junction J_3 associated with volume V_L is a crossflow junction and is designated by an X, see Figure 2.1.4-6).

No special component is provided to accomplish the input associated with a model such as illustrated in Figure 2.1.4-6. The volume V_L may be specified as a branch with the associated junctions or as a single volume with single junctions used to specify the connecting junctions. In either case, junctions J_1 and J_2 should be specified as smooth unless actual abrupt changes in area occur at either junction. The junction J_3 should be specified as smooth with a user input form loss factor to account for the turning and entrance losses. In addition, junction J_3 must be specified so that the half of the junction associated with volume V_L is modeled as a crossflow junction and the half associated with volume V_K is a normal junction. These options are specified through input of junction control flags.

It is also possible to model a 90-degree tee with the RELAP5/MOD2 code, however, unphysical numerical results may be obtained. Thus, the 90-degree tee model described previously is recommended and is a closer approximation to the actual fluid momentum interaction which occurs at a tee.

Gravity Effects at a Tee

In some branching situations where the through flow is small or where the flow is constrained by the geometry, body force effects may be significant. Examples that occur in PWR systems are the cold leg connections to the inlet annulus and downcomer, and the hot leg connection to the upper plenum and core. This type of branched flow is modeled as shown in Figure 2.1.4-10. Here the vertical direction is modeled as the through-flow direction (indicated by the volume orientation arrows). The cold or hot leg connections are modeled by crossflow junctions. The through flow direction of volume V_3 is chosen to correspond to the major flow path. In the case of a PWR inlet annulus through-flow in the horizontal direction is inhibited by the annular structure and in the case of the upper plenum to core connection the area for flow in the vertical direction is large compared to the flow

area in the horizontal direction. Some judgment is required to select the orientation. However, the crossflow branch connection will permit through-flow in the horizontal direction but with some accompanying pressure rise and drop associated with the fact that the momentum flux terms are neglected in the crossflow part of the junction.

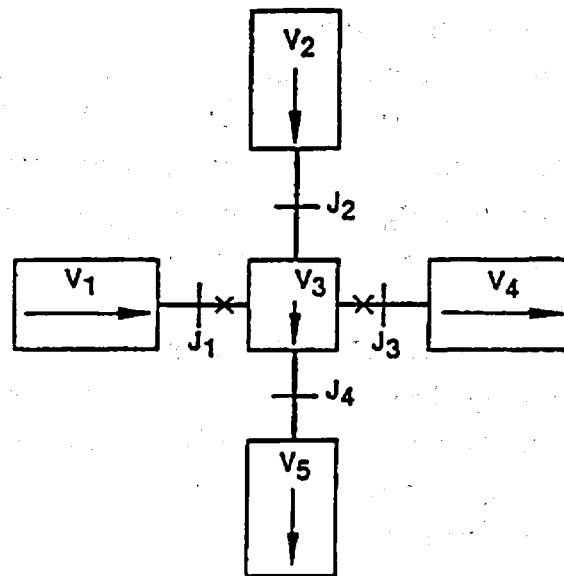


Figure 2.1.4-10. Gravity Effects on a Tee.

The model illustrated in Figure 2.1.4-10 has the additional advantage that the effect of vertical void gradients in the flow out of the horizontal connections may be more sharply defined as a result of the central volume, V_3 , which has a vertical height equal to the diameter of branch volumes V_1 and V_4 .

No special component model is provided for modeling the vertical tee and either a branch or a single volume may be used for volume V_3 . The branch component is more convenient since all junctions connecting to volume V_3 can be specified with the branch component.

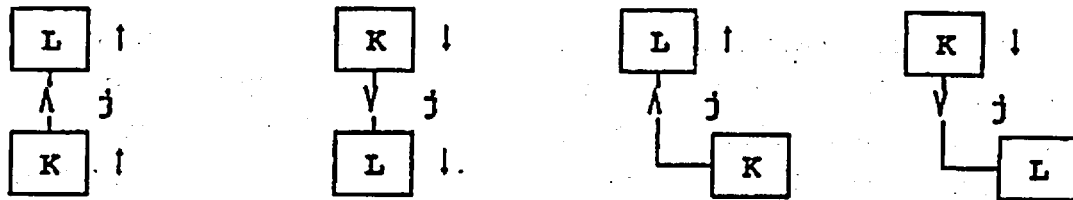
Crossflow Branch

A fourth type of branch flow path can be created by the use of a crossflow junction to couple two volumes. This type of branch is used to model crossflow between columns having centers at the same vertical elevation. The crossflow junction is assumed to have no elevation change; thus, one limitation of this type of branch is that the volume centers that are coupled must be at the same elevation. If volumes of differing elevation are coupled, an input processing error will occur in the loop elevation checking routines. The application of the crossflow junction for crossflow or leak path modeling is illustrated in Figure 2.1.4-7. The length scale associated with the crossflow junction is one half the diameter of the L volume. This length is only used for modeling the fluid inertia terms in the momentum equation and is always assumed to lie in a horizontal plane.

The pure crossflow branch is most easily modeled using a single junction component for the crossflow junction. However, either volume, V_1 or V_2 in Figure 2.1.4-7, can be modeled using the branch component and specifying the coupling junctions with that component.

2.1.4.5. Countercurrent Flow Limit (CCFL) Model

During the reflux condensation period of a small break LOCA transient in a PWR with U-tube steam generator, countercurrent flow limitation (CCFL) often will occur at the hot leg bend and at the U-tube inlet. The Wallis CCFL correlation³⁴ is added to calculate the steam and liquid flow rates for certain RELAP5 junctions. The applicability of the CCFL model is limited to the volume and junction configurations shown in Figure 2.1.4-11, in which K and L are RELAP5 volumes, the junction j is from the exit of volume K to the inlet of volume L, and ΔZ is the elevation change of each volume.



- a) $\Delta Z(K) > 0$ & $\Delta Z(L) > 0$ b) $\Delta Z(K) < 0$ & $\Delta Z(L) < 0$ c) $\Delta Z(K) = 0$ & $\Delta Z(L) > 0$ d) $\Delta Z(K) < 0$ & $\Delta Z(L) = 0$

Figure 2.1.4-11. Volumes and Junction Configurations Available for CCFL Model.

The general form of the Wallis CCFL correlation³⁴ is:

$$\left(j_g^* \right)^{1/2} + m \left(j_f^* \right)^{1/2} = c, \quad 2.1.4-75$$

where m is the negative slope and c is the y -intercept, respectively, of a plot of j_g^* versus j_f^* . The dimensionless gas flux, j_g^* , and the liquid flux, j_f^* , are defined by

$$j_g^* = j_g \left[\frac{\rho_g}{g D_j (\rho_f - \rho_g)} \right]^{1/2} \quad 2.1.4-76$$

and

$$j_f^* = j_f \left[\frac{\rho_f}{g D_j (\rho_f - \rho_g)} \right]^{1/2}, \quad 2.1.4-77$$

respectively, where j_g is the gas superficial velocity, j_f is the liquid superficial velocity, and D_j is the junction hydraulic diameter.

With regard to the solution method, if the CCFL model is requested by the user, the coding checks if countercurrent flow exists and if the liquid downflow exceeds the limit imposed by equation 2.1.4-75. If this is true, the sum momentum equation and the flooding limit equation is applied as has been done in RELAP5/MOD3.¹⁴⁴ The code's difference equation is replaced with the flooding limit equation during the semi-implicit intermediate velocity calculation (Subroutine VEXPLT). The difference equation contains the interphase friction, whereas the sum equation does not. This method is advantageous in that the phasic velocities still must satisfy the the sum equation which contains gravity and pressure terms. The numerical form of Equation 2.1.4-75 needed by the code is obtained by letting $c_g = j_g^*/v_g$ and $c_f = j_f^*/v_f$, solving for $m j_f^{1/2}$, and squaring the equation. This results in

$$m^2 c_{f,j}^n v_{f,j}^{n+1} = c^2 - 2c (c_{g,j}^n)^{1/2} (v_{g,j}^{n+1})^{1/2} + c_{g,j}^n v_{g,j}^{n+1} \quad 2.1.4-78$$

Linearization of $(v_{g,j}^{n+1})^{1/2}$ gives

$$(v_{g,j}^{n+1})^{1/2} = (v_{g,j}^n)^{1/2} + \frac{1}{2} (v_{g,j}^n)^{-1/2} (v_{g,j}^{n+1} - v_{g,j}^n) \quad 2.1.4-79$$

and substitution into equation 2.1.4-75 produces

$$\begin{aligned} m^2 c_{f,j}^n v_{f,j}^{n+1} + [c (c_{g,j}^n)^{1/2} (v_{g,j}^n)^{-1/2} - c_{g,j}^n] v_{g,j}^{n+1} \\ = c^2 - c (c_{g,j}^n)^{1/2} (v_{g,j}^n)^{1/2}. \end{aligned} \quad 2.1.4-80$$

The above method can be used when both the RELAP5 momentum equations and the CCFL correlation predict countercurrent flow. In situations where RELAP5 predicts countercurrent flow and the

CCFL correlation predicts current flow based on the RELAP5 calculated velocities, a different approach is used. The present RELAP5/MOD2 model does not address this situation. When this situation arises an iterative approach between the RELAP5 momentum solution and the CCFL correlation prediction is used until both solutions predict consistent flow behavior. During the iteration, the junction interphase drag of k-th iteration, f_{gf}^k , is multiplied by

$$C_{ccfl} = |v_{g,j}^k + v_{f,j}^k| / [(v_{g,j}^k)^2 + (v_{f,j}^k)^2]^{1/2}, \quad 2.1.4-81$$

such that

$$f_{gf}^{k+1} = C_{ccfl}^k f_{gf}^k \quad 2.1.4-82$$

This page intentionally left blank.

2.1.5. Special Component Models

RELAP5 consists of a variety of generic models which are used to build system models. The general philosophy has been to avoid system component models such as pressurizer, steam generator, core, etc. However, certain subsystem components are unavoidable due to unique processes or performance. RELAP5 contains models for subsystem components such as a separator, pump, valve, and accumulator. A summary of each of these models is included here.

2.1.5.1. Separator

The RELAP5 separator model is a nonmechanistic or black box model consisting of a special volume with junction flows as pictured in Figure 2.1.5-1. A steam-water inflowing mixture is separated by defining the quality of the outflow streams using empirical functions. No attempt is made to model the actual separation process from first principles.

The separator vapor outlet performance is defined by means of a special function for the vapor void fraction at J_1 . The donored junction vapor void fraction used to flux mass through the steam outlet is related to the vapor void fraction in the separator volume using the curve in Figure 2.1.5-2. For separator volume void fractions above the value of VOVER (an input parameter) a perfect separation is assumed and pure vapor is fluxed out junction J_1 . For separator volume void fractions less than VOVER a two-phase mixture is fluxed out. The VOVER parameter governs the vapor void fraction of the outflow. If VOVER is small the vapor outflow corresponds to an ideal separator. If VOVER equals 1.0 the vapor outlet junction behaves as a normal junction and the vapor outlet junction void fraction is equal to the separator volume average void fraction.

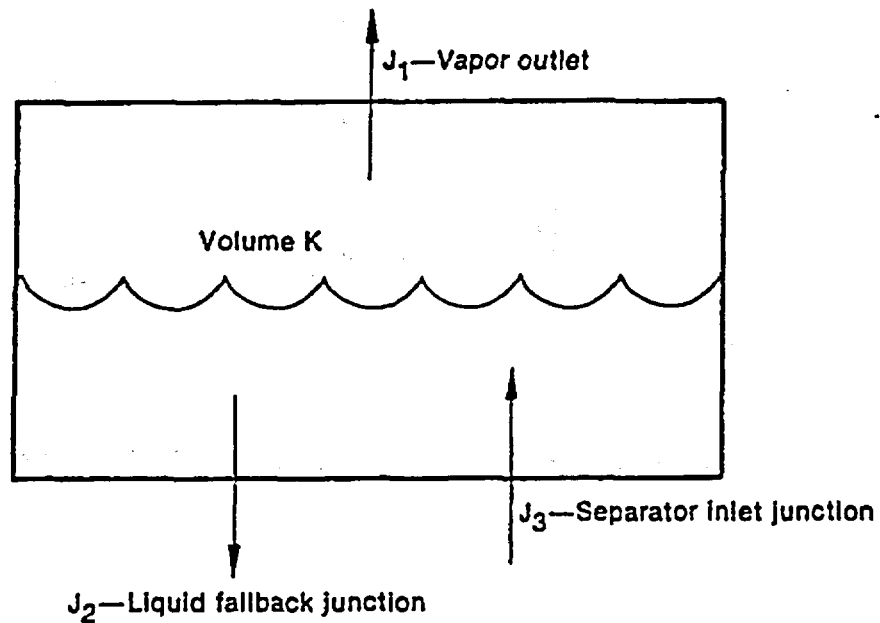


Figure 2.1.5-1. Typical Separator Volume and Junctions.

The flow of the separator liquid drain junction is modeled in a manner similar to the steam outlet except pure liquid outflow is assumed when the volume void fraction is less than the value of VUNDER, see Figure 2.1.5-3. Normal donored fluxes are used for the separator inlet junction. Although the void fractions used to flux mass and energy from the separator volumes are modified, the normal junction momentum equations are used to calculate the flow velocities.

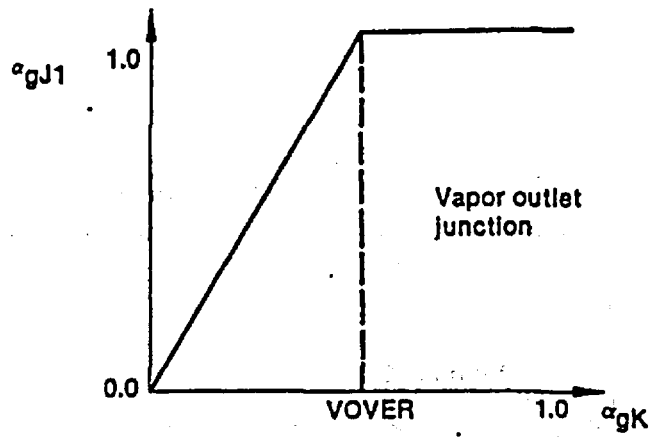


Figure 2.1.5-2. Vapor Outflow Void Donoring.

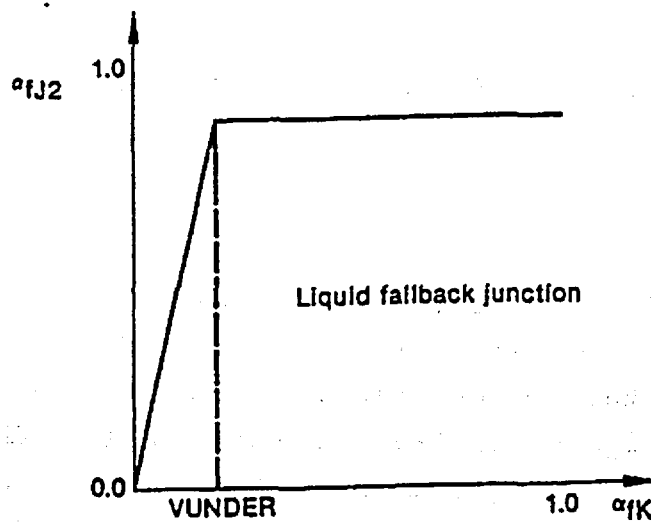


Figure 2.1.5-3. Liquid Fallback Void Donoring.

2.1.5.2. Pump Model

The pump is a volume oriented component and the head developed by the pump is apportioned equally between the suction and discharge junctions that connect the pump volume to the system. The pump model is interfaced with the two fluid hydrodynamic model by assuming the head developed by the pump is similar to a body force. Thus, the head term appears in the mixture momentum equation, but like the gravity body force, it does not appear in the momentum difference equation used in RELAP5. The term that is added to the mixture momentum equation is

$$\frac{1}{2}\rho gH ,$$

2.1.5-1

where H is the total head rise of the pump (m), ρ is the fluid density (kg/m³), and g is the acceleration due to gravity (m/s²). The factor 1/2 is needed because the term is applied at both the suction and discharge junctions.

In the semi-implicit numerical scheme, the pump is coupled explicitly so the numerical equivalent of Equation 2.1.5-1 is

$$\frac{1}{2}\rho^n g H^n \Delta t ,$$

2.1.5-2

where the n designates the previous time level and Δt is the time integration interval. This term is added to the right side of the mixture momentum equation.

In the nearly-implicit numerical scheme, the pump is coupled implicitly by way of its dependence on the volumetric flow rate (Q). It is assumed that the head depends on the volumetric flow rate, and a first order Taylor series expansion is used

$$H^{n+1} = H^n + \left(\frac{dH}{dQ} \right)^n (Q^{n+1} - Q^n) \quad . \quad 2.1.5-3$$

Thus, the numerical equivalent of Equation 2.1.5-1 in the nearly-implicit scheme is

$$\frac{1}{2} \rho_g^n g H^n \Delta t + \frac{1}{2} \rho_g^n g \left(\frac{dH}{dQ} \right)^n (Q^{n+1} - Q^n) \Delta t \quad . \quad 2.1.5-4$$

This term is added to the right side of the mixture momentum equation, which uses the linear implicit convection term from NUREG-4312¹ sections 3.1.1.4 and 3.1.1.7.

The pump dissipation is calculated for the pump volume as

$$\tau \omega - \frac{gH}{\rho} (\alpha_f \rho_f v_f + \alpha_g \rho_g v_g) A \quad , \quad 2.1.5-5$$

where τ is the pump torque and ω is the pump speed.

This term is evaluated explicitly in both the semi-implicit and nearly-implicit schemes, and it is partitioned between the liquid and vapor thermal energy equations in such a way that the rise in temperature due to dissipation is equal in each phase (the details of the dissipation mechanism in a two-phase system are unknown so the assumption is made that the mechanism acts in such a way that thermal equilibrium between the phases is maintained without phase change). Thus, the terms that are added to the right sides of the liquid and vapor thermal energy equations, are

$$\frac{\left[\tau \omega^n - \frac{gH^n}{\rho^n} \left(\alpha_f^n \rho_f^n v_f^n + \alpha_g^n \rho_g^n v_g^n \right) A \right] \Delta t \left(\alpha_f^n \rho_f^n C_{pf}^n \right)}{\left(\alpha_f^n \rho_f^n C_{pf}^n + \alpha_g^n \rho_g^n C_{pg}^n \right)} \quad 2.1.5-6$$

and

$$\frac{\left[r \omega^n - \frac{gH^n}{\rho^n} \left(\alpha_f^n \rho_f^n \bar{v}_f^n + \alpha_g^n \rho_g^n \bar{v}_g^n \right) A \right] \Delta t \left(\alpha_g^n \rho_g^n C_{pg}^n \right)}{\left(\alpha_f^n \rho_f^n C_{pf}^n + \alpha_g^n \rho_g^n C_{pg}^n \right)} \quad 2.1.5-7$$

respectively.

The pump head, H , and torque, r , are defined by means of an empirical homologous pump performance model and the pump speed, ω , is defined by a pump drive model. The derivative of the pump head with respect to the volumetric flow rate, dH/dQ , is obtained from the empirical homologous pump performance model using the assumption that the pump speed is constant.

Centrifugal Pump Performance Model

The basic pump performance data must be generated experimentally. Analytical programs have been developed that are reasonably successful in predicting near design pump performance for single-phase fluids. For off design operation or for operation with a two-phase fluid, the problems of analytical pump performance prediction are nearly insurmountable. The basic parameters that characterize the pump performance are the rotational speed, ω or N , the volumetric through flow, Q , the head rise, H , and the shaft torque, r . The relationship between these four parameters can be uniquely displayed by a four-quadrant representation of such data. A typical four quadrant curve is shown in Figure 2.1.5-4. Both positive and negative values for each of the four parameters are represented. The disadvantages in using such a data map for numerical purposes are the need for two-dimensional interpolation, the large number of points needed to define the entire range, and the fact that the map is infinite in extent. These objections can be largely

overcome by use of a homologous transformation based on the centrifugal pump similarity relationships. Such a transformation collapses the four quadrant data onto a single bounded dimensionless curve having eight basic octants. Typical homologous curves for the head and torque are illustrated in Figures 2.1.5-5 and 2.1.5-6 respectively where ω_r , Q_r , H_r , and τ_r are the rated values for the pump speed, volumetric flow rate, head, and torque, respectively. The homologous transformation is not unique and not all points of Figure 2.1.5-4 lie on the curves of Figures 2.1.5-5 and 2.1.5-6. However, the data are closely grouped and the single curve is a good approximation for the global pump performance.

The pump model allows the user the option of accounting for cavitation or two-phase degradation effects on pump performance. The user must supply a separate set of homologous, two-phase curves for head and torque that are in the form of difference curves. Difference curves are used because analysis of available two-phase pump data indicated that when the fluid being pumped had a void fraction between 0.2 and 0.9, little head was developed by the pump being tested. Outside this range of void fraction, the pump developed head varied from zero to undegraded single-phase performance. To consider the degraded performance, a set of dimensionless homologous curves was fit to the head data. Thus the fully-degraded two-phase head was expressed as a function of the standard pump model arguments.

To consider the ranges of void fraction where the pump was able to develop head (0 to 0.2 and 0.9 to 1.0), a multiplier as a function of void fraction was used. The multiplier varied from 0 to about 1.0 as the void fraction varied from 0 to 0.2, and the multiplier varied from about 1.0 to 0 as the void fraction varied from 0.9 to 1.0.

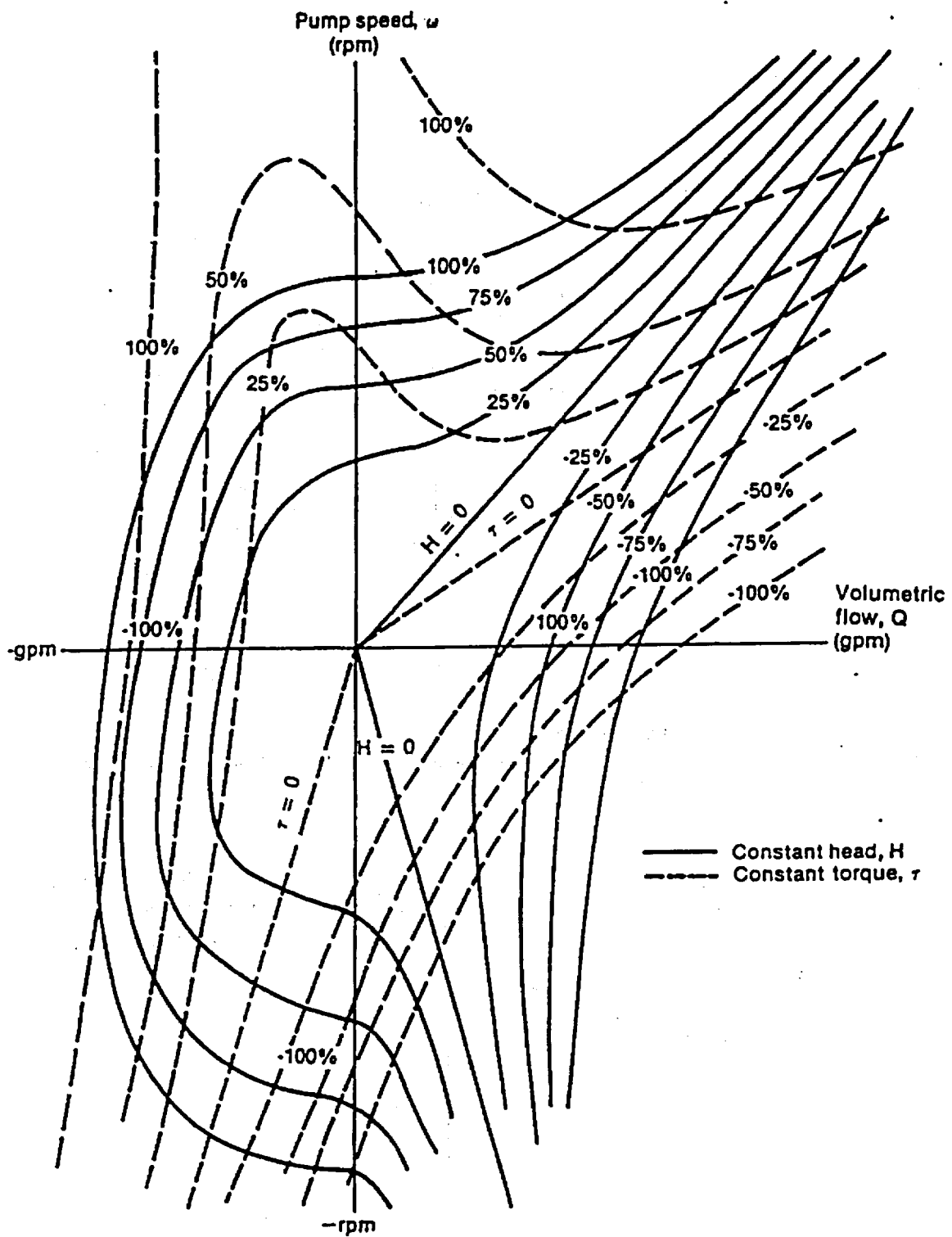


Figure 2.1.5-4. Typical Pump Characteristic Four-Quadrant Curves.

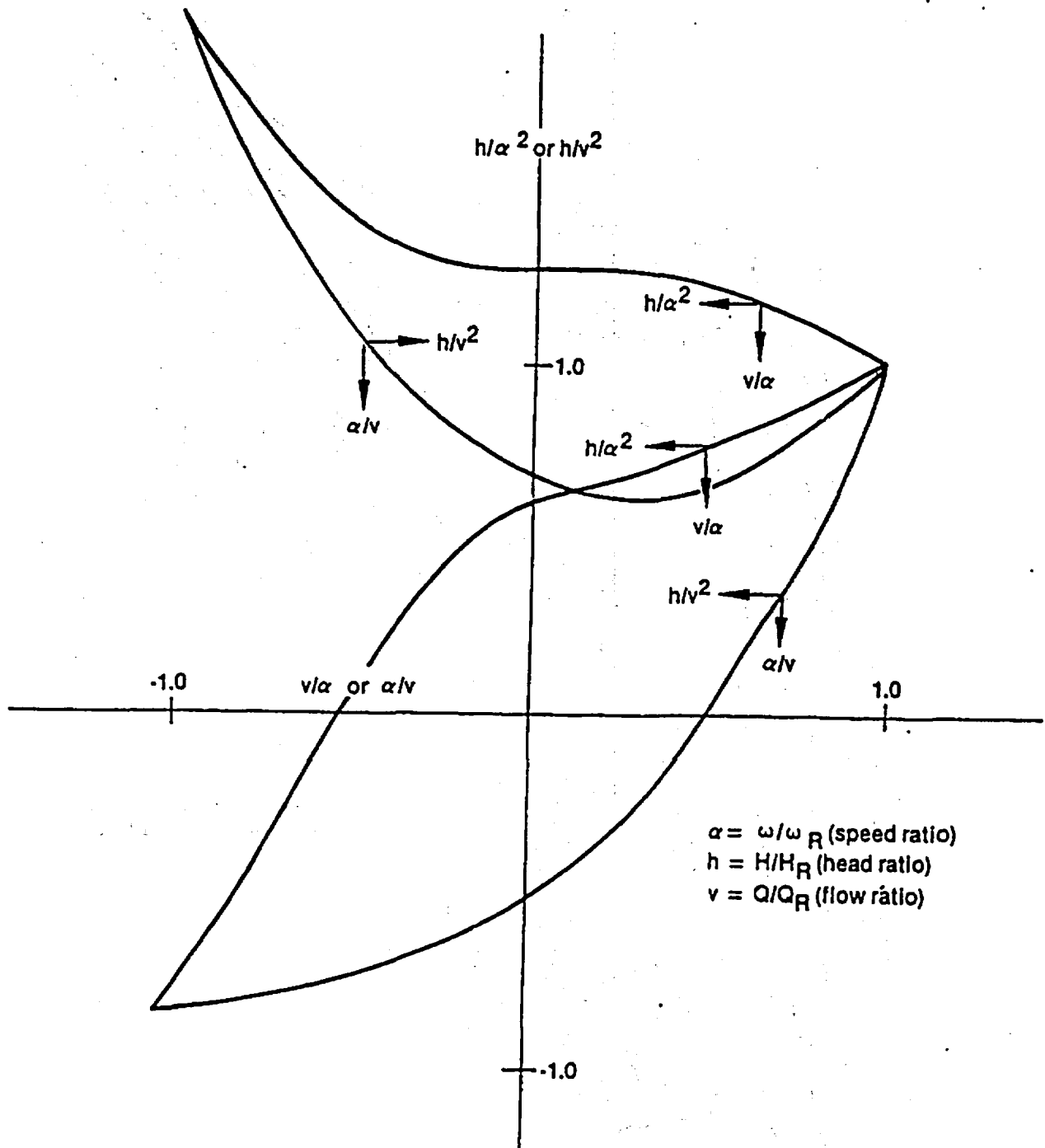


Figure 2.1.5-5. Typical Pump Homologous Head Curves.

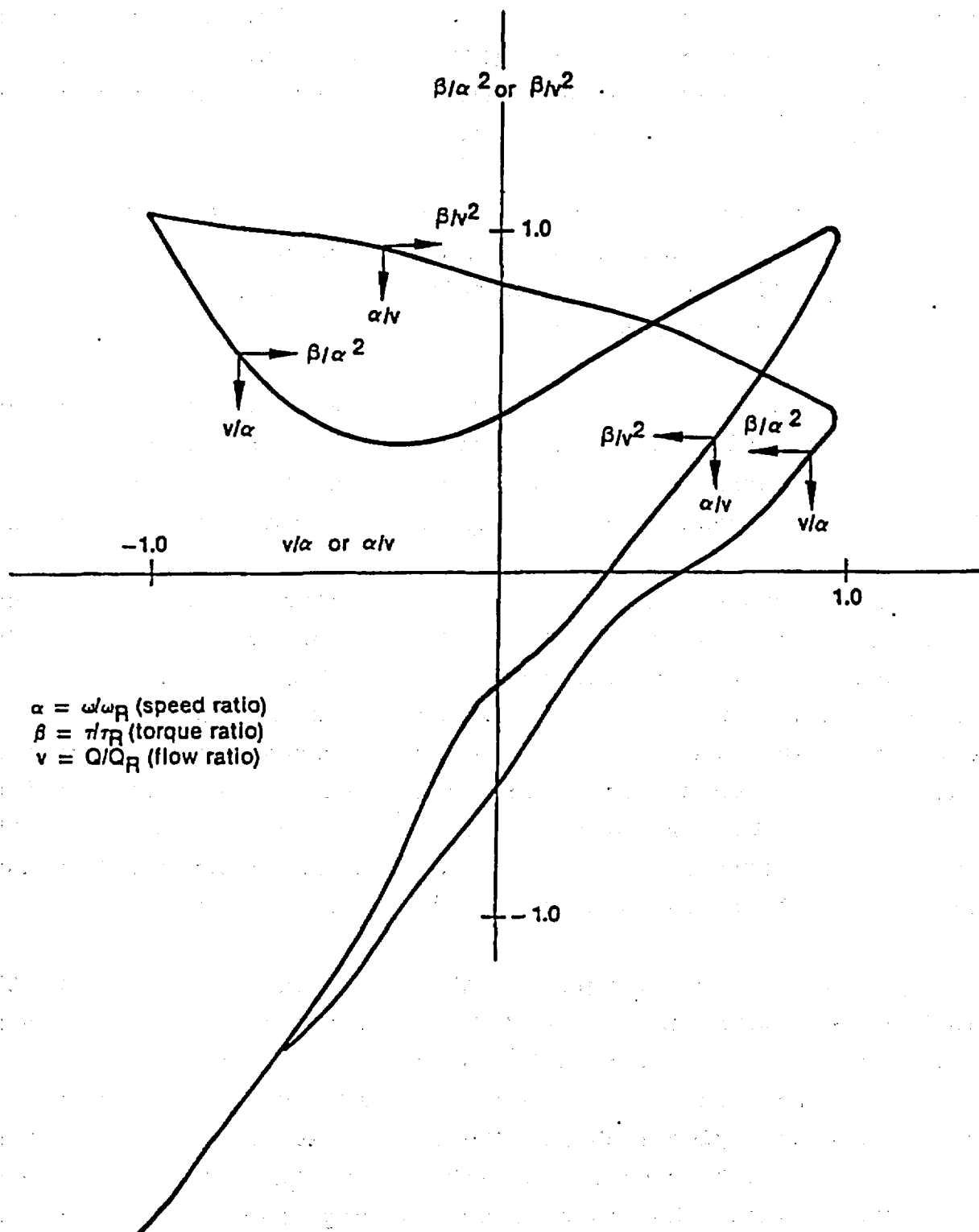


Figure 2.1.5-6. Typical Pump Homologous Torque Curves.

Available pump data from the 1-1/2 Loop Model Semiscale and Westinghouse Canada Limited (WCL) experiments were used in developing the two-phase pump data. Assumptions inherent in the pump model for two-phase flow include:

1. The head multiplier, $M_H(\alpha_g)$, determined empirically for the normal operating region of the pump, is also valid as an interpolating factor in all other operating regions.
2. The relationship of the two-phase to the single-phase behavior of the Semiscale pump is applicable to large reactor pumps. This assumes that the pump model of two-phase flow is independent of pump specific speed.

The single-phase pump head (dimensionless) curve for the Semiscale pump is shown in Figure 2.1.5-7 and the fully degraded two-phase pump head curves are shown in Figure 2.1.5-8. These represent complete pump characteristics (except for the reverse pump fully degraded region) for the Semiscale pump operating under two-phase conditions with the average of the void fractions of the pump inlet and outlet mixtures between 0.2 and 0.9. The lines drawn through the data were determined by least square polynomial fits to the data using known constraints.

A comparison of the two-phase data in Figure 2.1.5-8 with the single-phase data in Figure 2.1.5-7 shows that the two-phase dimensionless head ratio (h/v^2 or h/α^2) is significantly less than the single-phase dimensionless head ratio for the normal pump operation region (HAN and HVN). For negative ratios of v/α , such as those that occur in the HAD region, the pump flow becomes negative. When the pump flow is negative, the two-phase dimensionless head ratio is greater than the single-phase dimensionless head ratio. Two-phase flow friction losses are

Normal pump	$(+Q, +\alpha)$	} HAN HVN
Energy dissipation	$(-Q, +\alpha)$	
Normal turbine	$(-Q, -\alpha)$	} HAT HVT
Reverse pump	$(+Q, -\alpha)$	

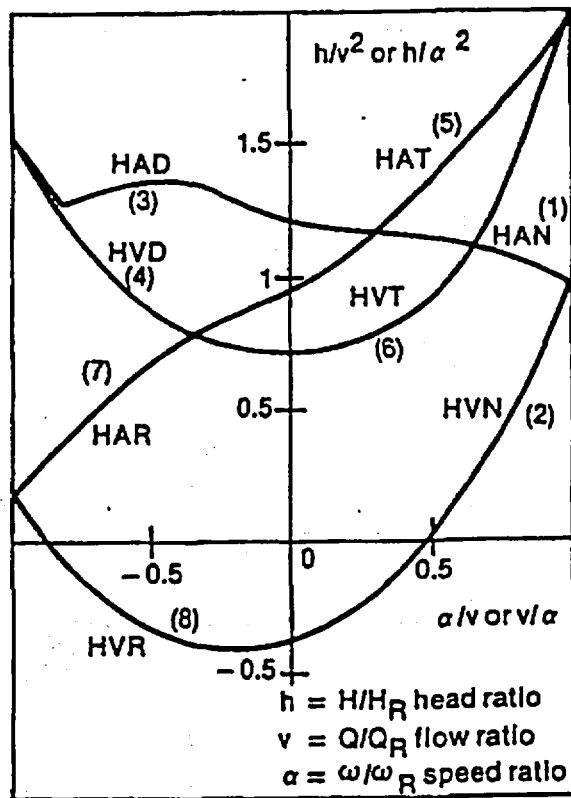


Figure 2.1.5-7. Single-Phase Homologous Head Curves for 1-1/2 Loop MOD1 Semiscale Pumps.

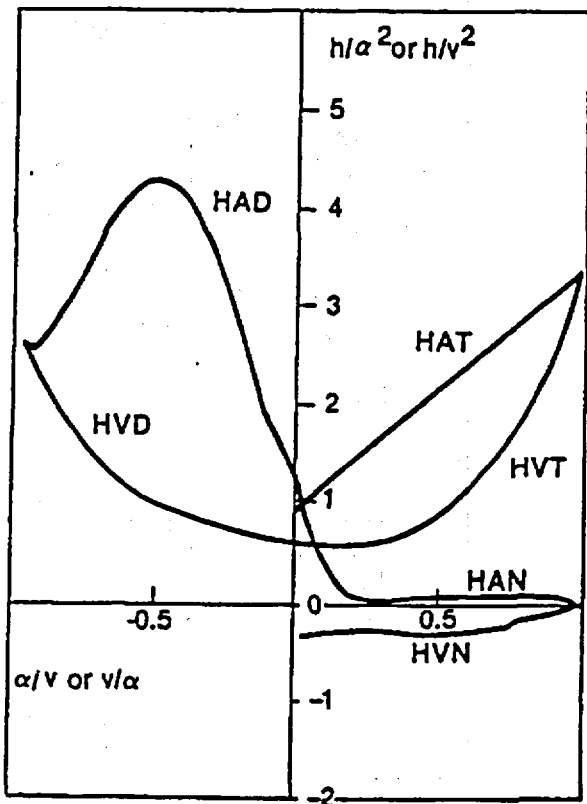


Figure 2.1.5-8. Fully Degraded Two-Phase Homologous Head Curves for 1-1/2 Loop MOD1 Semiscale Pumps.

generally greater than single-phase losses, and friction is controlling in this energy dissipation region (HAD). The other regions of two-phase dimensionless head ratio data show similar deviations from single-phase data.

Table 2.1.5-1 shows the difference between the single- and two-phase dimensionless head ratio data as a function of v/α and α/v for the various pumping regions shown in Figures 2.1.5-7 and 2.1.5-8. The differences shown in Table 2.1.5-1 are for the eight curve types used for determining pump head.

The head multiplier, $M_H(\alpha_g)$, and void fraction data shown in Table 2.1.5-2 were obtained in the following manner. The Semiscale and WCL pump data⁹² were converted to dimensionless head ratios of h/α^2 or h/v^2 . Values of the dimensionless head ratios were obtained for pump speeds and volumetric flow rates within 50% of the rated speed and flow rate for the pumps. The difference between the single- and two-phase dimensionless ratios was developed as a function of the average void fractions for the pump inlet and outlet mixtures. The difference between the single- and two-phase dimensionless ratios was then normalized to a value between 0 and 1.0. The normalized result was tabulated as a function of the void fraction.

If the two-phase option is selected, the pump head and torque are calculated from

$$H = H_{1\phi} - M_H(\alpha_g) (H_{1\phi} - H_{2\phi}) \quad 2.1.5-8$$

and

$$\tau = \tau_{1\phi} - M_r(\alpha_g) (\tau_{1\phi} - \tau_{\phi}) \quad 2.1.5-9$$

where

1ϕ = single-phase value,

2ϕ = two-phase, fully degraded value, $0.2 < \alpha_g < 0.9$,

M = multiplier on difference curve, and

α_g = average volume void fraction.

Centrifugal Pump Drive Model

The pump torque is used to calculate the pump speed after the pump has been shut off by the input trip signal. The speed is calculated by the deceleration equation

$$I \frac{d\omega}{dt} = r \quad 2.1.5-10$$

The solution of this equation is

$$\omega_{t+\Delta t} = \omega_t + \frac{r\Delta t}{I} \quad 2.1.5-11$$

where

r = net torque,

I = moment of inertia,

t = time,

Δt = time step, and

ω = angular velocity.

The rate of energy addition to the pump system is given by ωr and has been used in Equation 2.1.5-5 to calculate the pump dissipation.

Table 2.1.5-1. Semiscale Dimensionless Head Ratio Difference (single-phase minus two-phase) Data.

$$x = \frac{v}{\alpha} \quad \text{or} \quad \frac{\alpha}{v}$$

$$y = \frac{h}{\alpha^2} \Big|_{1\phi} - \frac{h}{\alpha^2} \Big|_{2\phi} \quad \text{or} \quad \frac{h}{v^2} \Big|_{1\phi} - \frac{h}{v^2} \Big|_{2\phi}$$

Curve Type	x	y	Curve Type	x	y	
1 (HAN)	0.00	0.00	4 (HVD)	-1.00	-1.16	
	0.10	0.82		-0.90	-0.78	
	0.20	1.09		-0.80	-0.50	
	0.50	1.02		-0.70	-0.31	
	0.70	1.01		-0.60	-0.17	
	0.90	0.94		-0.50	-0.08	
	1.00	1.00		-0.35	0.00	
				-0.20	0.05	
2 (HVN)	0.00	0.00		-0.10	0.08	
	0.10	-0.04		0.00	0.11	
	0.20	0.00	5 (HAT)	0.00	0.00	
	0.30	0.10		0.20	-0.34	
	0.40	0.21		0.40	-0.65	
	0.80	0.67		0.60	-0.95	
	0.90	0.80		0.80	-1.19	
	1.00	1.00		1.00	-1.47	
3 (HAD)	-1.00	-1.16		6 (HVT)	0.00	0.11
	-0.90	-1.24			0.10	0.13
	-0.80	-1.77	0.25		0.15	
	-0.70	-2.36	0.40		0.13	
	-0.60	-2.79	0.50		0.07	
	-0.50	-2.91	0.60		-0.04	
	-0.40	-2.67	0.70		-0.23	
	-0.25	-1.69	0.80		-0.51	
	-0.10	-0.50	0.90		-0.91	
	0.00	0.00	1.00		-1.47	
		7 (HAR)	-1.00	0.00		
			0.00	0.00		
		8 (HVR)	-1.00	0.00		
			0.00	0.00		

Table 2.1.5-2. Head Multiplier and Void Fraction Data.

α_g	$M_H(\alpha_g)$
0.00	0.00
0.10	0.00
0.15	0.05
0.24	0.80
0.30	0.96
0.40	0.98
0.60	0.97
0.80	0.90
0.90	0.80
0.96	0.50
1.00	0.00

The total pump torque is calculated by considering the hydraulic torque from the homologous curves and the pump frictional torque. The net torque with the drive motor shut off is

$$T = T_{hy} + T_{fr}$$

2.1.5-12

where

T_{hy} = hydraulic torque and

T_{fr} = frictional torque.

Pump frictional torque ($T_{fr} = TF$) is modeled as a cubic function of the pump rotational velocity. The FORTRAN notation for the cubic function is

$$S = \frac{V}{VR}$$

2.1.5-13

$$SA = |S| , \text{ and}$$

2.1.5-14

$$TF = -SIGN(TFO + TF1 \cdot SA + TF2 \cdot SA^2 + TF3 \cdot SA^3, S) ,$$

2.1.5-15

where V is pump rotational velocity, VR is rated pump rotational velocity, TFO, TF1, TF2, and TF3 are input data, and SIGN is a function whose result is the magnitude of the first argument with the sign of the second argument. An option is available to specify whether reverse rotation of the pump is allowed.

The electric drive motor will affect the speed behavior of the pump while the motor remains connected to its power source. The net torque with the drive motor on is incorporated into the pump model by adding the value of motor torque, τ_m , to the torque summation

$$\tau = \tau_{hy} + \tau_{fr} - \tau_m ,$$

2.1.5-16

where the sign of the motor torque is the same as that of the hydraulic and frictional torque for steady operating conditions, that is, zero net torque.

Induction motors are used to drive primary coolant pumps. At constant voltage, the motor torque is an explicit function of speed. This torque/speed relationship is normally available from the motor manufacturer.

Motor torque is supplied to the pump model as a tabular function of torque versus speed as given by the manufacturer's data. A typical torque/speed curve for an induction motor is shown in Figure 2.1.5-9.

The capability to simulate a locked rotor condition of the pump is included in RELAP5. This option provides for simulation of the pump rotor lockup as a function of input elapsed time,

maximum forward speed, or maximum reverse speed. At the time the rotor locks (and at all times thereafter), the pump speed is set equal to zero.

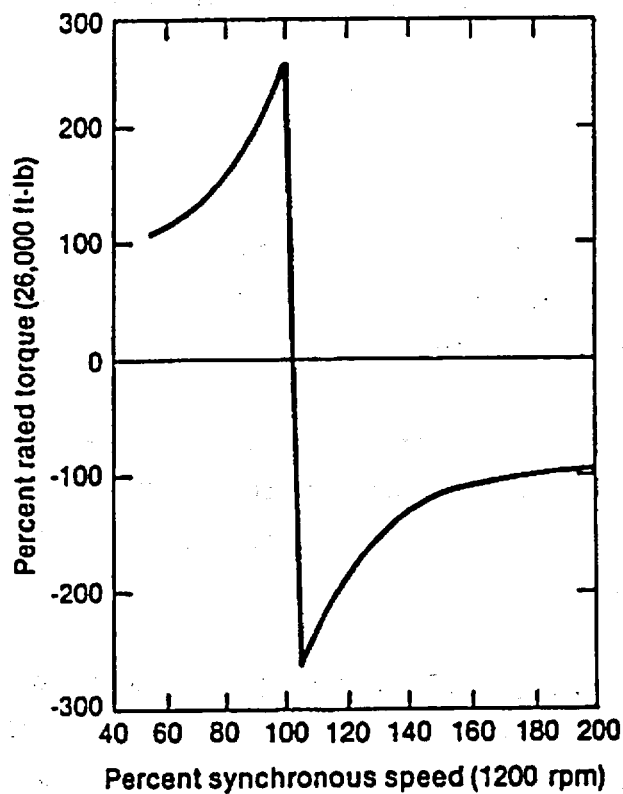


Figure 2.1.5-9. Torque Versus Speed, Type 93A Pump Motor (Rated Voltage).

2.1.5.3. Valves

Valves are quasi-steady models that are used either to specify an option in a system model or to simulate control mechanisms in a hydrodynamic system. The RELAP5 valve models can be classified into two categories: (a) valves that open or close instantly, and (b) valves that open or close gradually. Either type can be operated by control systems or by flow dynamics.

Valves in the first category are trip valves and check valves. The model for these valves does not include valve inertia or momentum effects. If the valve is used as a junction with an abrupt area change, then the abrupt area change model is used to calculate kinetic loss factors when the valve is open.

Valves in the second category are the inertial swing check valve, the motor valve, the servo valve, and the relief valve. The inertial valve and relief valve behavior is modeled using Newton's second law of motion. The abrupt area change model controls losses through the valve as the cross-sectional flow area varies with valve assembly movement. The motor and servo valve use differential equations to control valve movement. These two valves include the options to use the abrupt area change model to calculate losses across the valve or to use flow coefficients (C_v) input by the user. The C_v 's are converted to energy loss coefficients within the numerical scheme.

Valves are modeled in RELAP5 as junction components. The types of valves are defined as follows.

Trip Valve

The operation of a trip valve is solely dependent on the trip selected. With an appropriate trip, an abrupt full opening or full closing of the valve will occur. A latch option is also included for latching the valve in the open or closed position.

Check Valve

The operation of a check valve can be specified to open or close by static differential pressure, to open by static differential pressure and close by flow reversal, or to open by static differential pressure and close by dynamic differential pressure.

All of the check valves will be opened or closed based on static differential pressure across the junction according to

$$\left[P_K + \Delta P_{Kg} \right] - \left[P_L + \Delta P_{Lg} \right] - PCV > 0, \text{ valve opens, 2.1.5-17}$$

where

P_K, P_L = junction from and to volume thermodynamic pressures,

$\Delta P_{Kg}, \Delta P_{Lg}$ = static pressure head due to gravity, and

PCV = back pressure required to close the valve (user input).

For a static pressure controlled check valve the valve will open if Equation 2.1.5-17 becomes positive and will close if Equation 2.1.5-17 becomes negative. If Equation 2.1.5-17 is zero, the valve will remain as previously defined.

For a flow controlled check valve, the valve will open if Equation 2.1.5-17 is positive and will close only if a flow reversal occurs such that

$$GC < 0,$$

where GC is the dynamic pressure given as

$$GC = \frac{1}{2}(|\overline{\rho v}| \bar{v})_j = \frac{1}{2}|\alpha_f \rho_f v_f + \alpha_g \rho_g v_g|_j (\alpha_f v_f + \alpha_g v_g)_j \quad 2.1.5-18$$

For a dynamic pressure controlled check valve, the valve opens if Equation 2.1.5-17 is greater than zero. Once the valve is open, the forces due to pressure differential and momentum hold the valve open until

$$\left[P_K - \Delta P_{K_g} \right] - \left[P_L + \Delta P_{L_g} \right] + GC - PCV \begin{cases} < 0, \text{ valve closes} \\ = 0, \text{ remains as} \\ & \text{previously} \\ & \text{defined.} \end{cases} \quad 2.1.5-19$$

The terms α_f and α_g are the junction liquid and vapor volume fractions, respectively, ρ_f and ρ_g are the junction liquid and vapor densities, respectively, and v_f and v_g are the junction liquid and vapor velocities, respectively.

All check valves may be initialized as either open or closed. Leakage is also allowed if the valve is closed and the abrupt area change model is used to calculate the valve form losses.

Inertial Valve

This valve models the motion of the valve flapper assembly in an inertial type check valve. The abrupt area change model is used to calculate kinetic form losses assuming that the area between the flapper and the valve seat behaves as an orifice whose area changes in time as a function of the inertial valve geometry.

The motion of the flapper about the shaft axis is given by Newton's second law (angular version) as

$$r = I \alpha ,$$

2.1.5-20

where the external torques acting on the valve disk are given by

$$r = - W L \sin(\theta + \phi) - A_D L(\Delta P + P_{BP} + G_{head}) , \quad 2.1.5-21$$

where ΔP is the pressure drop across the valve, and α is the angular acceleration. Substituting Equation 2.1.5-20 into Equation 2.1.5-21 gives

$$I\alpha = - WL \sin\theta - \pi R^2 L(\Delta P + P_{BP} + G_{head}) , \quad 2.1.5-22$$

where ϕ has been dropped by assuming the valve is a horizontal pipe. Equation 2.1.5-22 is then written in finite-difference form as

$$\alpha^n = \frac{1}{I} - WL \sin\theta^n - \pi R^2 L(\Delta P^n + P_{BP} + G_{head}) , \quad 2.1.5-23$$

where the superscript, n , indicates the time level, $t + n \Delta t$. Integrating Equation 2.1.5-23 with respect to time yields the angular velocity

$$\omega^{n+1} = \omega^n + \alpha^n \Delta t . \quad 2.1.5-24$$

Similarly integrating Equation 2.1.5-24 gives the angular position

$$\theta^{n+1} = \theta^n + \omega^{n+1} \Delta t . \quad 2.1.5-25$$

The throat flow area for the valve is set by the following function ^{94,95}.

$$A_{throat} = \begin{cases} 2\pi R^2 \tan(\theta^{n+1}) & \theta \leq 26.565 \\ \pi R^2 & \theta > 26.565 . \end{cases} \quad 2.1.5-26$$

Several options are allowed with the use of this valve such as specifying minimum and maximum flapper angular positions when the valve is closed, specifying latch or no latch options, and specifying leakage.

Motor Valve

This valve model has the capability of controlling the junction flow area between two control volumes as a function of time. The operation of the valve is controlled by two trips: one for opening the valve, and a second for closing the valve. A constant rate parameter controls the speed at which valve area changes. The motor valve area variation can also be specified using a general table. When the general table is specified, the constant rate parameter controls the valve stem position and the general table relates the stem position to the valve flow area. Conversely, when the general table is not specified, the constant rate parameter controls the rate of change in valve area.

The abrupt area change model is used to calculate kinetic form losses with respect to the valve area. However, if the normalized valve flow area has a value less than 1.0E-10, the valve is assumed to be closed.

A second option allowed for the motor valve is the specification of valve flow coefficients, C_v . These coefficients may be specified using a general table of C_v versus normalized stem position and the smooth junction option must be specified. The conversion of C_v to an energy loss coefficient, K , is done in the numerical scheme using the formula

$$K = 2 \frac{A_{\text{valve}}^2}{C_v^2 \rho_0}$$

2.1.5-27

where

ρ_0 = density of water at 288.71 K (60.0 F).

Provisions also exist for applying multipliers to both stem position and C_v .

Servo Valve

The servo valve operation is similar to that for the motor valve. However, the valve area or stem position is controlled by a control variable rather than by a specified rate parameter. The servo valve also has the same options as the motor valve.

Relief Valve

For thermal-hydraulic analysis of overpressure transients it is necessary to simulate the effects of relief valves. In particular, it is desirable to model the valve dynamic behavior including simulation of valve flutter and hysteresis effects.

To assist in understanding the relief valve model three schematics of a typical relief valve are shown in Figures 2.1.5-10, 2.1.5-11, and 2.1.5-12. The three schematics represent the valve in the closed (Figure 2.1.5-10), partially open (Figure 2.1.5-11), and fully open (Figure 2.1.5-12) modes, respectively. In the schematics, the seven main components of a relief valve are shown, which are: the valve housing, inlet, outlet, piston rod assembly, spring, bellows, and valve adjusting ring assembly. The numerical model of the valve simply approximates the fluid forces acting on the valve piston and the valve reaction to these forces. The model of the fluid forces is based on a quasi-steady-state form of the impulse momentum principle and the valve reaction force is based on Newton's Second Law of motion.

A qualitative understanding of the operation of the relief valve can be gained by referring again to Figures 2.1.5-10, 2.1.5-11, and 2.1.5-12. If the valve inlet pressure is low the valve is closed, as shown in Figure 2.1.5-10. As the inlet pressure increases the valve piston will remain closed until the force of the upstream pressure on the valve exceeds the setpoint forces. The setpoint forces are the combined forces of the piston and rod assembly weight, the valve spring, the atmospheric pressure inside the bellows and the downstream back pressure around the outside of the bellows. Once the setpoint forces are exceeded the valve piston will begin to lift. Upon opening, the upstream fluid will begin to expand through the opening into the valve ring region. This initial expansion occurs through the angle α_0 and the flow changes direction through an average angle θ_0 as shown in Figure 2.1.5-10. As the flow accelerates, the momentum effects of the expansion and change in flow direction exert a thrust on the valve piston causing the valve to open further. As the valve partially opens the angle of expansion decreases to α_1 and the change in flow direction increases to θ_1 as shown in Figure 2.1.5-11. This effect in turn further increases the thrust on the valve piston causing it to fully open as shown in Figure 2.1.5-12. As these processes occur the valve reaction forces and fluid momentum forces vary in such a manner that the valve will not close until the upstream pressure decreases significantly below the valve setpoint pressure. In this respect a hysteresis effect is observed that is characteristic of relief valves.

The relief valve model consists of a set of equations designed to approximate the behavior described above. In implementing the model, the dynamic behavior of the fluid is calculated at each time step by the RELAP5/MOD2-B&W hydrodynamic solution scheme. The resultant phasic velocities and thermodynamic properties are then utilized to solve a quasi-steady equation approximating the fluid forces on the valve piston. The valve dynamic reaction

forces are then calculated and the new time valve piston speed and position are estimated.

The relief valve model is formulated by applying D'Alembert's principle in which the forces acting on the face of the valve piston are balanced, for which the valve reaction forces can be written as

$$(\text{Reaction Forces}) = F_R = m_v a_{v,x} + B (v_{v,x} - v_{\text{housing}}) + K_s x ,$$

2.1.5-28

where

m_v = mass of the valve mechanism that is in motion
(i.e., the valve piston and rod assembly combined with the spring and bellows),

$a_{v,x}$ = valve assembly acceleration in the x-direction,

B = damping coefficient,

$v_{v,x}$ = velocity of the valve mechanism in the x-direction,

$v_{\text{housing}} = 0$ = velocity of the valve housing,

K_s = spring constant, and

x = piston position (i.e., x-coordinate).

The positive x-direction is assumed to be in the direction of fluid flow at the valve inlet. The fluid forces can be formulated by summing the forces acting over the surfaces of the fluid flow channel such that

$$(\text{Fluid Forces}) = F_F = (P_i A_D) x$$

$$- (P_a A_{Ba}) x - (P_o A_{Bo}) - (P_e A_e) x - F_R ,$$

2.1.5-29

where

F_R = reaction forces,

P_i = valve inlet pressure,

A_D = valve piston face area exposed to the inlet flow stream,

P_a = atmospheric pressure inside the bellows,

A_{Ba} = valve piston area inside the bellows,

P_o = valve back pressure outside the bellows,

A_{Bo} = valve piston area outside the bellows,

A_e = valve ring exit area, and

P_e = valve ring exit pressure.

The subscript x denotes that the force component is in the x -direction. Since the fluid is flowing through a channel that both expands and changes direction, the fluid undergoes a change in momentum expressed by the impulse momentum principle as

$$F_F = \Delta(mv) = \dot{m}_F (v_{e,x} - v_{i,x}) , \quad 2.1.5-30$$

where

\dot{m}_F = mass flow rate of the fluid through the valve,

$v_{e,x}$ = fluid velocity exiting through the rings, and

$v_{i,x}$ = fluid velocity entering the valve inlet.

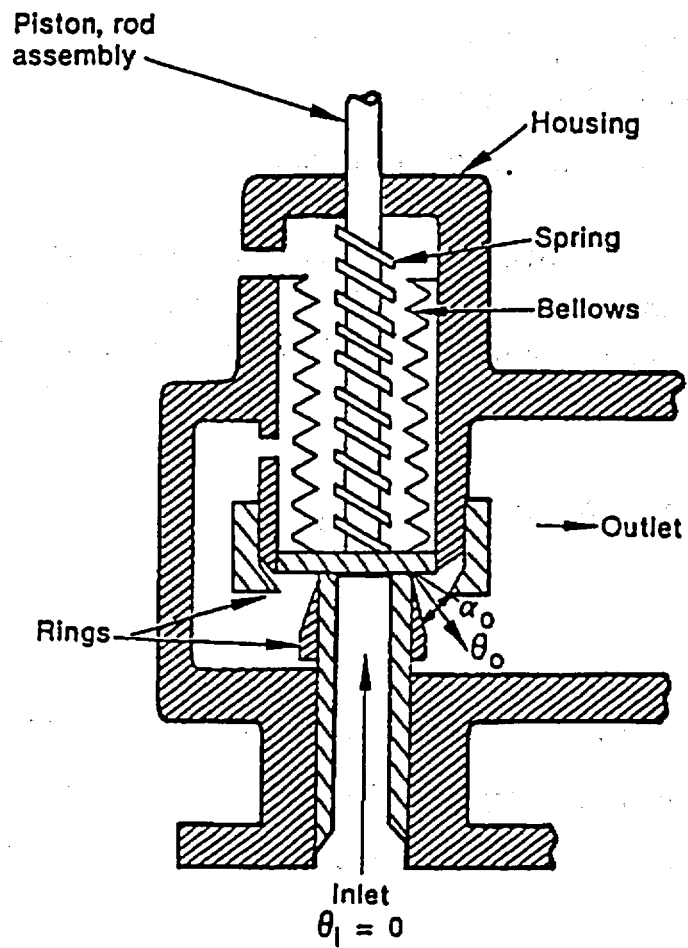
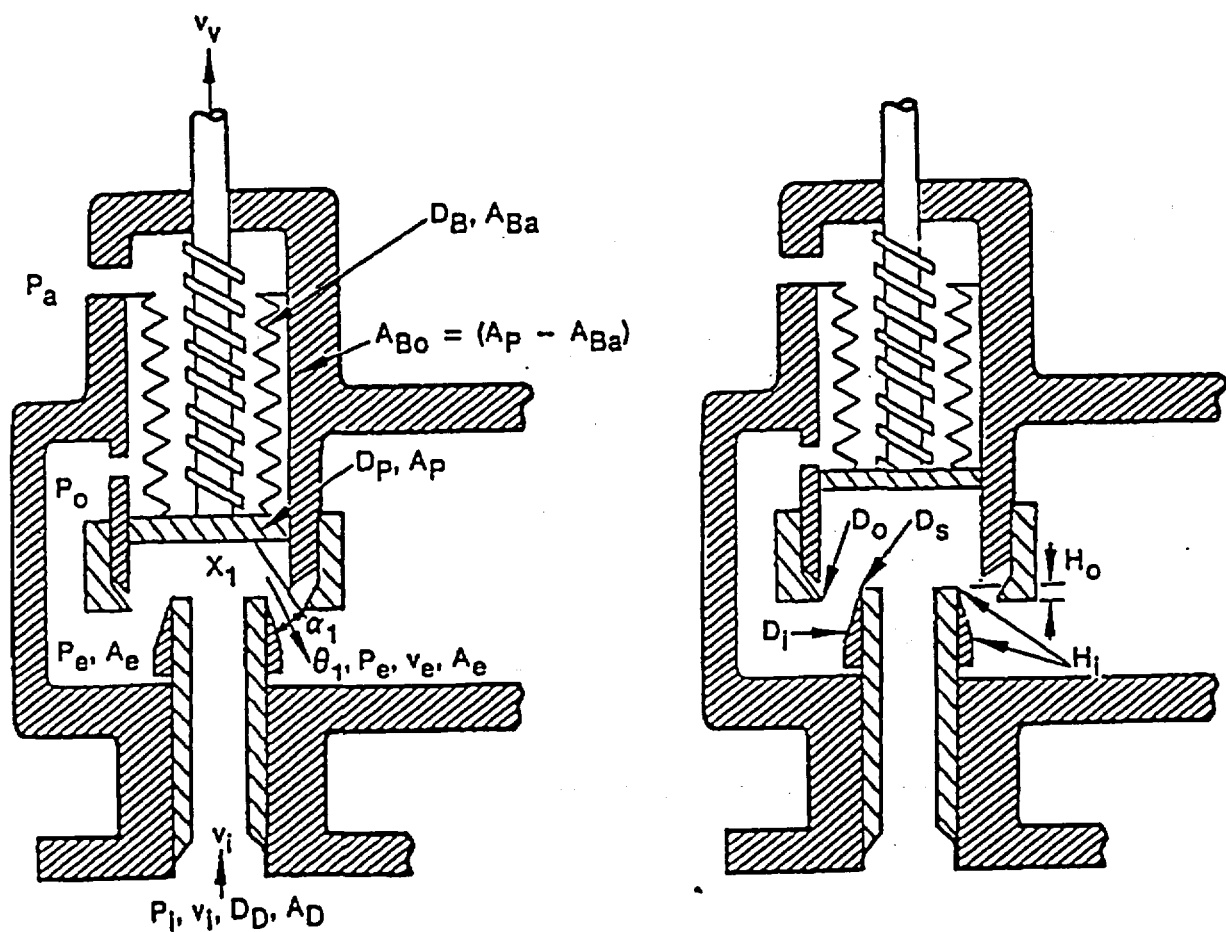


Figure 2.1.5-10. Schematic of a Typical Relief Valve in the Closed Position.



Figures 2.1.5-11. and 2.1.5-12. Schematic of a Typical Relief Valve in the Partially and Fully Open Positions, respectively.

Hence balancing the forces by combining Equations 2.1.5-28, 2.1.5-29 and 2.1.5-30 gives

$$m_v a_{v,x} + Bv_{v,x} + K_s x = -(P_a A_{Ba}) - (P_o A_{Bo}) - (P_e A_e) \cos\theta - \dot{m}_F (v_e \cos\theta - v_i) + P_i A_D . \quad 2.1.5-31$$

The valve acceleration can be expressed in terms of the valve velocity as

$$a_{v,x} = \frac{dv_{v,x}}{dt} + g , \quad 2.1.5-32$$

where g is the acceleration of gravity.

Combining Equations 2.1.5-31 and 2.1.5-32, treating the velocity damping term and spring force position terms implicitly and integrating over the time step gives

$$m_v (v_{v,x}^{n+1} - v_{v,x}^n) + Bv_{v,x}^{n+1} dt + K_s x^{n+1} dt + m_v g dt = [(P_i^n A_D) - (P_a^n A_{Ba}) - (P_o^n A_{Bo}) - (P_e^n A_e) \cos\theta_e^n - \dot{m}_F^n (v_e \cos\theta_e^n - v_i)] dt , \quad 2.1.5-33$$

where the superscripts n and $n+1$ represent the old and new time terms, respectively.

The position term, x^{n+1} , can be written in terms of the valve velocity by considering that

$$v_{v,x} = \frac{dx}{dt} . \quad 2.1.5-34$$

If Equation 2.1.5-34 is integrated over the time step then

$$x^{n+1} = x^n + v_{v,x}^{n+1} dt \quad . \quad 2.1.5-35$$

If the valve setpoint pressure is equated to $K_S x_0$ then combining Equations 2.1.5-33 and 2.1.5-35 and both adding and subtracting the term $K_S x_0$ gives the numerical form of the relief valve model, for which

$$\begin{aligned} m_v (v_{v,x}^{n+1} - v_{v,x}^n) + [(B + K_S dt) v_{v,x}^{n+1} + K_S (x^n - x_0) + m_v g] dt \\ = K_S x_0 dt + [(P_i^n A_D) - (P_a A_{Ba}) - (P_o^n A_{Bo}) - (P_e^n A_e) \cos \theta_e^n \\ - \dot{m}_F^n (v_e^n \cos \theta_e^n - v_i^n)] dt \quad . \quad 2.1.5-36 \end{aligned}$$

The size of the gravity term, g , is dependent on the valve orientation. For example, if the valve is oriented upward (i.e., $+x$ is upward) then the gravity term is expressed as $g = -|g|$.

In the numerical scheme, Equation 2.1.5-36 is solved for the new time valve piston velocity, v_v^{n+1} , in terms of the current time terms with superscript, n . The terms required to model the valve geometry and the valve damping, spring, and back pressure forces are input by the user.

The characteristic relief valve hysteresis effects are inherent in the formulation of Equation 2.1.5-36. For example, if the valve is closed then all velocity terms are zero and $x = x_0$. Therefore, acceleration of the valve piston in the positive x direction cannot occur until the upstream force $P_i A_D$ exceeds the spring set point and valve weight. Once the valve opens and the fluid accelerates, the forces due to the change in fluid momentum aid in holding the valve open. Therefore, the valve cannot close until the combined fluid pressure and momentum terms decrease

below the set point forces. Hence, the desired hysteresis is incorporated in the model.

2.1.5.4. Accumulator Model

An accumulator model is included in RELAP5/MOD2-B&W that features mechanistic relationships for the hydrodynamics, heat transfer from the tank wall and water surface, condensation in the vapor dome, and vaporization from the water surface to the vapor dome.

Hydrodynamic Model

An accumulator is modeled in RELAP5 as a lumped-parameter component. This modeling was chosen for two reasons; the spatial gradients in the accumulator tank are expected to be small, and special treatment of the equation of state can be utilized.

The accumulator model and associated notations are shown in Figure 2.1.5-13. The basic model assumptions are:

1. Heat transfer from the accumulator walls and heat and mass transfer from the liquid are modeled using natural convection correlations assuming similarity between heat and mass transfer from the liquid surface.
2. The gas in the gas dome is modeled as a closed expanding system composed of an ideal gas with constant specific heat. The steam in the dome exists at a very low partial pressure and hence its effect on the nitrogen state is neglected. However, energy transport to the gas dome as a result of vaporization/condensation is included.
3. Because of the high heat capacity and large mass of water below the interface, the water is modeled as an isothermal system.

4. The model for liquid flow includes inertia, wall friction, form loss and gravity effects.

Using these assumptions, the basic equations governing the thermal-hydraulics of the tank and discharge line for conservation of mass (nitrogen) can be written as

$$M_n = \text{constant} = \rho_n V_n \quad 2.1.5-37$$

where

M_n and ρ_n = gas mass and density, respectively, and
 V_n = gas dome volume

for conservation of energy.

Nitrogen

$$M_n \frac{\partial u_n}{\partial t} = - P_D \frac{\partial V_v}{\partial t} + \dot{Q}_D \quad 2.1.5-38$$

where

u_n = nitrogen internal energy
 P_D = vapor dome pressure, and
 \dot{Q}_D = heat transfer rate to the gas dome.

Wall

$$M_{\text{wall}} C_{v_{\text{wall}}} \frac{\partial T_{\text{wall}}}{\partial t} = -\dot{Q}_{\text{wall}} \quad 2.1.5-39$$

where

M_{wall} = metal mass in the tank wall,

$C_{V_{\text{wall}}}$ = metal specific heat,

T_{wall} = mean metal temperature, and

Q_{wall} = heat transfer rate to the wall.

For momentum^a

$$\rho A \left(L \frac{\partial v}{\partial t} + \frac{1}{2} v^2 \right) + Fv = - A \frac{\partial P}{\partial x} + \Delta P_z, \quad 2.1.5-40$$

where

A = flow channel cross-sectional area,

v = velocity,

F = frictional loss coefficient, and

ΔP_z = elevation pressure differential.

For the gas state relationships

$$P_D V_v = M_n R_n T_D \quad 2.1.5-41$$

and

$$U_n = M_n C_{V_n} T_D \quad 2.1.5-42$$

^aEquation 2.1.5-40 is the combined tank and discharge line momentum equations. The wall drag coefficient, F , is given as $1/2 p_w f L_L/D A_{LV}$, where D = surge line diameter.

Using Equations 2.1.5-41 and 2.1.5-42, the nitrogen energy equation (Equation 2.1.5-40), can be rewritten as

$$M_n C_{v_n} \frac{dT_D}{dt} = - P_D v A_L + \dot{Q}_D \quad . \quad 2.1.5-43$$

Differentiating Equation 2.1.5-41, eliminating the constant term $M_n R_n$ and substituting the result into Equation 2.1.5-43 yields

$$P_D \left(1 + \frac{R_n}{C_{v_n}} \right) \frac{dv_v}{dt} + v_v \frac{dP_D}{dt} = \frac{R_n}{C_{v_n}} \dot{Q}_D \quad . \quad 2.1.5-44$$

Equations 2.1.5-40, 2.1.5-43, and 2.1.5-44 comprise the system of three differential equations used in the accumulator hydrodynamic model. They are used to numerically advance T_D , v_v , and P_D in time.

Heat Transfer to the Gas Dome

In the accumulator, energy transport by heat transfer is modeled to the gas dome using a typical convective transport equation of the form

$$Q_i = h_i A_i (T_i - T_d) \quad , \quad 2.1.5-45$$

where

subscript i = thermal transport interface,

h_i = convective transport coefficient,

A_i = interface surface area, and

$T_i - T_d$ = interface to gas dome temperature difference.

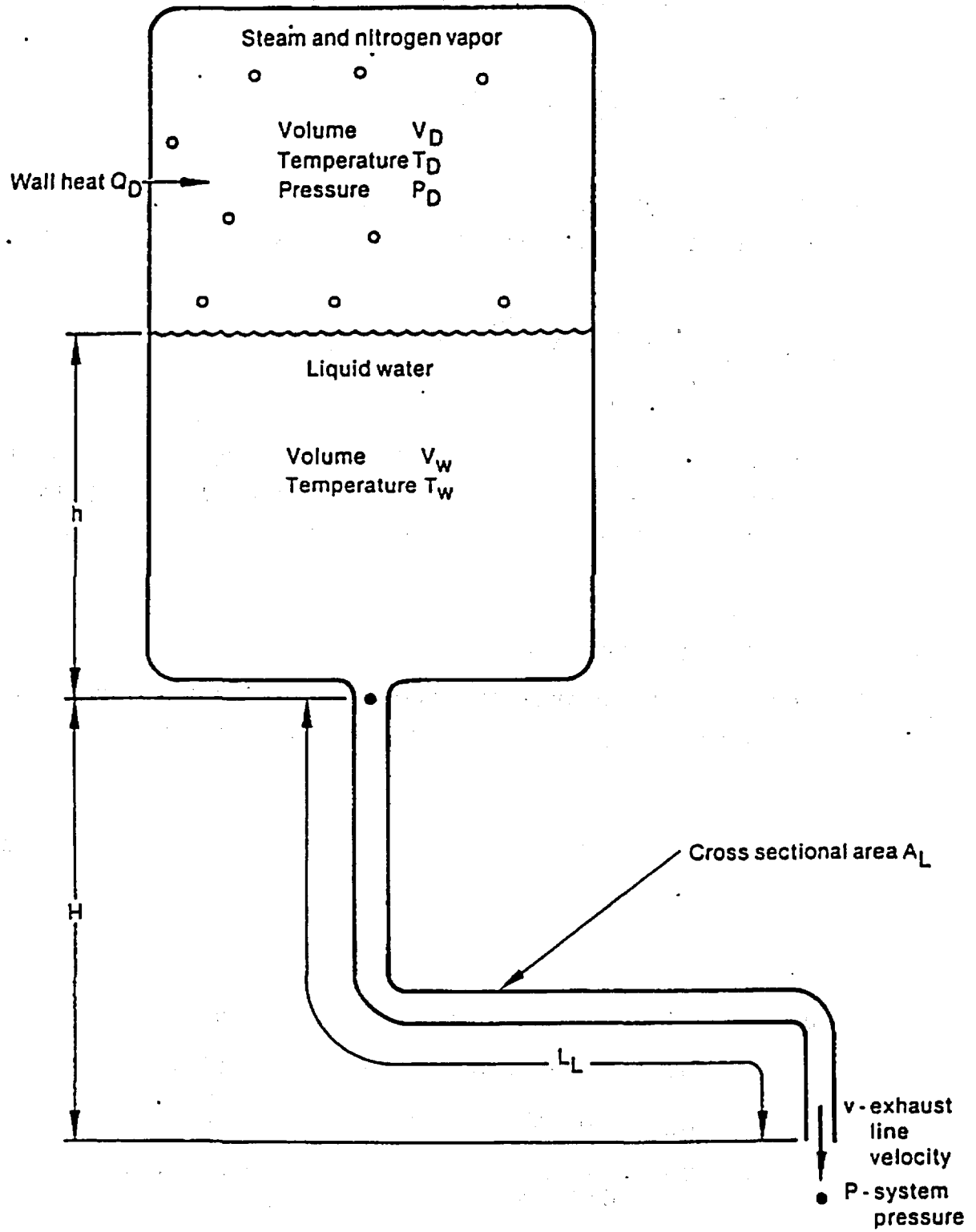


Figure 2.1.5-13. Typical Accumulator.

It should be noted that heat and mass transfer in the accumulator surge line are neglected.

Two turbulent natural convection heat transfer models are used and combined by superposition. First, heat transfer with the cylindrical walls of the tank is considered using a turbulent natural convection correlation⁹⁶ for heat transfer within a vertical cylinder with closed ends for which

$$h_1 = 0.1 \frac{k_d}{\frac{1}{2} D_{TK}} (Gr Pr)^{\frac{1}{3}} \frac{L}{\delta} \quad 2.1.5-46$$

and

$$A_1 = \pi D_{TK} L, \quad 2.1.5-47$$

where

h_1 = gas dome to cylinder heat transfer coefficient,

L = gas dome cylinder length,

δ = gas dome characteristic diameter,

k_d = gas thermal conductivity,

$\frac{1}{2} D_{TK}$ = integration interval normal to the surface of the cylinder,

Gr = gas dome Grashof number, and

Pr = gas dome Prandtl number.

Second, heat transfer with the disk shaped ends of the cylinder is considered, where the top disk is the metal top of the tank and the bottom disk is the liquid-gas interface. For this model a turbulent natural convection correlation⁵⁶ is used for heat

transfer between two horizontal disks separated vertically where, for each disk,

$$h_2 = 0.15 \frac{k_d}{L} (Gr Pr)^{\frac{1}{3}} \frac{L}{\delta} \quad 2.1.5-48$$

and

$$A_2 = \frac{\pi D_{TK}^2}{4} \quad 2.1.5-49$$

In the correlations given by Equations 2.1.5-46 and 2.1.5-49 the product of the Grashof and Prandtl numbers represents the convective thermal circulation in the gas dome, where the Grashof number represents the circulation and the Prandtl number represents the thermal diffusion. Only the Grashof number is a function of the gas dome dimensions and temperature difference for which

$$Gr = \frac{g \beta_d |T_i - T_d| \delta^3}{\nu_i^2}, \quad 2.1.5-50$$

where

g = acceleration due to gravity,

β_d = gas isobaric coefficient of thermal expansion,

$T_i - T_d$ = magnitude of the interface, gas dome temperature difference,

ν_i = gas kinematic viscosity, and

δ = characteristic overall diameter of the gas dome.

If the Prandtl number is written in terms of the gas dome thermal diffusivity then

$$Pr = \frac{\mu_d}{\rho_d \alpha_d} , \quad 2.1.5-51$$

where

ρ_d = gas density and

α_d = thermal diffusivity.

The characteristic diameter is defined in terms of the typical volume to surface area ratio as

$$\delta = \frac{4 V_d}{A_i} , \quad 2.1.5-52$$

where

A_i = combined gas dome cylinder, disk top, and bottom surface areas.

Mass Transfer to the Gas Dome

When the accumulator is in its stagnant initial condition the gas dome and liquid are in thermal equilibrium and the gas dome is at essentially 100% humidity. However, as the accumulator blows down, the gas dome expands and cools while the liquid remains essentially isothermal. As a result there is simultaneous vaporization at the liquid-gas interface and condensation in the gas dome.

At the liquid-gas interface as vaporization occurs the vapor diffuses across the temperature gradient into the gas dome. Assuming that the process can be approximated by a quasi-steady

formulation, then for diffusion in a stagnant gas the mass transfer for the process can be written as

$$\dot{M}_{\text{vap}} = - \zeta A_i \frac{dC}{dx}, \quad 2.1.5-53$$

where

\dot{M}_{vap} = rate of vapor diffusion,

ζ = diffusion coefficient,

A_i = surface area of the liquid-gas interface, and

$\frac{dC}{dx}$ = vapor concentration gradient.

The concentration can be expressed in terms of partial pressure such that

$$C = \frac{P_v}{P_d} \rho_g, \quad 2.1.5-54$$

where

C = vapor concentration,

P_v = local vapor partial pressure, and

ρ_g = vapor density (saturated vapor at P_v).

Hence at the dome pressure, the concentration gradient can be written as

$$\frac{dC}{dx} = \frac{1}{P_d} \frac{dP_v \rho_g}{dx}. \quad 2.1.5-55$$

Combining Equations 2.1.5-53 and 2.1.5-55 and integrating gives

$$\dot{M}_{\text{vap}} L_d = - \frac{\zeta A_i}{P_d} \left(\bar{p}_v \int_{x=0}^{x=L_d} d\rho_g + \bar{\rho} \int_{x=0}^{x=L_d} dP_v \right), \quad 2.1.5-56$$

where the integration is performed by parts.

Both of the differential terms $d\rho_g$ and dP_v can be written in terms of temperature differentials if 100% relative humidity is assumed, so that

$$P_v = P^S(T_g),$$

where

$P^S(T_g)$ = saturation pressure at the temperature T_g .

Hence the density differential can be expanded as

$$d\rho_g = \left[\left(\frac{\partial \rho_g}{\partial P_g} \right)_T \frac{dP_g}{dT} + \left(\frac{\partial \rho_g}{\partial T} \right)_{P_g} \right] \Delta T, \quad 2.1.5-57$$

where

$$\left(\frac{\partial \rho_g}{\partial P_g} \right)_T = \kappa_g \rho_g \quad \text{and} \quad 2.1.5-58$$

$$\left(\frac{\partial \rho_g}{\partial T} \right)_{P_g} = - \beta_g \rho_g. \quad 2.1.5-59$$

Combining Equations 2.1.5-57, 2.1.5-58, and 2.1.5-59, and substituting Clapeyron's equation for the dP_g/dT term gives

$$d\rho_g = \bar{\rho}_g \left[\kappa_g \left(\frac{h_{fg}}{T_g v_{fg}} \right) - \beta_g \right] dT, \quad 2.1.5-60$$

where Clapeyron's equation is

$$dP^s = \left(\frac{h_{fg}}{T_g v_{fg}} \right) dT, \quad 2.1.5-61$$

and where the term $(h_{fg}/T_g v_{fg})$ is treated as a constant. Combining Equations 2.1.5-56, 2.1.5-60, and 2.1.5-61 the diffusion equation can be rewritten as

$$\dot{M}_{\text{vap}} = \frac{c}{L_d} \frac{A_i}{P_d} \left\{ \bar{P}_g \bar{\rho}_g \left[\kappa_g \left(\frac{h_{fg}}{T_g v_{fg}} \right) - \beta_g \right] + \bar{\rho}_g \left(\frac{h_{fg}}{T_g v_{fg}} \right) \right\} (T_f - T_w). \quad 2.1.5-62$$

The dome average terms are evaluated at the dome average temperature, $T_g = T_d$, and T_w is the tank top wall temperature.

Equation 2.1.5-62 can be made analogous to a convective equation by expressing the mass transfer coefficient as

$$h_{2s} = \frac{c}{L_d}, \quad 2.1.5-63$$

where

h_{2s} = mass transfer coefficient in a stagnant gas.

Then, by applying Reynold's analogy a turbulent natural convection mass transfer coefficient can be derived in terms of the heat transfer coefficient, h_2 , from Equation 2.1.5-48 such that

$$h_{2s} = h_2 \left(\frac{r}{k_D}\right) \left(\frac{\alpha_d}{r}\right)^{1/3} \quad 2.1.5-64$$

Equation 2.1.5-64 can then be substituted in place of (ζ/L) in Equation 2.1.5-63 such that

$$\begin{aligned} \dot{M}_{\text{vap}} = h_2 \left(\frac{r}{k_D}\right) \left(\frac{\alpha_d}{r}\right)^{1/3} \left(\frac{A_i}{P_d}\right) \left\{ \bar{p}_g \bar{\rho}_g \left[k_g \left(\frac{h_{fg}}{T_d v_{fg}}\right) - \beta_g \right] \right. \\ \left. + \bar{\rho}_g \cdot \left(\frac{h_{fg}}{T_g v_{fg}}\right) \right\} (T_f - T_w) , \end{aligned} \quad 2.1.5-65$$

which gives the rate at which water vapor is transported into the accumulator gas dome by turbulent diffusion.

Since the energy transported to the gas dome by the vaporization process must come from the liquid and since the energy per unit mass required for vaporization is h_{fg} , then the rate of energy transport to the gas dome by vaporization is

$$\dot{Q}_{\text{vap}} = \Gamma_{\text{vap}} (h_{fg})_{T_f} = \dot{M}_{\text{vap}} (h_g)_{T_f} , \quad 2.1.5-66$$

where Γ_{vap} is the rate of vaporization at the liquid gas interface.

In the gas dome, as the accumulator blows down, the gas cools and condensation by turbulent diffusion occurs. The rate of condensation may be approximated by assuming that the gas dome

remains at 100% humidity and considering simple humidity relationships. The humidity ratio can be written as

$$w = \frac{M_g}{M_n} = \frac{N_g P_g}{N_n P_D}, \quad 2.1.5-67$$

where

M_g, M_n = vapor, gas masses, respectively,

N_g, N_n = vapor, gas molecular weights, respectively, and

P_g = vapor partial pressure.

Taking the derivative of Equation 2.1.5-67 gives

$$\frac{dM_g}{dt} = \frac{1}{P_D} \left[M_n \frac{N_g}{N_n} \frac{dP_g}{dt} - M_g \frac{dP_D}{dt} \right]. \quad 2.1.5-68$$

From Gibb's equation, the relationship between the vapor and liquid condensate in the dome is

$$v_{g_{P_g, T_D}} \frac{dP_g}{dT_D} - s_{g_{P_g, T_D}} = v_{f_{P_D, T_D}} \frac{dP_D}{dT_D} - s_{f_{P_D, T_D}}. \quad 2.1.5-69$$

Substituting the relationship

$$\frac{dP}{dt} = \frac{dP}{dT} \frac{dT}{dt} \quad 2.1.5-70$$

into Equation 2.1.5-69 and rearranging gives

$$\frac{dP_g}{dt} = \frac{v_{f_{P_D, T_D}}}{v_{g_{P_g, T_D}}} \frac{dP_D}{dt} - \frac{[h_{g_{P_g, T_D}} - h_{f_{P_D, T_D}}]}{T_D v_{g_{P_g, T_D}}} \frac{dT_D}{dt}. \quad 2.1.5-71$$

Combining Equations 2.1.5-68 and 2.1.5-71 with Equations 2.1.5-43 and 2.1.5-44 gives

$$\frac{dM_g}{dt} = \frac{1}{P_D} \left(M_a \frac{N_g}{N_a} - M_g \right) \frac{V_{f_{P_D, T_D}}}{V_{g_{P_g, T_D}}} \frac{1}{V_v} \left[\dot{Q}_D \frac{R_n}{C_v} - P_D \left(1 + \frac{R_n}{C_v} \right) A_1 V \right] + \frac{1}{P_D} \frac{N_g}{N_a} \left[\frac{h_{g_{P_g, T_D}} - h_{f_{P_D, T_D}}}{T_D V_{g_{P_g, T_D}}} \right] \frac{1}{C_v} (\dot{Q}_D - P_D A_1 V) \quad 2.1.5-72$$

and the rate of condensate formation is given as

$$\dot{M}_c = - \frac{dM_g}{dt} + \dot{M}_{vap} \quad 2.1.5-73$$

The energy transported by the condensate to the interface can be expressed as

$$\dot{Q}_{m_c} = \dot{m}_c h_{f_{T_D}} \quad 2.1.5-74$$

Also, since the condensation is taking place in the gas dome, the energy given up by the condensation process is given up to the gas dome at the rate expressed as

$$\dot{Q}_{M_c} = \dot{M}_c h_{fg_{T_D}} \quad 2.1.5-75$$

Finally, since it is assumed that the condensate is transported to the interface at the condensation rate

$$\dot{m}_c = \dot{M}_c \quad 2.1.5-76$$

and the net energy given up to the gas dome by the condensation process can be expressed as

$$\dot{Q}_c = \dot{Q}_{\dot{M}_c} - \dot{Q}_{\dot{m}_c} = \dot{m}_c (h_{fg_{T_D}} - h_{f_{T_D}}) \quad . \quad 2.1.5-77$$

Energy Transported to the Gas Dome by Combined Heat and Mass Transfer

The total energy transported to the gas dome can be rewritten by combining Equations 2.1.5-45, 2.1.5-46, 2.1.5-48, 2.1.5-66, and 2.1.5-77 and summing to give

$$\begin{aligned} \dot{Q}_D = & (h_1 A_1 + h_2 A_2) (T_w - T_d) + h_2 A_2 (T_f - T_d) + \dot{M}_{vap} h_{g_{T_f}} \\ & + \dot{m}_c \left[h_{fg_{T_d}} - h_{f_{T_d}} \right] \quad . \quad 2.1.5-78 \end{aligned}$$

Numerical Implementation

The numerical scheme used for the accumulator model includes special features for coupling the solution scheme to the main code in such a way that it is time step independent. This scheme, as in RELAP5, is semi-implicit and special considerations are employed to preserve the nitrogen energy and mass.

The numerical scheme uses finite difference techniques to solve the differential equations. The momentum equation is formulated

by integrating Equation 2.1.5-40 over space and writing the time variation in difference form as

$$\begin{aligned} & \left[\rho_f \left(L_{f_L} + L_{f_{TK}} \right) \left(\frac{A_L}{A_{TK}} \right) + F_f \Delta t + \rho_g \left(L_{g_L} + L_{g_{TK}} \right) \left(\frac{A_L}{A_{TK}} \right) + F_g \Delta t \right] v_{f_L}^{n+1} \\ & = - \left(P^{n+1} - P_D^{n+1} \right) \Delta t + \Delta P_z \Delta t + \left[\rho_f \left(L_{f_L} + L_{f_{TK}} \right) \left(\frac{A_L}{A_{TK}} \right) \right. \\ & \quad \left. + \rho_g \left(L_{g_L} + L_{g_{TK}} \right) \left(\frac{A_L}{A_{TK}} \right) \right] v_{f_L}^n - \text{CONVF} - \text{CONVG}, \quad 2.1.5-79 \end{aligned}$$

where

P^{n+1} = pressure downstream from the accumulator junction.

The inertia term is represented by

$$\rho_f \left(L_{f_L} + L_{f_{TK}} \right) \left(\frac{A_L}{A_{TK}} \right) + \rho_g \left(L_{g_L} + L_{g_{TK}} \right) \left(\frac{A_L}{A_{TK}} \right), \quad 2.1.5-80$$

where L_{f_L} , $L_{f_{TK}}$, L_{g_L} , and $L_{g_{TK}}$ are the lengths of the liquid and gas in the surge line and tank, respectively. These terms are computed at each time step and hence vary explicitly with time having the effect that as the accumulator blows down the inertia term changes from a liquid dominant to a vapor dominant term. The liquid and gas friction terms, respectively, are formulated as

$$F_f = \frac{\rho_f}{2} \left(\lambda \frac{L_{f_L}}{D_L} + K_L \frac{L_{f_L}}{L_L} \right) v_{f_L}^n \quad 2.1.5-81$$

for the liquid, and

$$F_g = \frac{\rho_g}{2} \left(\lambda \frac{L_{g_L}}{D_L} + K_L \frac{L_{g_L}}{L_L} \right) v_{g_L}^n \quad 2.1.5-82$$

for the vapor. Friction is neglected in the tank and the line friction factor is assumed to be the constant turbulent-turbulent Darcy friction factor given as

$$\lambda = \left[1.74 - 2 \log \frac{2\epsilon}{D_L} \right]^{-2} \quad 2.1.5-83$$

The loss factor term, K_L , is assumed to be distributed over the surge line length, L_L . The term D_L is the surge line hydraulic diameter and ϵ is the surge line wall roughness. The elevation head term, ΔP_z , is formulated as

$$\Delta P_z = - \frac{g \Delta z_{TK} \left(\rho_f L_{f_{TK}} + \frac{1}{2} \rho_g L_{g_{TK}} \right)}{L_{TK}} - \frac{g \Delta z_L \left(\rho_f L_{f_L} + \rho_g L_{g_L} \right)}{L_L} \quad 2.1.5-84$$

where Δz_{TK} and Δz_L are the tank and surge line elevation changes, respectively, and g is the gravitational acceleration. The liquid and vapor momentum flux terms, CONVF and CONVG, respectively are formulated as

$$\text{CONVF} = \frac{1}{2} \rho_f \left[1 - \left(\frac{A_L}{A_{TK}} \right)^2 \right] \Delta t v_{f_L}^n \left(2v_{f_L}^{n+1} - v_{f_L}^n \right) \quad 2.1.5-85$$

if there is liquid in the tank,

$$\text{CONVF} = 0.0 \quad 2.1.5-86$$

when there is no liquid in the tank,

$$\text{CONVG} = \frac{1}{2} \rho_g \left[\left(\frac{A_L}{A_{TK}} \right)^2 - \frac{1}{4} \left(\frac{A_L}{A_{TK}} \right)^2 \right] \Delta t v_{g_L}^n \left(2 v_{g_L}^{n+1} - v_{g_L}^n \right) \quad 2.1.5-87$$

if there is vapor in the surge line, and

$$\text{CONVG} = 0.0$$

2.1.5-88

where there is no vapor in the surge line. By formulation in this manner the momentum equation is solved over the pressure gradient from the centroid of the gas dome to the accumulator junction. However, the momentum of the fluid downstream from the accumulator junction is not included. Also since fluxing of the gas through the junction is not allowed, we have

$$v_{g_L}^{n, n+1} = v_{f_L}^{n, n+1}$$

2.1.5-89

until the accumulator empties of liquid. The effect of this formulation is that as the accumulator blowsdown the liquid-gas interface moves out of the accumulator tank and surge line. Thus, the centroid of the gas dome moves towards the centroid of the combined tank and surge line.

The pressure solution is obtained by combining Equations 2.1.5-38 and 2.1.5-42 and multiplying by R_n/C_{v_n} , which results in

$$M_n R_n \frac{dT}{dt} = - \frac{R_n P_D}{C_{v_n}} \frac{dv_v}{dt} + \frac{R_n}{C_{v_n}} \dot{Q}_D, \quad 2.1.5-90$$

where Q_D is given by Equation 2.1.5-78. Equations 2.1.5-41 and 2.1.5-90 are then combined resulting in

$$P_D \left[1 + \frac{R_n}{C_{v_n}} \right] \frac{dv_v}{dt} + v_v \frac{dP_D}{dt} = \frac{R_n}{C_{v_n}} \dot{Q}_D . \quad 2.1.5-91$$

Since the liquid is incompressible

$$\frac{dv_v}{dt} = - \frac{dv_f}{dt} = A_L v_{f_L} \quad 2.1.5-92$$

and substitution in Equation 2.1.5-91 and expanding in nonconservative finite difference form gives

$$P_D^n \left[1 + \frac{R_n}{C_{v_n}} \right] A_L \Delta t v_{f_L}^{n+1} + v_v^n (P_D^{n+1} - P_D^n) = \frac{R_n}{C_{v_n}} \dot{Q}_D^n \Delta t . \quad 2.1.5-93$$

The energy equation may then be solved directly for the new time gas temperature by combining Equations 2.1.5-41, 2.1.5-44, 2.1.5-91, and integrating, which gives

$$T_D^{n+1} = T_D^n e^{\left[\frac{R_n}{C_{v_n}} \ln \left[\frac{v_v^n}{v_v^{n+1}} \right] + \Delta t \frac{\dot{Q}_D^n}{P_D^n v_v^n} \right]} . \quad 2.1.5-94$$